6-1-2004

Analysis of the cup drawing process and optimization of the blank holder force

Hossam Gharib
The American University in Cairo AUC

The American University in Cairo
School of Science and Engineering
Interdisciplinary Engineering Programs

ANALYSIS OF THE CUP DRAWING PROCESS AND OPTIMIZATION OF THE BLANK HOLDER FORCE

by

Hossam Hamdy Gharib
B.Sc. in Mechanical Engineering
With double specialization in
Design and Industrial

A thesis submitted in partial fulfillment of the requirements for the degree of:

Master of Science in Engineering

With specialization in:

Mechanical Design

Under the supervision of:

Dr. Maher Y. A. Younan
Prof. of Mechanics and Design, Mechanical Engineering Department
The American University in Cairo

Dr. Abdallah S. Wifi
Professor
Mechanical Design and Production Department, Faculty of Engineering
Cairo University

Dr. Ashraf O. Nassef
Associate Professor, Mechanical Engineering Department
The American University in Cairo

Spring 2004

ACKNOWLEDGEMENTS

Above all, I would like to thank God for the strength, power, and patience he provided me with all through my life. I need to thank my instructors and advisors, Dr. Maher Younan, Dr. Abdallah Wifi, and Dr. Ashraf Nassef. They provided me with the knowledge and guidance that were of great help in accomplishing this work.

My gratitude and appreciation goes to my father and mother. They supported me in all aspects of life and were a continuous source of encouragement and advice. An everlasting gratitude and thankfulness goes to my fiancé Radwa for standing by my side through it all.

I also want to express by admire and gratitude to my dear friend Hany Fayek. He provided me with great help and support through his technical advice and experience. Also, he has been a good listener at times when I needed motivation and encouragement.

Many thanks go to Dr. Ermen Tekkaya in the Middle East Technical University in Ankara. His Master thesis that he sent me was of great help and guidance to my work. Also, I would like to thank Dr. Hassan Moslemi Naeini in Tarbiat Modarres Univesrity in Tahran. He sent me copy of technical papers in my field of study that were of great usefulness.

ACKNOWLEDGEMENT TO THE U.S. EGYPTIAN PARTNERSHIP FUNDED PROJECT

The work done in this thesis is part of the U.S. Egyptian partnership funded projects. The project is between Missouri University and the American University in Cairo. The project is titled “Modeling and Management of Process Induced Shape Distortion in Sheet Forming Processes”. The project code is MAN6-006 and the contract/agreement number is 170.

ABSTRACT

The process of deep drawing of a cylindrical cup is analyzed and optimized for the minimum punch force. An analytical model is developed for the cup drawing process by determining the variation of stresses and strains over the deforming sheet at any stage of deformation until a full cup is formed. The model uses finite difference approach and numerical analysis to solve for equilibrium, continuity, and plasticity equations. Then, optimization of the blank holder force (BHF) is carried out using the developed analytical model. Optimization is carried out using genetic algorithms to determine the optimum linear BHF scheme that minimizes punch force and avoids limits of flange wrinkling and wall tearing.

Verification of the analytical model is achieved by comparing the results with experimental results from the literature. The analytical model results are also compared with those of a developed finite element model on ABAQUS. The finite element model is developed using continuum axisymmetric elements for the sheet metal blank and analytical surfaces for the punch, die, and blank holder parts. Both the experimental verification and the finite elements comparison showed good correlation with the analytical model.

The analytical model is used to conduct a parametric study on the effect of the different die and process parameters on the process. The parameters investigated are the die and punch profiles radii, blank holder force, die coefficient of friction, and drawing ratio. The study showed good correlation with other parametric studies conducted by previous investigators.

An optimization strategy for the BHF scheme is proposed which searches for the BHF scheme that minimizes the maximum punch force and avoids process limits. This strategy is applied for the linear type BHF scheme and compared to the constant BHF. The optimized linear BHF scheme showed good improvement to the results compared to the constant scheme. Also, the BHF scheme is optimized for different cases of drawing ratios and die coefficients of friction in order to analyze the nature of

the optimum linear BHF scheme. It was found that the slope of the linear BHF scheme increases with the increase in the drawing ratio in a linear manner. Also, the intercept of the function showed a nearly linear variation with the drawing ratio. A general equation is deduced for the optimum blank holder force at any drawing ratio for the cup under study.

TABLE OF CONTENTS

LIST OF TABLES

LIST OF FIGURES

NOMENCLATURE

C, n	: Constants in the material flow equation
B_o	: drawing ratio
D_a	: flange radius reduction
E	: Young's modulus
E_o	: reduced modulus of buckling of the sheet metal
F_o	: tangent modulus of buckling of the sheet metal
F_{BH}	: blank holder force
$(F_{BH})_{cr}$	: critical blank holder force
F_P	: punch force
$(F_P)_{max}$	: maximum punch force
$(F_P)_{cr}$	: critical punch force
(F_r)	: radial force
$(F_r)_{cr}$	: critical radial force that initiates necking
F_{error}	: error function used in the numerical solution convergence in region I
H	: vertical distance between die profile center and punch profile center
N	: distance between die profile center and punch profile center normal to the tangent line (T)
K	: horizontal distance between die profile center and punch profile center
L	: punch travel
R_a	: initial blank radius
R_{j-1},R_j,…	: initial radii of particular points in the sheet metal blank
T	: length of tangent between die and punch profiles
i,j	: Suffices that designate location of a point in time and space respectively
np	: number of points in the deforming sheet
np	: number of stages of deformation
p_{cr}	: critical blank holder pressure to suppress wrinkling of the blank
r_1	: radius to the mean surface of sheet at the moving boundary between regions III and IV
r_2	: radius to the mean surface of sheet at the moving boundary between

regions IV and V

r_a : current rim radius

r_b : current boundary radius of the rim region between regions I and II

r_c : radius to the die lip

r_d : die throat radius

r_e : punch radius

r_f : radius of the flat base of punch

r_m : average radial position of two points

Δr : incrementing parameter the describes the displacement of the sheet rim

Δr^* : difference between radial position of two points

$r_{j-1}, r_j, \ldots$: current radii of points of initial radii $R_{j-1}, R_j, \ldots$

$t_{j-1}, t_j, \ldots$: current thickness of material at $r_{j-1}, r_j, \ldots$

t_0 : initial thickness of material

t_a : thickness of sheet in region I

t_F : mean thickness of sheet in region II

t_D : mean thickness of sheet in region III

t_W : mean thickness of sheet in region IV

t_P : mean thickness of sheet in region V

t_B : mean thickness of sheet in region VI

t_{error} : error function used in the numerical solution convergence in regions II to V

u_0, u_1 : intercept and slope of the optimized blank holder force function that is in terms of the reduction of flange radius

v_0, v_1 : intercept and slope of the optimized blank holder force function that is in terms of the punch travel

α_B, α_H, α_D : relations between the drawing ratios β's

β_o : current drawing ratio

β_c : ratio of flange inner radius to punch radius

δ : specific hole diameter

$\varepsilon_\theta, \varepsilon_r, \varepsilon_t$: principal circumferential, radial and thickness strains respectively

$\bar{\varepsilon}$: equivalent strain

$\bar{\varepsilon}_{eq}$: equivalent strain at a mean radius in the flange

$\Delta\varepsilon_f$: objective function to be minimized in the moving boundary search

ϕ : angle of contact between the sheet and the die profile or between the sheet and the punch profile for a point in the sheet

ϕ_{error} : error function used in the numerical convergence of angle ϕ in regions III to V

μ_{BH} : coefficient of friction between sheet and blank-holder or sheet and die surface

μ_{DP} : coefficient of friction between sheet and die profile

μ_{PP} : coefficient of friction between sheet and punch profile

μ_D : coefficient of friction between sheet and die surface, which includes the die profile and the part in contact with the flange of the deforming sheet

ν : poisson's ratio

θ : contact angle on die or punch profiles defining moving boundaries (1) and (2) respectively

θ_{error} : error function used in convergence of the contact angle θ

ρ_d : die profile radius

$\rho_d^{'}$: die profile radius to the mean surface of sheet

ρ_p : punch profile radius

$\rho_p^{'}$: punch profile radius to the mean surface of sheet

$\sigma_\theta, \sigma_r, \sigma_t$: principal circumferential, radial and thickness stresses respectively

$\overline{\sigma}$: Von Mises yield stress

$\overline{\sigma}_o$: initial yield stress

σ_c : radial stress at flange inner radius r_c

ω_{cr} : critical specific wave amplitude for wrinkling

ψ : angular coordinate in the horizontal plane

CHAPTER 1

INTRODUCTION

Sheet metal forming is a huge industry that provides countless products for everyday life. For many years, sheet metal deformation has been an art. However, the strong demand for improvement of the industry has demanded researchers to dig deep into the science of the process. Deep-drawing, being one of the main processes in sheet metal forming, has many applications including kitchen utensils, beverage cans, military steel helmets, and car body parts.

Deep Drawing is considered a plastic deformation process in which a given workpiece is brought into a desired shape by conserving the mass and continuity of the material. It is based on plastically deforming a sheet metal which is initially in the form of a flat plate into the desired shape of a product. The process consists of a sheet metal blank that is restrained by a blank holder against a die. A punch moves against the blank to deform it into the required shape. The basic process components are shown in Fig. 1-1

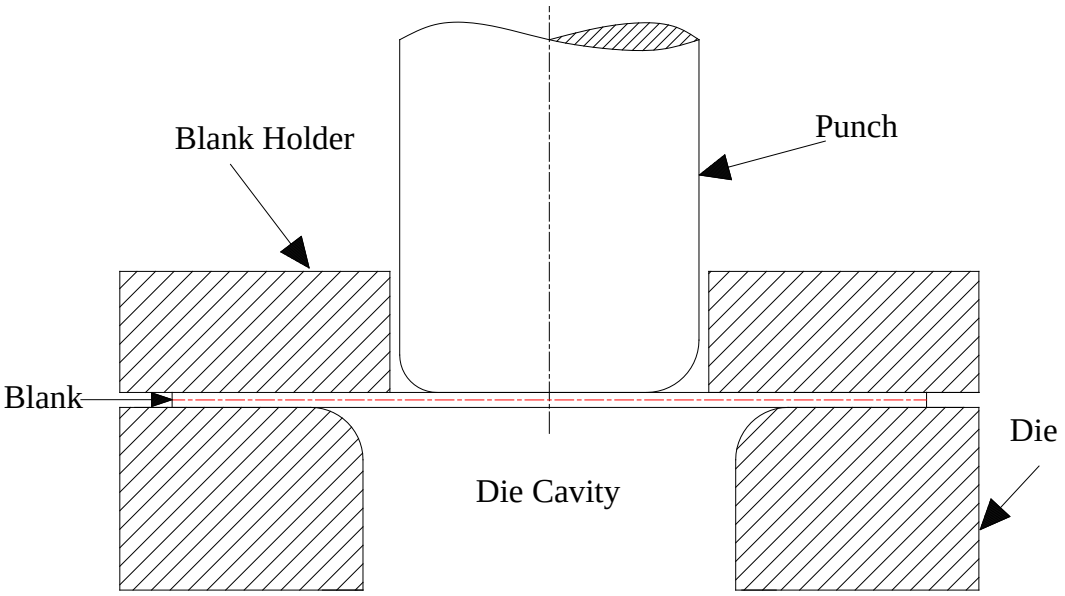

Fig. 1-1: The basic components of the deep drawing process

As shown in Fig. 1-2, the deforming sheet can be divided into regions (zones), where each region has different loading conditions and deformation behavior. In the case of a cylindrical cup, the sheet can be divided into six regions. These regions can be described as:

- Region I (Flange in contact with the blank-holder): It consists of the part of the material present over the die where it experiences a state of radial drawing under friction with the blank holder and the die surface. In this region, wrinkling or local buckling of the sheet blank due to compressive stress is possible. So, the blank-holder role is to press normally on this area to suppress wrinkling of the flange and forces the sheet to have a constant thickness.
- Region II (Flange not in contact with the blank-holder): This is the remaining part of the flange undergoing radial drawing. The material in this region is not in contact with the blank holder. Thus, thickness variation is possible, where the material starts with a large thickness at radius r_b and thins until it reaches radius r_c (die lip).
- Region III (Die Profile): This region undergoes both radial drawing with friction over die profile and bending/unbending effect. This combined loading causes sudden decrease in thickness at the die lip (radius r_c). The position of the point of departure of the material from the die profile to the wall of the cup (radius r_1) is varying through time. This represents a problem with a moving boundary, which is not known *a priori* in the analysis and requires special treatment to determine its correct position.
- Region IV (Straight Wall): this region forms the wall of the cup where it starts from the departure of sheet from the die profile until it meets the punch profile at radius r_2. The material in this region suffers a state of biaxial stress. The point of contact of the sheet with the punch profile (at radius r_2) is also considered a moving boundary.
- Region V (Punch Profile): This region constitutes the part of the sheet being stretched under friction and bent over the punch profile. Fracture of the sheet metal usually occurs at the boundary between this region and region IV.
- Region VI (Flat Bottom below the punch): Material is drawn under biaxial state of stress in this region. Stresses and strains are nearly uniform and constant over this area.

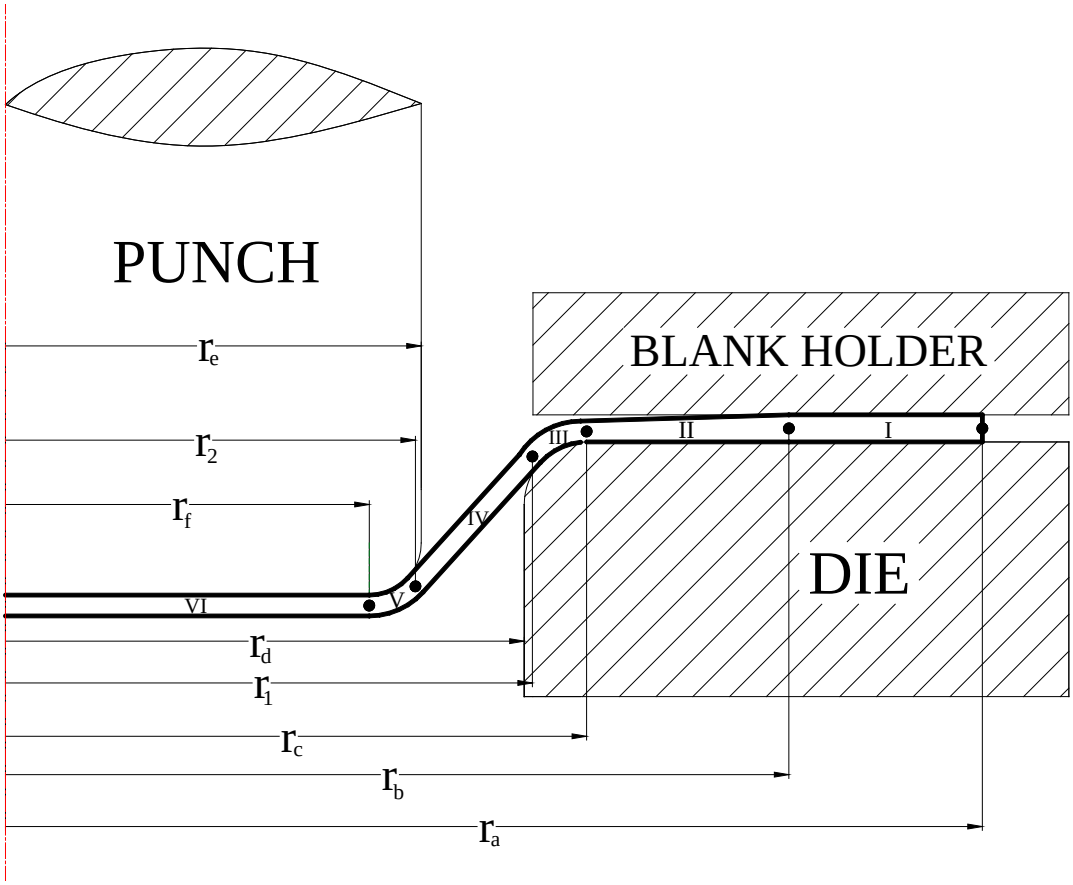

Fig. 1-2: Features in Cylindrical Cup Deep-Drawing

Defects are of major concern in sheet metal forming operations. Defects due to wrinkles and excessive localized thinning alter the product geometry from the designed one causing difficulties in joining and assembly of sheet products and limits the product serviceability. They are function of material properties, process parameters, and die design. The two main material properties that affect the process defects are the strain hardening and normal anisotropy. Process parameters are blank holding force, punch speed, sheet thickness, and interface friction condition. On the other hand, die design variables include punch and die profile radii, and clearance between the punch and the die.

In deep drawing, it is required to produce the deepest cup while avoiding defects. One way to achieve this goal is to increase the number of redraws in which the part is produced in several draws. However, this method can be expensive since it requires more time and money. So, it is required to reduce the number of redraws and at the same time produce the deepest possible cup. This goal can be achieved by optimizing the process parameters and/or die design variables with the objective of avoiding process defects. In that respect, two approaches can be followed:

(1) Experimental Design can be useful in determining the optimum process parameters and die design variables that satisfy the requirements stated above. However, experimental work is usually very expensive and time consuming to perform.

(2) Analytical/Numerical modeling can be used to model and analyze the process through all stages of deformation. This is combined with an optimization algorithm that satisfies the process objectives. This approach is less time consuming and more economical than experimental design.

In the present study, an Analytical/Numerical modeling approach is adopted. First, the model is developed to analyze the stresses and strains in the cup drawing process. The model is established on the solution of force equilibrium and plasticity relations using finite difference method. In the second phase of the study, the attention is focused on the role played by the blank holder force (BHF). The BHF is allowed to vary with process time to determine an optimized scheme that produces a defect free cup.

CHAPTER 2

LITERATURE REVIEW AND SCOPE OF THE STUDY

2.1 Literature Review

Understanding the science of deep drawing has started since the early decades of the twentieth century. Several attempts have been carried out to understand the mechanics and behavior of the deep drawn part. This understanding allowed for the control of the process defects. Wrinkling and tearing limits criteria have been developed to be used in the process design. Following is an account of the research carried out in the deep drawing process including process analysis, limits criteria, and process design.

2.1.1 Deep Drawing Analysis

There have been several efforts to solve and analyze the deep drawing problem. A comprehensive study of the elementary mechanics of the drawing process was carried out by Chung and Swift [1]. They provided experimental and analytical investigations into the cup drawing process. Their experimental testing was focused on analyzing the effect of varying the die design parameters and material properties on final strains, work, and punch load. On the other hand, the analytical study analyzed the cup starting from the rim up to the cup wall. They used modified Tresca criterion, Levy-Mises stress strain relations, equilibrium equations, strain compatibility relations, blank holding force on the rim, straight wall between the die and the punch, and isotropic material. Their analysis produced results in the flange and die profile very close to their experimental work. This analytical investigation was considered the foundation for the following works.

In 1964, Woo [2] carried out an investigation for the cup drawing process by handling some of the assumptions made by Chung and Swift [1]. He used a Von Mises yield criterion, blank holding force distributed on an area of the flange, shell membrane theory, finite difference method, and numerical integration. However, he

neglected bending/unbending effect, but suggested that their effect is not significant on the stresses and strains if the ratio between the die profile radius to the initial sheet thickness is greater than 6. He divided the analysis into two parts. The first started from the sheet rim up to the end of radial drawing over the die profile. While, the second started from the stretch-forming in region V (at radius r_f) up to region IV (at radius r_1). Then, a boundary matching technique was referred to at the moving boundary between the die profile and the cup wall. However, no results were given for both solution parts after applying the matching technique.

Woo followed his previous analysis with later works which included solutions to the boundary matching problem and normal anisotropy in Woo [3] and tractrix type dies in Woo [4] and Al-Makky and Woo [5]. He provided a complete solution to his previous analysis in which boundary matching was applied. He applied his analysis to the problem of hemispherical punch where he solved for stresses and strains over the whole sheet. A different approach to the determination of the moving boundary was presented in the solution of tractrix type dies [4] and [5]. In all his analytical investigations, Woo provided experimental verification to support his results.

Kaftanoglu and Alexander [6] and Kaftanoglu and Tekkaya [7] have developed a theory for axisymmetrical sheet metal deformation problems. They were able to predict the progress of the variables during the course of the axisymmetrical stretch-forming process up to the start of fracture. The theory includes the effects of plastic anisotropy in the thickness direction, approximation to thickness stress, variable coefficient of friction as a function of deformation, non-linear strain hardening, and pre-strain. A finite difference method was used in the solution and results showed good agreement with experimental work. However, bending and unbending effect was not taken into account in this approach.

Similar to the previous works, a complete analytical/numerical solution which included solution to all regions was presented by Reissner and Ehrismann [8] and Reissner and Schmid [9]. They presented a solution approach for solving the problem starting from the sheet rim up to the punch centerline. They used force equilibrium equations, Hill's anisotropic yield criterion, normal anisotropy, and isotropic work hardening. They also used finite difference for marching from one point to the other

over the sheet and over stages of deformation. In the work of Reissner and Ehrismann [8], redraws were analyzed for the production of two-part cans. Energy based failure criterion was used to determine bottom cracking as a process limit. Also, wrinkle formation was analyzed using virtual work method. However, they did not explain how the moving boundary between regions III and IV is determined.

A mixed method between discrete elements and finite difference was developed by Tatenami et al. [10] and Nakamura et al. [11]. The model incorporated bending and unbending at the die profile, friction between the material and punch-die profiles and variation of the stresses and strains over the sheet thickness. They applied the incremental theory of plasticity and isotropic theory to an elasto-plastic solid of mild steel. Their results for strain history and stress distribution agree with experimental testing. They concluded that the membrane theory is not suitable for problems undergoing large bending because of the considerable change of thickness.

Simple analytical models for the cup forming process which included force equilibrium and plasticity relations were due to Mahdavian and He [12] and Chang and Wang [13]. Mahdavian and He [12] analyzed the variation of stresses and strains in the cup from the rim up to the wall without including the punch bottom and profile. They used pure bending/drawing process with nonlinear strain-hardening and frictional force between blank and die. Effect of different coefficients of friction and constant yield stress versus strain hardening were investigated. As a continuation, Chang and Wang [13] presented an analytical model to solve the problem up to the contact of the deforming sheet with the punch profile. They decomposed the drawing and redrawing processes into a series of radial drawing and bending under tension calculations. Thickness distribution on the wall of the formed cup was obtained for the drawing and redrawing operations.

Other solution approaches for the deep drawing problem include upper-bound solutions such as the work of Noh and Yang [14], geometric solutions such as the work of Sowerby et al. [15], and slip line field methods like the work of Gloeckl and Lange [16].

Normal anisotropy is an important material parameter that influences the deep drawing process. Yoshida and Miyauchi [17] constructed experiments of both ferrous

materials and aluminum and copper alloys. They found out that fracture strength increases with an increase in normal anisotropy in case of ferrous metals, while the opposite occurs in aluminum and copper alloys. Also, it has been discovered that wrinkling resistance of materials increases with increasing normal anisotropy.

Based on Woo's analytical model, Hansen et al. [18] investigated the effect of anisotropy on the cup drawing process. They modeled the problem of the cylindrical cup from region I up until region III. Also, experiments were carried out to compare with the analytical results, and were in good agreement. They concluded that variation of anisotropy has large influence on the wall thickness distribution in the drawn cup. On the other hand, anisotropy has a small influence on the punch stroke – punch load curve.

Temperature effect on the limiting drawing ratio (LDR) was examined by Wong et al. [19]. LDR is known as the ratio between the initial sheet diameter to punch diameter that provides a complete cup without failure. They have found that the use of uniform temperature increase for the total material under deformation in deep-drawing yields only slight improvement in the limiting drawing ratio. However, applying a temperature gradient across the punch-sided and die-sided material obtained a punch stroke depth of twice that at room temperature.

Finite elements started its applications in large plastic deformation since the 1970's. One of the first applications of finite elements to the deep drawing problem was due to Wifi [20]. He developed a model for hemispherical cup based on elasto-plastic isotropic material with strain hardening. His model included bending, effect of shear stresses, and thickness variation. However, friction was assumed constant.

Another later investigation on hemispherical cup was carried out by Wang and Budiansky [21], which included modified interface conditions between contacting surfaces. However, they neglected bending and variation across the material thickness. Their model was based on nonlinear theory of membrane shells, normal anisotropy, and work hardening. Some discrepancy from the experimental work was noted, which is mainly due to the use of constant coefficient of friction and exclusion of the prestrain concept.

A general large plastic deformation metal forming model was developed by Kobayashi and Kim [22]. The model was based on rigid-plastic approach, but did not take into account plastic anisotropy and strain-hardening. A similar approach was worked out by Yamada et al. [23], but for elastic-plastic material.

Since the late 1980's, the use of finite elements for the analysis of the deep-drawing problems has increased. Different researches have been carried out to analyze various geometries, process parameters, die designs, and element types. These include the works of Saran et al. [24], Harpell et al. [25], Hayashida et al [26], and Moreira et al. [27].

2.1.2 Process Limits Investigations

In deep drawing, the two defects of flange wrinkling and tearing are considered process limits. The wrinkling or buckling of thin sheet metal is caused by a compressive instability. It occurs when the dominant stresses are compressive, tending to cause thickening of the material. This is influenced by many factors like mechanical properties of the sheet material, geometry of the sheet, contact conditions, and plastic anisotropy. On the other hand, localized necking or tearing occurs when the stress state leads to an increase in the surface area of the sheet while decreasing the thickness. The mechanism of localized necking initiation is very complicated, but it depends on the geometry of the part, the forces involved, the material properties, and the initial homogeneity of the sheet. It is important to have a certain criterion of prediction for these two process limits in order to fully deep draw a product without defects. Following is a review of some of the efforts made to predict these limits.

One of the early investigators into flange wrinkling was Senior [28]. He explained theoretically the critical dimensions of a deep-drawn flange that can cause wrinkling. However, his wrinkling critical limits are only applicable to a flange without a blank holder. Kawai [29] conducted valuable theoretical and experimental investigation of flange wrinkling. He carried out a semi-empirical analysis to predict the critical blank holding pressure below which wrinkling would occur. This critical blank holder pressure formula was based on the cup and sheet geometry, stresses, and friction in the flange. He also provided formulas that can predict the critical conditions of wrinkling in the case where a blank holder is not used.

Améziane-Hassani and Neale [30] presented an analysis of wrinkling in sheet metals. They constructed wrinkling limit curves (WLCs) which represented the combinations of the critical principal stresses for wrinkling. These curves were constructed using a bifurcation analysis for plastic buckling. They also carried out a study of the effects of material properties and sheet geometry on the critical conditions for wrinkling. Their analysis was based on the implementation of a finite element scheme. Another application to the bifurcation theory was carried out by Kim et al. [31]. The wrinkling initiation and growth was analyzed by finite element analysis including the bifurcation theory. They investigated the effect of blank holding force and anisotropy on the wrinkling behavior.

Cao and Wang [32] proposed an analytical model for plate wrinkling under tri-axial loading. They calculated the critical buckling stress and wavelength as functions of normal pressure using a combination of energy conservation and plastic bending theory. However, they required the use of finite elements for the simulation in order to be able to calculate the wrinkling wavelength.

There have been many efforts for determining the fracture limit in the sheet metal of the deep drawing part. A usual necking site is located near the punch profile which is known as the dangerous section. Analysis of the fracture load at this location was investigated by Deng et al. [34]. They used Hill's theory of plasticity and Swift diffuse instability criterion to predict the drawing fracture load and limit drawing ratio (LDR) of an axisymmetric cup drawing. They found that tool geometry has an effect on the weakening of the loading capacity of the sheet metal blank due to inducing a triaxial stress state and a bending effect at the dangerous section. It was verified that the decrease in the loading capacity of the workpiece due to tool geometry is about 6-10%. Also, they concluded that the optimum punch profile radius was found to be between 5 and 7 times the initial sheet thickness. However, their LDR equation requires knowing some material parameters that are not commercially available.

A very powerful and common tearing prediction and control in sheet metals are the forming limit diagrams (FLDs). These are diagrams comparing both minor and major strains in the deformed sheet. They are usually constructed using experiments that determine limit failure strains in the sheet metal. However, some efforts have

been directed towards constructing such diagrams using theoretical and analytical failure techniques.

The first appearance of the FLDs concept was in 1961 by Keeler and Backofen [35]. They tested several materials including steel, copper, brass and aluminum sheets by stretching them over solid punches and providing fracture limits for those materials. Later, FLDs were constructed experimentally for various materials with the common form known today as a map in principal strains (major and minor) which separated safe strain states from severe states of failure.

There are a large number of theortical approaches for the construction of FLDs. One of them is the Marciniak's approach of assuming an initial inhomogeneity in the material. Lahoti et al. [36] used this approach to predict the forming limit curve in biaxial stretching of sheets. They included the material anisotropy, strain rate dependent flow behavior of the sheet material and the orientation of inhomogeneity.

Instability was explored by El-Sebaie and Mellor [37] where they determined two types of instability. The first is under uniaxial tension in the flange and usually at the die opening. It was found to depend on strain hardening exponent (n) and likely to materials that have been previously cold worked. The second instability is under plane strain tension over the punch profile and depends on the normal anisotropy. Also, they developed an analytical model to solve the axisymmetrical deep-drawing problem. However, they ignored friction, assumed plane strain condition, and neglected die profile curvature effect. Also, they presented theoretical results for the limiting drawing ratio (LDR) in the deep drawing of cylindrical cups.

LDR was also investigated by Sonis et al. [38], where they proposed an analytical model to determine the limiting drawing ratio for the first draw as well as for redraws. They considered normal anisotropy, coefficient of friction, strain hardening and die profile radius. Their model can be used to determine the minimum number of passes or redraws required to achieve the final component geometry.

A more conservative fracture criterion assumes that necking in sheet metal will be initiated when the material reaches an equivalent strain equals to the strain hardening exponent. This situation occurs at the dangerous section between the cup

wall and the punch profile where the material undergoes a state of uniaxial stress. This approach was investigated by Marciniak and Duncan [39] and applied by Ahmetoglu et al. [40] to determine the critical fracture limit in the deep drawing of non symmetric parts.

An investigation that combined both wrinkling and fracture limits was carried out by Lei [41] and Lei and Kang [42]. They provided a prediction and control criteria of both the wrinkle limit and fracture limit for the deep drawing of a cylindrical cup. The fracture limit was based on the fracture critical radial tensile stress at the punch profile similar to the work of Deng et al. [34]. They compared their wrinkle criterion with those of other researchers. They claimed that their criterion is suitable for narrow-flange and wide-flange cylindrical cups.

2.1.3 Process Design Investigations

The design of a deep drawn component requires avoiding process limits discussed earlier. This can be established by varying the die design or the process parameters. The usual approach is controlling the blank holder force (BHF) scheme. This approach is aimed at the determination of the so called “process window” which provides the blank holder force path which gives the highest drawing ratio without causing wrinkling or tearing in the material.

The conventional way of applying the blank holder on the sheet metal is the constant load scheme. However, other schemes of varying blank holder load during the stages of deformation can be applied. Some of these schemes can be linearly decreasing or increasing, vibrating, or proportional to the punch force. Thiruvarudchelvan and Lewis [43] and Thiruvarudchelvan and Loh [44] conducted experiments for applying a blank holder load that is proportional to the punch load. They used an annular urethane pad compressed between two parts of a punch, which expands and applies pressure against the blank holder. The friction between the urethane pad and the blank holder applies a blank holding force approximately proportional to the punch force. They found that the maximum BHF needed for wrinkle free cups is about 34% of the maximum punch force. It was concluded that a BHF proportional to the punch force reduces thickness strain and punch force.

Using finite elements, Cao and Boyce [45] optimized the process of deep drawing a conical cup by a variable blank holder force history to avoid both wrinkling and tearing. Also, Sheng et al. [46] optimized the BHF scheme for a conical cup by adjusting the magnitude of the BHF continuously during the finite element simulation process. So, they were able to predict the suitable BHF scheme in a single process simulation. Lorenzo et al. [47] used an integrated approach to determine the optimal blank holder load path in an axisymmetric deep drawing process. They combined both finite element explicit simulation of the process with a closed-loop control system based on fuzzy logic reasoning.

Moshksar and Zamanian [48] studied the critical die and punch profile radii, and limiting drawing ratios for optimization of the axisymmetric deep drawn aluminum cups. They discovered that the process is sensitive to the die and punch profiles, where the maximum punch load is inversely proportional to the die nose radius. On the other hand, increasing the punch profile reduces the possibility of fracture, which means increasing drawability.

Design of experiments was used by Browne and Hillery [49] and Colgan and Monaghan [50] to determine the most important factors influencing the deep drawing of a cylindrical cup. They used statistical analysis to determine the effect of punch and die profile radii, punch velocity, clamping force, friction and draw depth on the thinning and punch force. Browne and Hillery [49] found that the blank holder force, punch and die profiles, lubrication, and position of lubrication are significant factors on the punch force. A similar conclusion was reached by Colgan and Monaghan [50] who concluded that the geometry of the tooling is generally most important, especially the die radius. The smaller the die radius the greater the drawing force induced and the greater is the overall thinning of the cup sidewall.

2.2 Motivation and Scope of the Present Work

The different studies carried out by researchers as shown previously provided an insight into the development of the deep drawing process. At first, the main interest has been to understand the mechanics of the problem. Thus, various experimental and

theoretical investigations were performed to analyze the process. They were mainly aimed at understanding the effect of the different factors in the process including material properties, process parameters and die design parameters. Also, process limits have been of major concern in the presented research studies, which help in producing a defect free product. Combining the process analysis techniques and process limits criteria, investigators have been able to optimize the deep drawing process for different objectives.

The main concern of the deep drawing industry is to optimize the process parameters in order to get a complete deep drawn product with least defects and high LDR. In order to achieve this optimization objective, a large number of runs will need to be performed in order to search for the optimum or near optimum solution. Most researchers have been using experimental design or finite elements for process optimization. Carrying out the optimization process through experimental design approach would require many runs in order to fit a proper objective function depending on the number of variables and the degree of fitting. Also, the use of finite elements to evaluate the function will require a lot of time which would reach one hour for one function evaluation on a 2.5GHz computer processor. This time can vary depending on the part geometry, material properties, loading conditions, and FE model. At some cases it will need months to satisfy an optimization objective. Therefore, a less time consuming approach is more reasonable and practical if optimization or process design is the objective. An appropriate and less time consuming solution approach is the analytical one. However, there has been no complete closed form solution for the simple problem of deep-drawing a cylindrical cup. Still, a complete analytical solution of the problem requires the use of numerical analysis.

The aim of the present study is to develop an optimization system to be used in determining the optimum BHF scheme that minimizes punch force without running into any of the process limits. The optimization process is implemented on a developed analytical/numerical solution. This analytical solution is intended to provide a thorough understanding of the mechanics of the process. Also, it offers less solution time than finite elements. However, its accuracy depends on the assumptions considered in the analysis.

The developed analytical model uses the finite difference method to solve for stresses and strains over the whole sheet from the rim up to the centerline of the punch. The analytical model considers nonlinear strain hardening, Von Mises isotropic yield criterion, thickness variation, friction between blank and deep drawing tools, and isotropic material. Verification of the developed analytical model is performed against experimental results from the literature. The results of the analytical model are compared with those of a developed finite element model. Also, a parametric study is conducted by varying some process and die design parameters to investigate their effect on the process.

The second phase of the research is concerned with the optimization of the BHF scheme. The developed analytical model is used to determine the suitable BHF scheme that minimizes punch force in order to draw a full cup without wrinkling or tearing. Wrinkling is controlled using the blank holder force limit criterion suggested by Kawai [30]. On the other hand, tearing is restrained using the uniaxial stress limit criterion which was suggested by Marciniak [39].

Several cases including different drawing ratios and die coefficients of friction are optimized for the minimum punch force. Genetic Algorithms (GAs) is used as the optimization tool to determine the optimum BHF linear scheme.

The present thesis is comprised of 6 chapters. Chapter 1 and 2 give an overview of the work and literature review.

In Chapter 3, the theoretical basics of the analytical model are presented including plasticity relations, force equilibrium equations, and continuity equations. Then, the numerical solution of the constitutive equations at each region is presented. This is followed by the determination of the moving boundaries and the computer code of the analytical model. The chapter is concluded with a description of the cases that are analyzed using the developed analytical model.

The optimization strategy of the BHF is presented in Chapter 4 with more emphasis on the role of the BHF and its associated process window. Also, the two process limits prediction criteria used in the optimization process are explained. Then, the optimization process is described including the objective function, variables and

constraints. This is concluded with a description of the computer code used in the BHF optimization and the cases whose BHF is optimized.

The results and discussion are given in chapter 5. The analytical model is verified against experimental results and compared with a finite element model. Then, a parametric study is carried out on some process and die design parameters to determine their effect on the process. Then, optimization of the BHF is carried out on two cup models. The first one is to compare the optimized BHF with a constant BHF and the other to analyze the nature of the optimized scheme.

Finally, chapter 6 gives a conclusion on the present study and recommendations for future work.

CHAPTER 3

THEORETICAL ANALYSIS AND MODELING OF THE CUP DRAWING PROCESS

The basic analytical theory used in the solution of the problem of deep-drawing a cylindrical cup is based mainly on the works of Chung and Swift [1], Woo [2], [3], and [5] and Kaftanoglu and Tekkaya [7] and Reissner and Ehrismann [8]. In the following sections, the analytical model constitutive equations together with their numerical solution are presented. Also, the unknown moving boundaries are discussed and a suggested procedure for their determination is introduced. The analytical model is established on the following assumptions:

- Elastic strains are neglected, since they are small compared with plastic strains
- Isotropic material
- Von Mises isotropic yield criterion
- Non-linear isotropic strain-hardening
- Radial (meridional), circumferential, and thickness directions are considered principal directions
- Bending/unbending effects are neglected since their effect is negligible for a die profile radius to sheet thickness ratio greater than 6 [2]
- Shear stress is neglected across the thickness

The principal directions in the problem of deep-drawing a cylindrical cup are the radial (meridional), circumferential and thickness directions. Stresses in the deforming sheet at the different regions are shown in Fig. 3-1, where:

σ_r = radial stress

σ_θ = circumferential stress

σ_t = Thickness stress

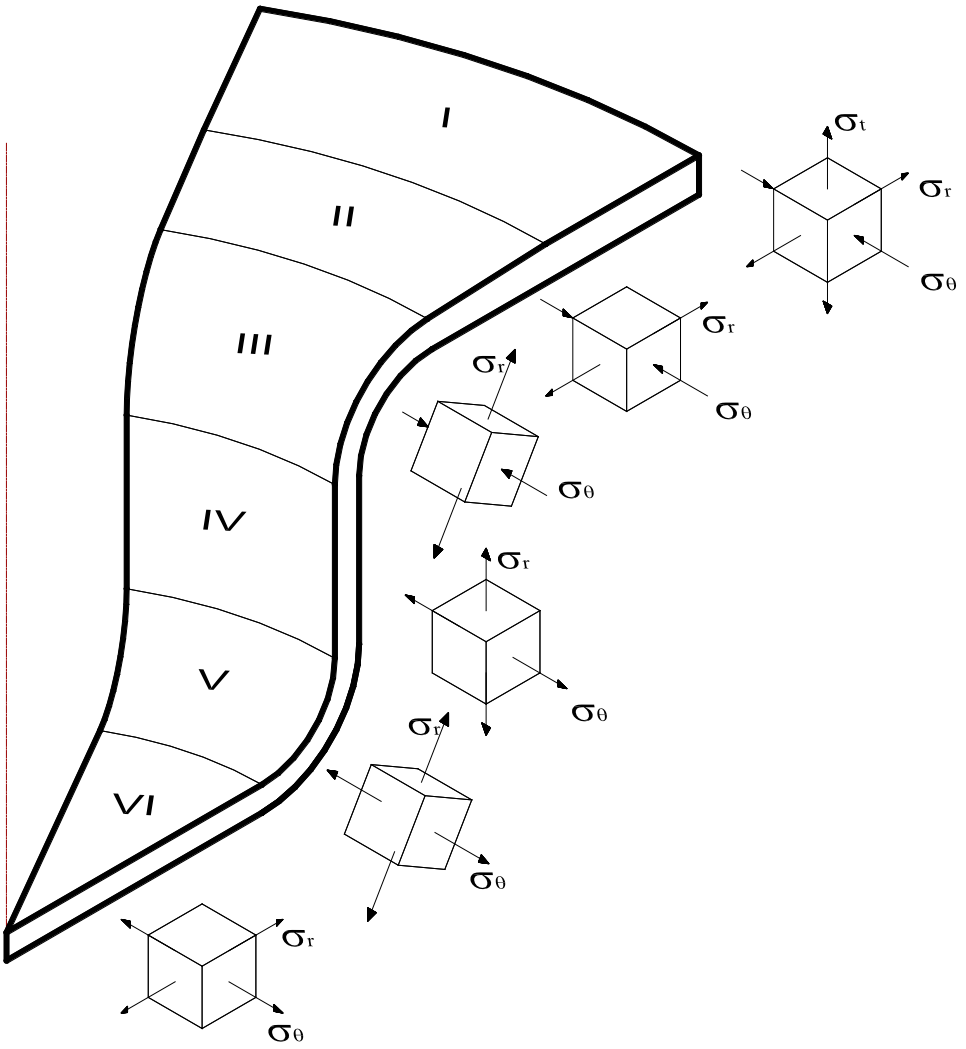

Fig. 3-1: Principal directions in the deformed cup

3.1 Problem Definition and Finite Difference Discretization

The objective of the analytical model is to evaluate the stresses and strains in the deforming sheet of the deep drawn cup. The analysis is carried out for each stage of deformation and over all the deformation regions that were discussed in chapter 1 and shown in Fig. 1-2. As indicated in Fig. 3-2, the deep drawing process starts with a flat circular blank of initial radius R_a and thickness t_o. The finite difference solution divides the blank from rim to punch centerline into discrete number of points (*np*) designated with subscript (*j*). Each point in the initial circular blank has a radius R_j and marches in time for a finite number of stages (*ns*) designated with subscript (*i*). The time used is just a fictitious time which is governed by the incremental motion of

the blank rim. At each stage of deformation, the outer rim has a radius r_a and each j point on the sheet has a radius $r_{i,j}$ and thickness $t_{i,j}$

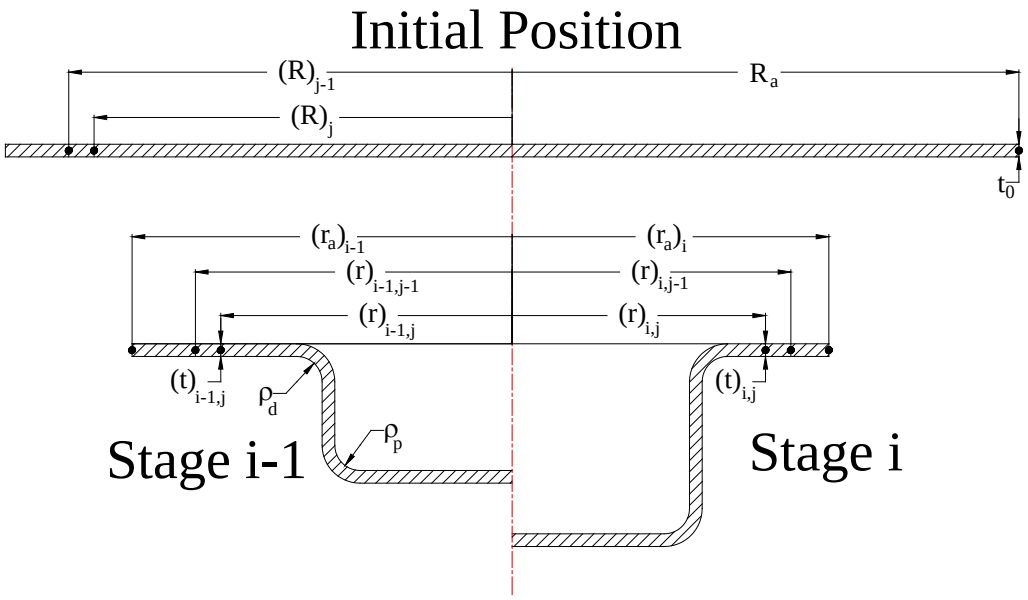

Fig. 3-2: Finite difference discretization of a cup (based on [8])

3.2 Plasticity Equations

The plasticity equations given in this section are based on references [2] and [39]

Effective Stress

For a material free from Bauschinger effects, Von Mises or effective stress is defined as follows:

$$\bar{\sigma} = \sqrt{\frac{1}{2}\left[(\sigma_r - \sigma_\theta)^2 + (\sigma_\theta - \sigma_t)^2 + (\sigma_t - \sigma_r)^2\right]} \tag{3.1}$$

Plastic Strains

Plastic strains for the three principal directions; circumferential, thickness, and radial (meridional) directions can be expressed as:

$$\varepsilon_\theta = \ln\left(\frac{r}{R}\right) \tag{3.2}$$

$$\varepsilon_t = \ln\left(\frac{t}{t_o}\right) \tag{3.3}$$

From the condition of constancy of volume,

$$d\varepsilon_r + d\varepsilon_\theta + d\varepsilon_t = 0 \quad , \quad \varepsilon_r + \varepsilon_\theta + \varepsilon_t = 0 \tag{3.4}$$

Thus,

$$\varepsilon_r = -\varepsilon_\theta - \varepsilon_t \tag{3.5}$$

Effective Strain

The effective incremental strain can be stated as:

$$d\bar{\varepsilon} = \sqrt{\frac{2}{9}\left[\left(d\varepsilon_r - d\varepsilon_\theta\right)^2 + \left(d\varepsilon_\theta - d\varepsilon_t\right)^2 + \left(d\varepsilon_t - d\varepsilon_r\right)^2\right]} \tag{3.6}$$

Using equation (3.4), the effective incremental strain becomes:

$$d\bar{\varepsilon} = \sqrt{\frac{4}{3}\left[\left(d\varepsilon_\theta + d\varepsilon_t\right)^2 - d\varepsilon_\theta d\varepsilon_t\right]} \tag{3.7}$$

Stress-Strain Relationship

The Levy-Lode stress-strain relationship states that:

$$\frac{d\varepsilon_r - d\varepsilon_\theta}{\sigma_r - \sigma_\theta} = \frac{d\varepsilon_\theta - d\varepsilon_t}{\sigma_\theta - \sigma_t} = \frac{d\varepsilon_t - d\varepsilon_r}{\sigma_t - \sigma_r} = \frac{3}{2}\frac{d\bar{\varepsilon}}{\bar{\sigma}}$$

Hence, the stress-strain relations can be written as:

$$\sigma_\theta - \sigma_r = \frac{2}{3}\frac{\bar{\sigma}}{d\bar{\varepsilon}}\left(d\varepsilon_\theta - d\varepsilon_r\right) = \frac{2}{3}\frac{\bar{\sigma}}{d\bar{\varepsilon}}\left(2d\varepsilon_\theta + d\varepsilon_t\right) \tag{3.8}$$

$$\sigma_t - \sigma_r = \frac{2}{3}\frac{\bar{\sigma}}{d\bar{\varepsilon}}\left(d\varepsilon_t - d\varepsilon_r\right) = \frac{2}{3}\frac{\bar{\sigma}}{d\bar{\varepsilon}}\left(2d\varepsilon_t + d\varepsilon_\theta\right) \tag{3.9}$$

Flow Equation

The flow equation that describes the strain hardening of the material is the Ludwik-Hollomon power law which is given by:

$$\bar{\sigma} = C\bar{\varepsilon}^n \tag{3.10}$$

Where, C = strength coefficient

n = strain hardening exponent

3.2.1 Finite Difference Form of Plasticity Equations

Writing the previous equations into finite difference format (based on reference [2]):

Plastic Strains

$$(\varepsilon_\theta)_{i,j} = \ln\left(\frac{r_{i,j}}{R_j}\right) \tag{3.11}$$

$$(\varepsilon_t)_{i,j} = \ln\left(\frac{t_{i,j}}{t_o}\right) \tag{3.12}$$

Therefore, the incremental plastic strains are:

$$(\Delta\varepsilon_\theta)_{i,j} = (\varepsilon_\theta)_{i,j} - (\varepsilon_\theta)_{i-1,j} \tag{3.13}$$

$$(\Delta\varepsilon_t)_{i,j} = (\varepsilon_t)_{i,j} - (\varepsilon_t)_{i-1,j} \tag{3.14}$$

$$(\Delta\varepsilon_r)_{i,j} = -(\Delta\varepsilon_\theta)_{i,j} - (\Delta\varepsilon_t)_{i,j} \tag{3.15}$$

Effective incremental strain

$$(\Delta\bar{\varepsilon})_{i,j} = \sqrt{\frac{4}{3}\left[\left((\Delta\varepsilon_\theta)_{i,j} + (\Delta\varepsilon_t)_{i,j}\right)^2 - (\Delta\varepsilon_\theta)_{i,j}(\Delta\varepsilon_t)_{i,j}\right]} \tag{3.16}$$

Total effective strain for a point can be obtained by adding up effective incremental strains up to the current stage (*cs*):

$$\bar{\varepsilon}_{i,j} = \sum_{i=1}^{cs} \Delta\bar{\varepsilon}_{i,j} \tag{3.17}$$

Flow Equation

$$\bar{\sigma}_{i,j} = C\bar{\varepsilon}_{i,j}^{\,n} \tag{3.18}$$

Stress-Strain relations

$$(\sigma_\theta)_{i,j} - (\sigma_r)_{i,j} = \frac{2}{3}\frac{(\bar{\sigma})_{i,j}}{(\Delta\bar{\varepsilon})_{i,j}}\left(2(\Delta\varepsilon_\theta)_{i,j} + (\Delta\varepsilon_t)_{i,j}\right) \tag{3.19}$$

$$(\sigma_t)_{i,j} - (\sigma_r)_{i,j} = \frac{2}{3}\frac{(\bar{\sigma})_{i,j}}{(\Delta\bar{\varepsilon})_{i,j}}\left(2(\Delta\varepsilon_t)_{i,j} + (\Delta\varepsilon_\theta)_{i,j}\right) \tag{3.20}$$

3.3 Equilibrium and Continuity Equations for the Different Cup Regions

Each of the six regions has different equilibrium equations and geometrical relations. Thus, what follows presents the equations specific for each region (based on references [2] and [8]).

3.3.1 Region I (Flange in contact with the blank-holder)

The stresses acting on a slab or discrete element in region I are shown in Fig. 3-3. These stresses are radial stress (σ_r), circumferential stress (σ_θ), and thickness stress (σ_t) due to blank holder force. Thickness stress causes frictional stress ($-\mu_{BH}\sigma_t$) at the slab upper surface in contact with the blank holder and lower surface in contact with the die surface.

Equilibrium Equation

The equilibrium of forces along the radial direction on an element in the flange under load of the blank-holder can be written as:

$$d\sigma_r = \left(\frac{\sigma_\theta - \sigma_r}{r}\right)dr + \frac{2\mu_{BH}\sigma_t}{t}dr$$

This can be written in integral and finite difference form as:

$$\left(\sigma_r\right)_{i,j} = \left(\sigma_r\right)_{i,j-1} + \int_{r_{i,j-1}}^{r_{i,j}} \left(\frac{\sigma_\theta - \sigma_r}{r}\right)dr + \frac{2\mu_{BH}}{t}\int_{r_{i,j-1}}^{r_{i,j}} \sigma_t dr \tag{3.21}$$

Continuity Equation

The position of a point at a certain stage can be determined by using constancy of volume between two points (*j-1* and *j*):

Initial Volume = $\pi\left(R_{j-1}^2 - R_j^2\right)t_o$

Current Volume = $\pi\left(r_{i,j-1}^2 - r_{i,j}^2\right)t_a$

In region I, thickness is uniform and equals t_a

Therefore, an equation of continuity can be written as:

$$\left(R_{j-1}^2 - R_j^2\right)t_o = \left(r_{i,j-1}^2 - r_{i,j}^2\right)t_a \tag{3.22}$$

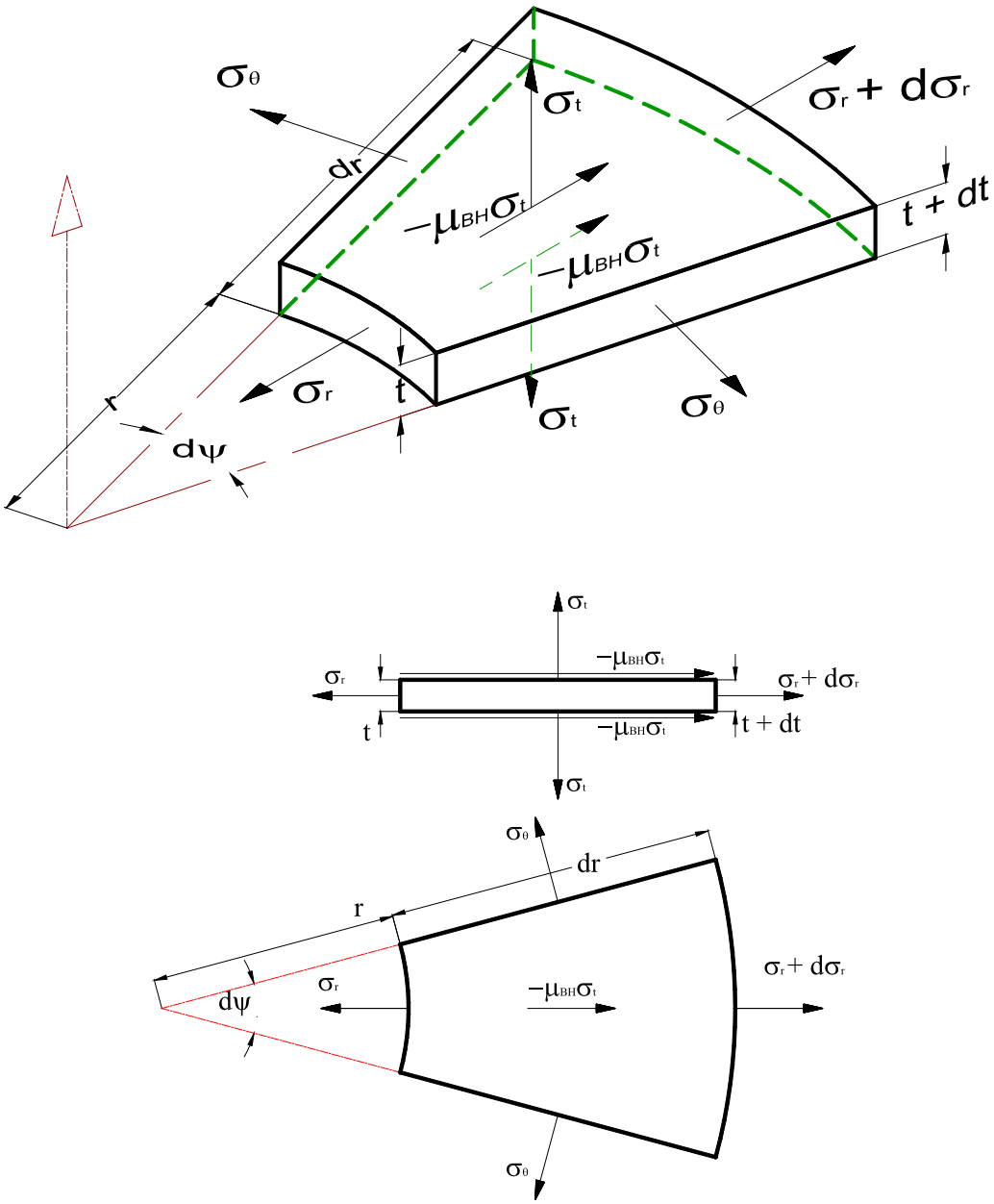

Fig. 3-3: Stresses in a slab element in region I

3.3.2 Region II (Flange not in contact with the blank-holder)

Neglecting the thickness stress, the stresses acting on region II are shown in Fig. 3-4.

Equilibrium Equation

The equilibrium equation of forces is similar to that of region I. However, friction is not introduced due to the absence of contact between the sheet and the blank-holder. Thus, the equation is given as:

$$d(\sigma_r t) = \left(\frac{\sigma_\theta - \sigma_r}{r}\right) t dr$$

This can be written in integral and finite difference form as:

$$(\sigma_r t)_{i,j} = (\sigma_r t)_{i,j-1} + \int_{r_{i,j-1}}^{r_{i,j}} \left(\frac{\sigma_\theta - \sigma_r}{r}\right) t dr \tag{3.23}$$

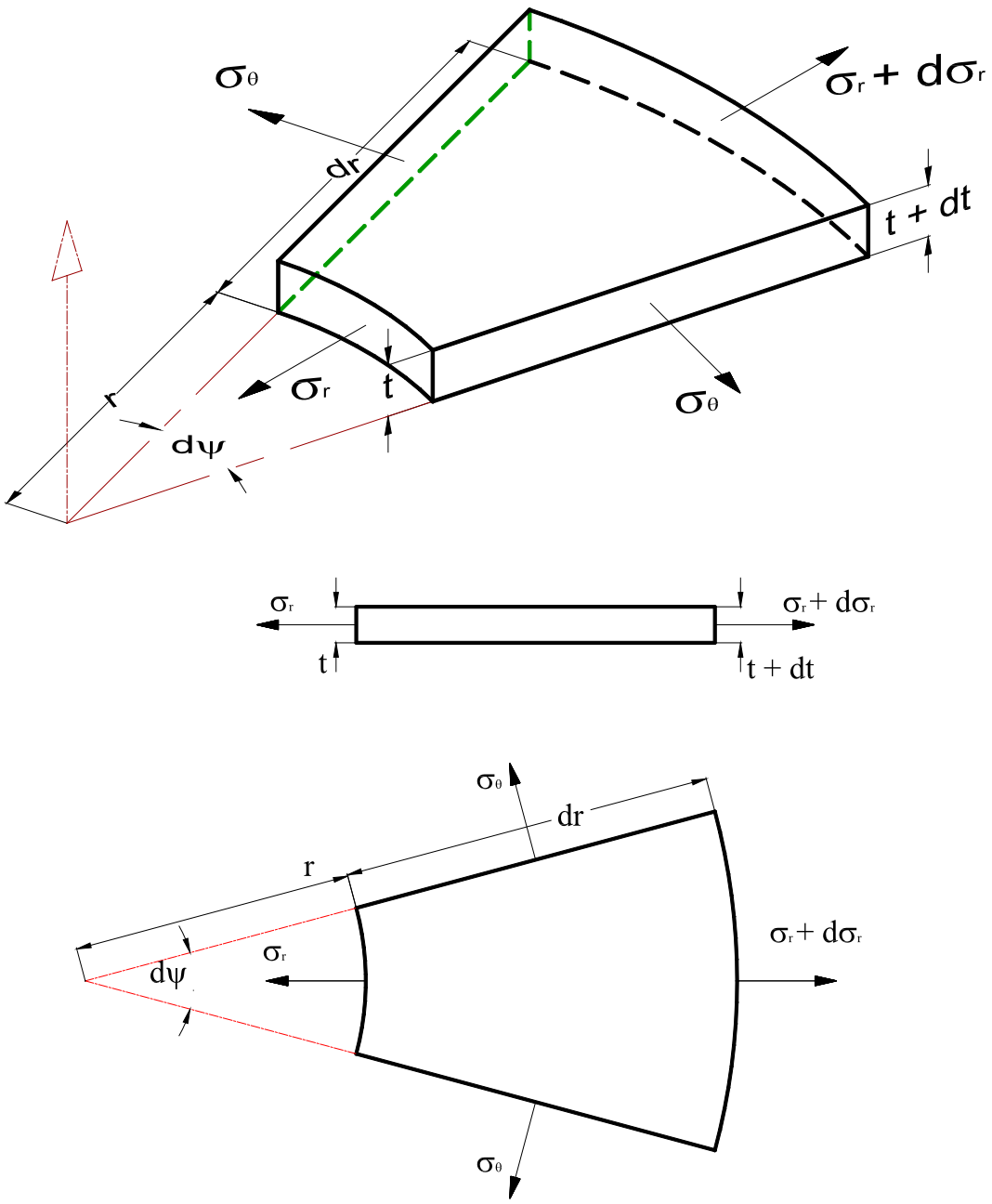

Fig. 3-4: Stresses in a slab element in region II

Continuity Equation

Unlike region I, thickness varies from one point to the next. So, the continuity equation can be written as:

$$\left(R_{j-1}^2 - R_j^2\right)t_o = \left(r_{i,j-1}^2 - r_{i,j}^2\right)\frac{\left(t_{i,j-1} + t_{i,j}\right)}{2} \tag{3.24}$$

3.3.3 Region III (Die Profile)

The stresses acting on a slab element on the die profile region is shown in Fig. 3-5. The radial (σ_r) and circumferential (σ_θ) stresses act on the membrane surface of the element. The thickness stress (σ_t) is directed from the die profile center and acts normally on the slab element inner surface, which is in contact with the die profile surface. This induces a frictional stress ($\mu_{DP}\sigma_t$) at the element inner surface.

Equilibrium Equation

By analyzing the stresses in the element, two equations of static equilibrium of forces in the horizontal and vertical directions can be obtained. Thickness stress (σ_t) is eliminated by substituting it from one equation to the other in terms of the other stresses. Therefore, the following equilibrium equation is obtained:

$$d\left(\sigma_r t\right) = \frac{\rho_d^{'}}{r_c - \rho_d^{'}\sin\phi}\left[\sigma_\theta t(\cos\phi + \mu_{DP}\sin\phi) - \sigma_r t\cos\phi\right]d\phi - \mu_{DP}\sigma_r t$$

Where, $\rho_d^{'} = \rho_d + \frac{t}{2}$

This can be written as:

$$\left(\sigma_r t\right)_{i,j} = \left(\sigma_r t\right)_{i,j-1} - \int_{\phi_{i,j-1}}^{\phi_{i,j}}\left[\sigma_\theta t(\cos\phi + \mu_{DP}\sin\phi) - \sigma_r t\cos\phi\right]\frac{\rho_d^{'}}{r_c - \rho_d^{'}\sin\phi}d\phi + \int_{\phi_{i,j-1}}^{\phi_{i,j}}\mu_{DP}\sigma_r t d\phi \tag{3.25}$$

Continuity Equation

From the constancy of volume of an element on the die profile, the following continuity equation can be used to determine the position of a point *j* at stage *i*:

$$\left(R_{j-1}^2 - R_j^2\right)t_o = 2(\rho_d^{'})^2\left[\frac{r_c}{\rho_d^{'}}\left(\phi_{i,j} - \phi_{i,j-1}\right) + \left(\cos\phi_{i,j} - \cos\phi_{i,j-1}\right)\right]\left(\frac{t_{i,j-1} + t_{i,j}}{2}\right) \tag{3.26}$$

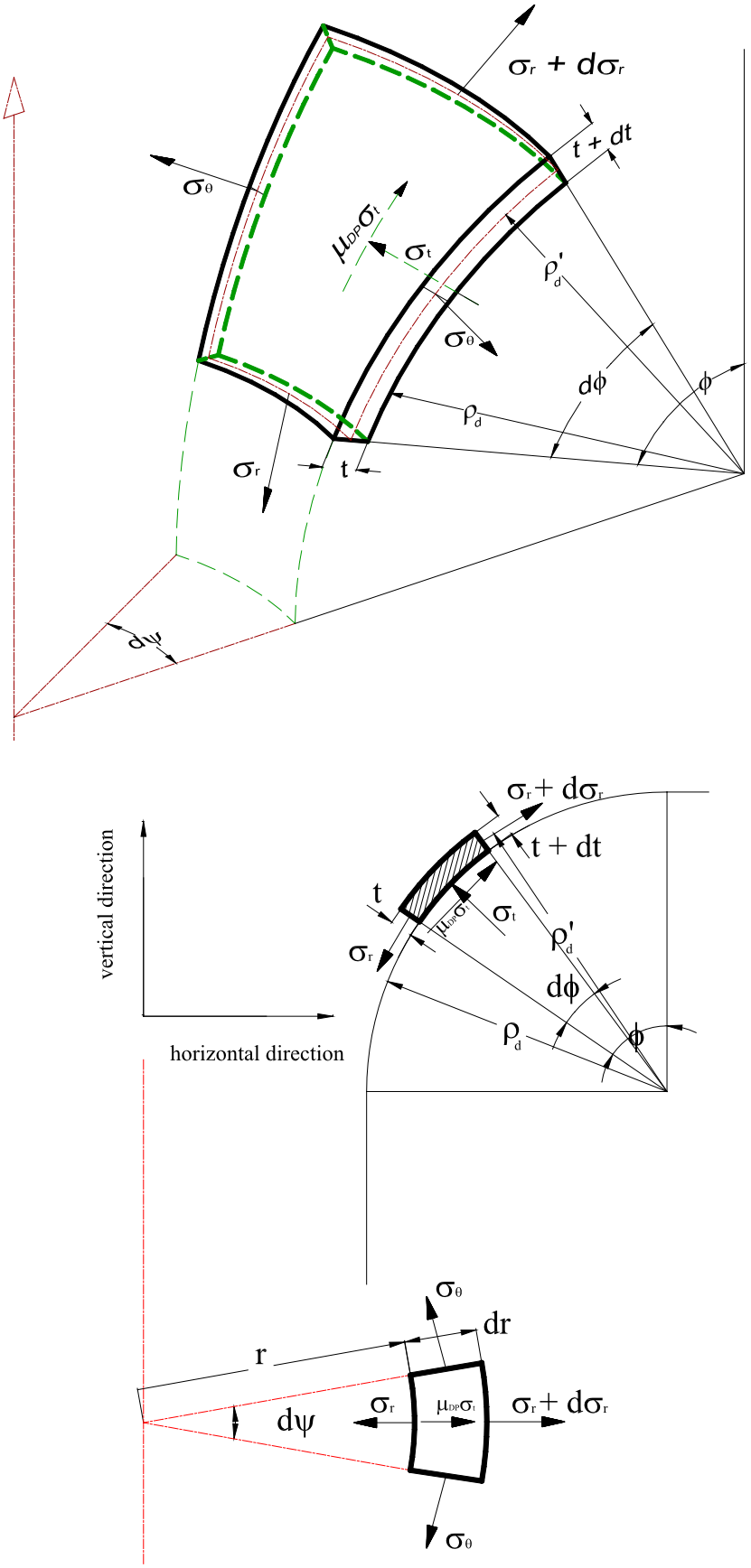

Fig. 3-5: Stresses in a slab element in region III

3.3.4 Region IV (Straight Wall)

Stresses acting on an element in the cup wall are shown in Fig. 3-6. Thickness stress is assumed to be negligible in this region since the cup wall is free from contact on its surface. Therefore, the element is only affected by a state of biaxial stress.

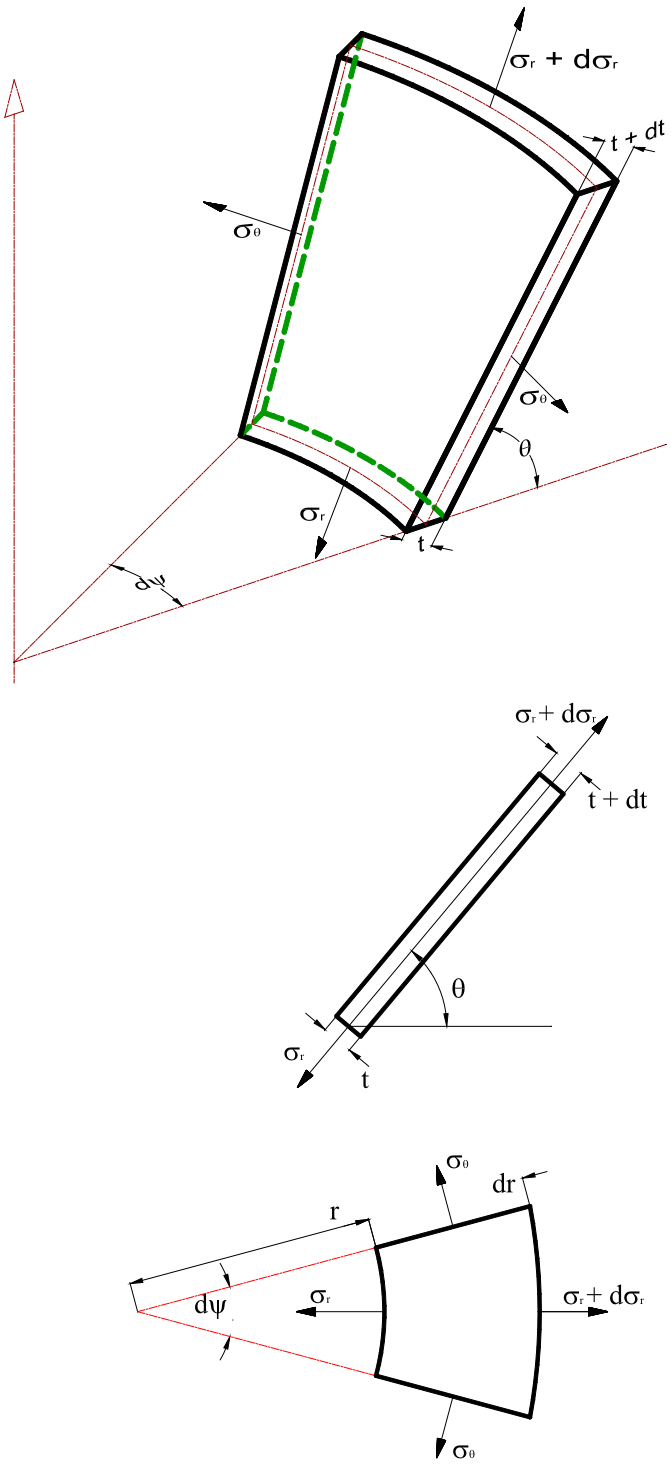

Fig. 3-6: Stresses in a slab element in region IV

Equilibrium Equation

The same equation for radial drawing in region II is used in the straight wall.

$$(\sigma_r t)_{i,j} = (\sigma_r t)_{i,j-1} + \int_{r_{i,j-1}}^{r_{i,j}} \left(\frac{\sigma_\theta - \sigma_r}{r} \right) t dr \tag{3.23}$$

Continuity Equation

An element in the wall of the cup will form a tangent line between the die and the punch profiles. It will be inclined by an angle (θ). So, the continuity equation is:

$$\left(R_{j-1}^2 - R_j^2\right) t_o = \left(r_{i,j-1}^2 - r_{i,j}^2\right) \left(\frac{t_{i,j-1} + t_{i,j}}{2 \cos \theta_i} \right) \tag{3.27}$$

3.3.5 Region V (Punch Profile)

In Fig. 3-7, the stresses acting on an element in the punch profile region are shown, which are similar to those on an element in the die profile region. The thickness stress (σ_t) acts normally on the inner surface of the element in contact with the punch profile. Thus, it induces a frictional stress ($\mu_{PP}\sigma_t$).

Equilibrium Equation

Similar to the equilibrium equation in region III which is based on the static equilibrium of forces in the horizontal and vertical directions, the equation for equilibrium of forces is given by:

$$d(\sigma_r t) = \frac{\rho_p^{'}}{r_f + \rho_p^{'} \sin \phi} \left[\sigma_\theta t (\cos \phi + \mu_{PP} \sin \phi) - \sigma_r t \cos \phi \right] d\phi + \mu_{PP} \sigma_r t$$

Where, $\rho_p^{'} = \rho_p + \frac{t}{2}$

This can be written as:

$$(\sigma_r t)_{i,j} = (\sigma_r t)_{i,j-1} + \int_{\phi_{i,j-1}}^{\phi_{i,j}} \left[\sigma_\theta t (\cos \phi + \mu_{PP} \sin \phi) - \sigma_r t \cos \phi \right] \frac{\rho_p^{'}}{r_f + \rho_p^{'} \sin \phi} d\phi + \int_{\phi_{i,j-1}}^{\phi_{i,j}} \mu_{PP} \sigma_r t d\phi \tag{3.28}$$

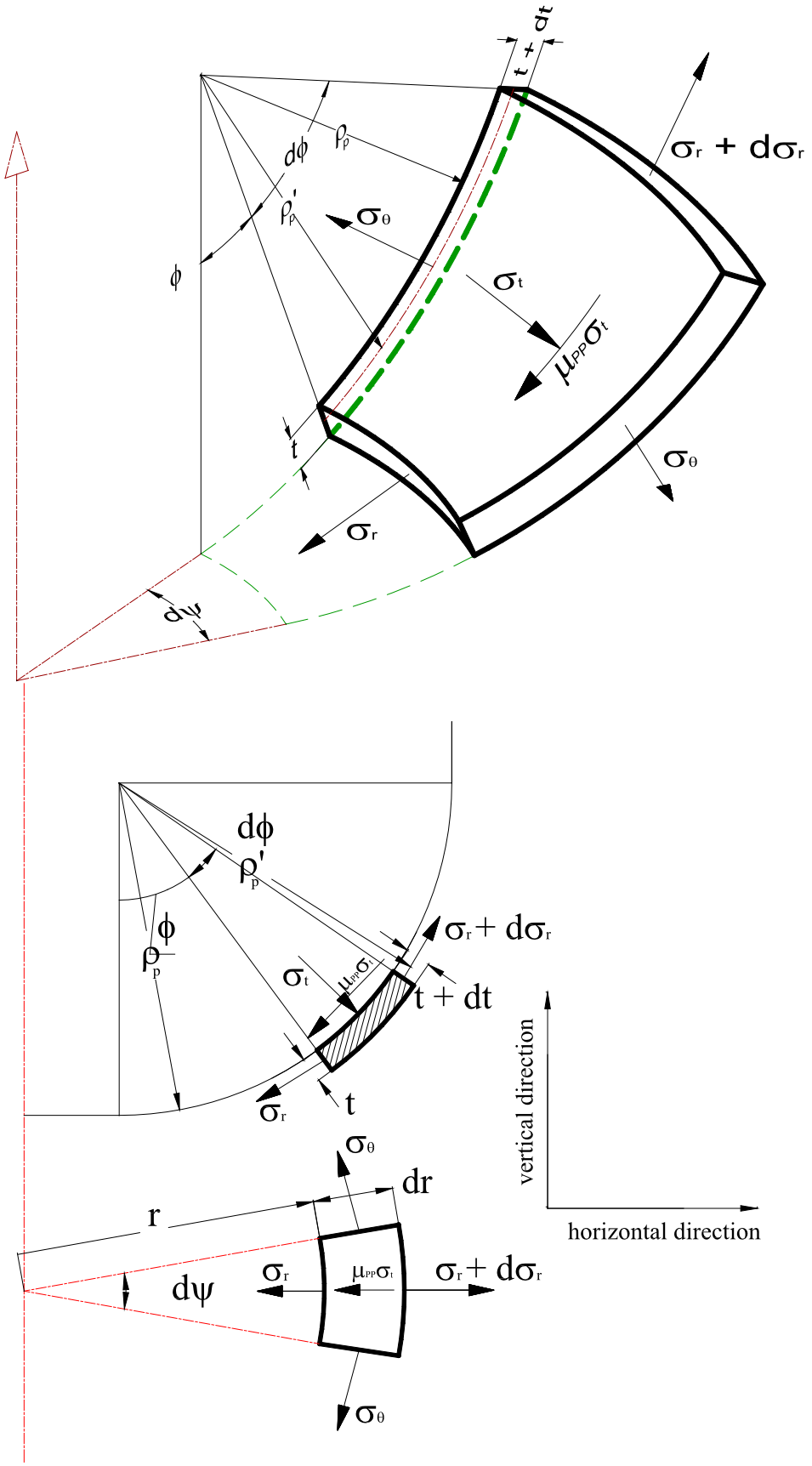

Fig. 3-7: Stresses in a slab element in region V

Continuity Equation

This equation is similar to that of region III

$$\left(R_{j-1}^2 - R_j^2\right)t_o = 2(\rho_p^{'})^2\left[\frac{r_f}{\rho_p^{'}}\left(\phi_{i,j-1} - \phi_{i,j}\right) - \left(\cos\phi_{i,j-1} - \cos\phi_{i,j}\right)\right]\left(\frac{t_{i,j-1} + t_{i,j}}{2}\right) \tag{3.29}$$

3.3.6 Region VI (Flat Bottom below punch)

This region has the same state of stress as region II as shown in Fig. 3-4.

Equilibrium Equation

Similar to region II:

$$\left(\sigma_r t\right)_{i,j} = \left(\sigma_r t\right)_{i,j-1} + \int_{r_{i,j-1}}^{r_{i,j}}\left(\frac{\sigma_\theta - \sigma_r}{r}\right)t dr \tag{3.23}$$

Continuity Equation

Similar to region II:

$$\left(R_{j-1}^2 - R_j^2\right)t_o = \left(r_{i,j-1}^2 - r_{i,j}^2\right)\frac{\left(t_{i,j-1} + t_{i,j}\right)}{2} \tag{3.24}$$

3.4 Boundary Conditions

As mentioned earlier in the introduction in chapter 1, the deforming sheet is divided into six regions where each region has different constitutive equations. The solution for stresses and strains starts from the blank rim and ends at the punch centerline. It is important when solving for each region to determine its boundary conditions to initiate the solution. The problem of the cylindrical cup has a total of seven boundaries; four of them are moving boundaries through stages of deformation, while the other three have fixed positions over stages. Moving boundaries are not known a priori and change from one stage to the other. The seven boundaries are shown in Fig. 3-8, and their status is given in Table 3-1.

Table 3-1: Status of boundaries between regions

Boundary	Label	Status
Sheet rim at radius r_a	(a)	Moving
Boundary between regions I and II at radius (r_b)	(b)	Moving
Boundary between regions II and IV at radius (r_c)	(c)	Fixed
Boundary between regions III and IV at radius (r_1)	(1)	Moving
Boundary between regions IV and V at radius (r_2)	(2)	Moving
Boundary between regions V and VI at radius (r_f)	(f)	Fixed
Centerline of the punch at zero radius	(g)	Fixed

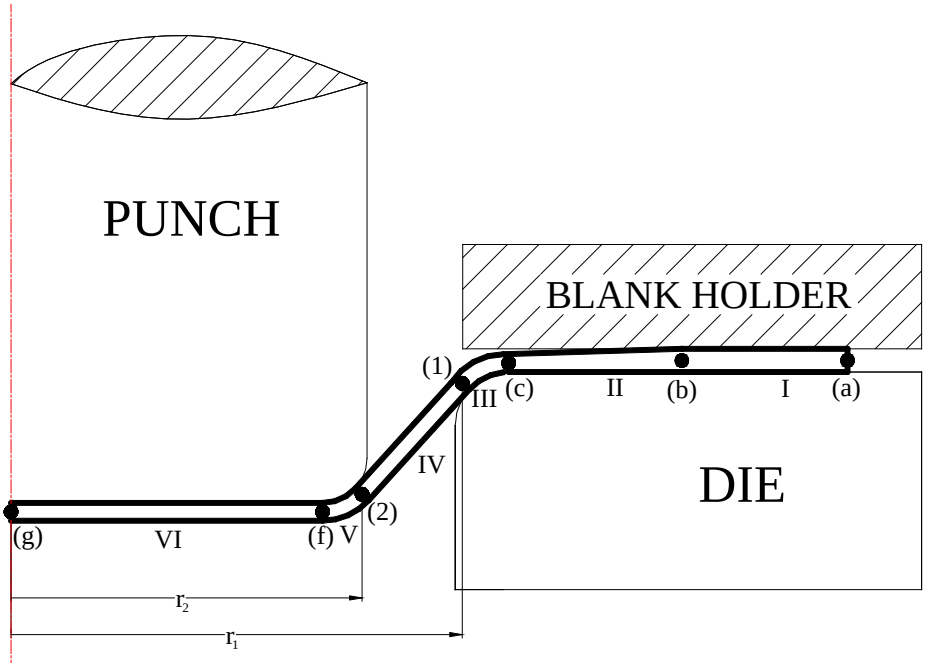

Fig. 3-8: Boundaries between the different regions

3.5 Numerical Solution

The solution of the deep-drawing problem using finite difference requires iterating through different variables until convergence. This is achieved by satisfying equilibrium and continuity equations as well as the stress-strain relations subject to the given flow equation and boundary conditions. Thus, it is possible to determine the stresses and strains at each point as well as radial displacement and thickness variation. Following is the solution procedure for each region of the deforming cup, which is based on the works of Woo [2] and Reissner and Ehrismann [8].

3.5.1 Region I (Flange in Contact with blank-holder)

Region I is slightly different in calculation than other regions since thickness (t_a) is assumed to be constant over the region under the load of the blank-holder. The solution procedure is as follows:

(1) It starts by assuming a value for t_a from which thickness strain $(\varepsilon_t)_{i,j}$ (equation (3.12)) can be calculated. Initial assumption for t_a is such that $(t_a)_i = (t_a)_{i-1}$. For i=1, $(t_a)_i = t_0$

(2) At the rim (j = 1), the following takes place:

a. $r_{i,1} = r_a$, which is the incrementing parameter for each stage of deformation. Each stage is incremented by a decrease in r_a by a value Δr.

Therefore, $r_{i,1} = r_{i-1,1} - \Delta r$

For i = 1, $r_{i,1} = R_1 - \Delta r$

b. Radial stress equals zero, $(\sigma_r)_{i,1} = 0$

(3) For other points in region I, from the continuity equation (3.22), the position of a point ($r_{i,j}$) is determined as follows:

$$r_{i,j} = \sqrt{r_{i,j-1}^2 - \left(R_{j-1}^2 - R_j^2\right)\frac{t_o}{(t_a)_i}} \tag{3.30}$$

(4) Knowing the radial position ($r_{i,j}$) of a point, circumferential strain $(\varepsilon_\theta)_{i,j}$ (equation (3.11)) can be calculated.

(5) Incremental plastic strains $(\Delta\varepsilon_\theta)_{i,j}$, $(\Delta\varepsilon_t)_{i,j}$, and $(\Delta\varepsilon_r)_{i,j}$ can then be calculated from equations (3.13), (3.14), and (3.15).

(6) Then, it is possible to calculate effective incremental strain and total effective strain from equations (3.16) and (3.17) successively. This allows for the calculation of the effective stress $\overline{\sigma}_{i,j}$ from the flow equation (3.18).

(7) The differences of stresses $[(\sigma_\theta)_{i,j} - (\sigma_r)_{i,j}]$ and $[(\sigma_t)_{i,j} - (\sigma_r)_{i,j}]$ are determined from equations (3.19) and (3.20).

(8) These two difference values are used in the calculation of the equilibrium equation (3.21) which is numerically integrated using the trapezoidal rule as follows (see Appendix A1 for the derivation):

$$(\sigma_r)_{i,j} = \frac{1}{1-\frac{\mu_{BH}}{t_a}\left(r_{i,j}-r_{i,j-1}\right)}\left[(\sigma_r)_{i,j-1}\left(1+\frac{\mu_{BH}}{t_a}\left(r_{i,j}-r_{i,j-1}\right)\right)\right.$$
$$\left.+\left\{\frac{1}{2}\left(\left(\frac{\sigma_\theta-\sigma_r}{r}\right)_{i,j}+\left(\frac{\sigma_\theta-\sigma_r}{r}\right)_{i,j-1}\right)+\frac{\mu_{BH}}{t_a}\left((\sigma_t-\sigma_r)_{i,j}+(\sigma_t-\sigma_r)_{i,j-1}\right)\right\}\left(r_{i,j}-r_{i,j-1}\right)\right] \quad (3.31)$$

(9) Calculation marches from one point (*j-1*) to the next point (*j*) until one of the following conditions occur:

- The value of the thickness stress $(\sigma_t)_{i,j} \geq 0$
- The radial position $r_{i,j} < r_c$, which occurs in the final stages of deformation when the blank holder is pressing on the whole flange and thus region II disappears

At this instant, a check is performed to satisfy equilibrium condition between the normal forces in all elements in region I and the applied blank-holder force. That is:

$$\sum_{ra}^{rb} \sigma_t \, 2\pi \, r_m \Delta r^* \approx F_{BH} \quad (3.32)$$

Where, Δr^* = difference between radial position of two points = $r_{i,j-1} - r_{i,j}$

r_m = average radial position of two points = $\frac{r_{i,j-1}+r_{i,j}}{2}$

(10) If this condition is not satisfied, calculations are repeated again from step (1) to step (9) with a new value for t_a. Iterations on t_a are carried out until equation (3.32) is satisfied. At this instance, calculations with region I are terminated. The iterations on t_a are performed as a minimization problem for a function in one variable (t_a), where the function to be minimized is:

$$F_{error} = \left| \sum_{ra}^{rb} \sigma_t \, 2\pi \, r_m \Delta r^* - F_{BH} \right| \quad (3.33)$$

In other words, the search for the minimum of equation (3.33) is performed through varying the value of t_a. One-dimensional search methods including bisection, secant, and quadratic interpolation methods are used for this minimization objective [55].

(11) To start region II, it is required to determine the stresses and strains at boundary (b) at radius r_b. The position of this boundary point is unknown *a priori* since it is a moving boundary. So, a first guess for r_b is taken to be equal to the last point in region I. In other words, $(r_b)_i = r_{i,j-1}$ as shown in Fig. 3-9.

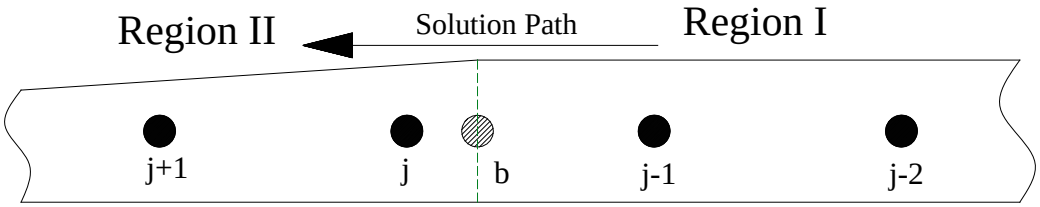

Fig. 3-9: The moving boundary (b) between regions I and II

The initial radial position of point b (R_b) is also unknown. However, by assuming a value for $(r_b)_i$, it can be determined from the continuity equation (3.22) as follows:

$$R_b = \sqrt{R_{j-1}^2 - \left(r_{i,j-1}^2 - r_{i,j}^2\right)\frac{(t_a)_i}{t_o}} \tag{3.34}$$

Solution for point b is carried out similar to the search procedure in step (10) by searching for the value of r_b that gives a thickness stress $(\sigma_t)_b$ value that is nearly equal to zero. Then, stresses and strains are calculated for this point to start the next region calculations.

3.5.2 Regions II to V (From radius r_b to punch centerline)

Stresses and strains in region VI (Flat bottom of punch) are assumed to be constant over all the points in the region [9]. Thus, there is no need to carry out the calculations for region VI. Instead, stresses and strains at this region are taken to be equal to those at the boundary point (f) at radius r_f, which are obtained by the termination of region V calculations. So, the finite difference solution is only carried out from region I until region V.

The calculations procedure for regions II to V is similar. However, there is a difference in the equilibrium and continuity equations used at each region. The main calculation procedure is discussed below with reference to any differences in calculations from one region to the other whenever required.

For any point in the region under consideration, the following steps are followed.

(1) The thickness of a point j is assumed to be equal to the thickness of the previous point, i.e. $t_{i,j} = t_{i,j-1}$ as a first approximation. In case of the first point in the region, $t_{i,j}$ is assumed to be equal to the boundary point between the current region and the previous region.

(2) The radial position ($r_{i,j}$) of the current point is obtained from the continuity equation, which differs according to the region under consideration as follows.

Current Radial Position for Region II

From equation (3.24):

$$r_{i,j} = \sqrt{r_{i,j-1}^2 - 2t_o\left(\frac{R_{j-1}^2 - R_j^2}{t_{i,j-1} + t_{i,j}}\right)} \tag{3.35}$$

Current Radial Positions for Regions III and V

The following procedure is used to calculate the current radial position ($r_{i,j}$):

(a) Equation (3.26) for **region III** can be written as:

$$c_1\left(\phi_{i,j} - \phi_{i,j-1}\right) + \left(\cos\phi_{i,j} - \cos\phi_{i,j-1}\right) - c_2 = 0$$

Where, $c_1 = \frac{r_c}{\rho_d^{'}}$, $c_2 = \frac{\left(R_{j-1}^2 - R_j^2\right)t_o}{(\rho_d^{'})^2\left(t_{i,j-1} + t_{i,j}\right)}$

While for **region V**, equation (3.29) can be written as:

$$c_3\left(\phi_{i,j-1} - \phi_{i,j}\right) - \left(\cos\phi_{i,j-1} - \cos\phi_{i,j}\right) - c_4 = 0$$

Where, $c_3 = \frac{r_f}{\rho_p^{'}}$, $c_4 = \frac{\left(R_{j-1}^2 - R_j^2\right)t_o}{(\rho_p^{'})^2\left(t_{i,j-1} + t_{i,j}\right)}$

(b) As a first approximation,

For **region III:** $\phi_{i,j} = \phi_{i,j-1} + \frac{c_2}{c_1}$

For **region V :** $\phi_{i,j} = \phi_{i,j-1} - \frac{c_4}{c_3}$

(c) Then, using Newton's Raphson root locating formula [55], a new value $\phi_{i,j}^{'}$ can be calculated as:

For **region III:**

$$\phi'_{i,j} = \phi_{i,j} - \frac{c_1\left(\phi_{i,j} - \phi_{i,j-1}\right) + \left(\cos\phi_{i,j} - \cos_{i,j-1}\right) - c_2}{c_1 - \sin\phi_{i,j}} \tag{3.36}$$

For **region V:**

$$\phi'_{i,j} = \phi_{i,j} - \frac{c_3\left(\phi_{i,j-1} - \phi_{i,j}\right) - \left(\cos\phi_{i,j-1} - \cos_{i,j}\right) - c_4}{-c_3 - \sin\phi_{i,j}} \tag{3.37}$$

(d) A check is carried out using the following error function

$$\phi_{error} = \left|\frac{\phi'_{i,j} - \phi_{i,j}}{\phi'_{i,j}}\right| \times 100 \tag{3.38}$$

If $\phi_{error} > 0.01$, a new value for $\phi'_{i,j}$ is calculated using equation (3.36) or (3.37) where $\phi_{i,j}$ is replaced with $\phi'_{i,j}$. Iterations continue until $\phi_{error} < 0.01$.

(e) Then, the radial position of a point in **region III** is**:**

$$r_{i,j} = r_c - \rho'_d \sin\phi_{i,j} \tag{3.39}$$

While for **region V:**

$$r_{i,j} = r_f + \rho'_p \sin\phi_{i,j} \tag{3.40}$$

<u>Current Radial Position for Region IV</u>

From equation (3.27),

$$r_{i,j} = \sqrt{r_{i,j-1}^2 - 2t_o \cos\theta_i \frac{\left(R_{j-1}^2 - R_j^2\right)}{\left(t_{i,j-1} + t_{i,j}\right)}} \tag{3.41}$$

(3) Incremental strains, effective incremental strain, effective strain, and effective stress are calculated the same way as in region I, using equations (3.13) to (3.18).

(4) $[(\sigma_\theta)_{i,j} - (\sigma_r)_{i,j}]$ is calculated from equation (3.19).

(5) Thickness stress (σ_t) in regions II to VI is assumed to be equal zero. Therefore, σ_t is eliminated from equation (3.20) from which $(\sigma_r)_{i,j}$ can be calculated. The unit radial force for the point under consideration is determined by multiplying $(\sigma_r)_{i,j}$ obtained from equation (3.20) by the assumed $t_{i,j}$ from step (1), which gives $(\sigma_r t)_{i,j}$.

(6) Another value for the unit radial force, $(\sigma_r t)'_{i,j}$, is calculated from the equilibrium equation of the region under consideration, which is solved numerically using the trapezoidal rule as follows:

Equilibrium Equation for Regions II and IV

Equation (3.23) is solved as:

$$(\sigma_r t)'_{i,j} = (\sigma_r t)_{i,j-1} + \frac{1}{2}\left[\left(\left(\frac{\sigma_\theta - \sigma_r}{r}\right)t\right)_{i,j} + \left(\left(\frac{\sigma_\theta - \sigma_r}{t}\right)t\right)_{i,j-1}\right]\left(r_{i,j} - r_{i,j-1}\right) \tag{3.42}$$

Equilibrium Equation for Region III

Equation (3.25) is solved as:

$$\begin{aligned}(\sigma_r t)'_{i,j} = {} & (\sigma_r t)_{i,j-1} \\ & - \frac{\phi_{i,j} - \phi_{i,j-1}}{2}\left[\left(\left[\sigma_\theta t(\cos\phi + \mu_{DP}\sin\phi) - \sigma_r t\cos\phi\right]\frac{\rho'_d}{r_c - \rho'_d\sin\phi} - \mu_{DP}\sigma_r t\right)_{i,j}\right. \\ & \left. + \left(\left[\sigma_\theta t(\cos\phi + \mu_{DP}\sin\phi) - \sigma_r t\cos\phi\right]\frac{\rho'_d}{r_c - \rho'_d\sin\phi} - \mu_{DP}\sigma_r t\right)_{i,j-1}\right]\end{aligned} \tag{3.43}$$

Equilibrium Equation for Region V

Equation (3.28) is solved as:

$$\begin{aligned}(\sigma_r t)'_{i,j} = {} & (\sigma_r t)_{i,j-1} \\ & + \frac{\phi_{i,j} - \phi_{i,j-1}}{2}\left[\left(\left[\sigma_\theta t(\cos\phi + \mu_{PP}\sin\phi) - \sigma_r t\cos\phi\right]\frac{\rho'_p}{r_f + \rho'_p\sin\phi} + \mu_{PP}\sigma_r t\right)_{i,j}\right. \\ & \left. + \left(\left[\sigma_\theta t(\cos\phi + \mu_{PP}\sin\phi) - \sigma_r t\cos\phi\right]\frac{\rho'_p}{r_f + \rho'_p\sin\phi} + \mu_{PP}\sigma_r t\right)_{i,j-1}\right]\end{aligned} \tag{3.44}$$

(7) The value $(\sigma_r t)'_{i,j}$ obtained using the equilibrium equation and the value $(\sigma_r t)_{i,j}$ calculated from the stress-strain relations are compared using the following error function.

$$t_{error} = \left|\frac{(\sigma_r t)'_{i,j} - (\sigma_r t)_{i,j}}{(\sigma_r t)'_{i,j}}\right| \times 100 \tag{3.45}$$

(8) If the error function is greater than 0.01, calculations are repeated from step (2) to step (7) with a new value for the current point thickness ($t'_{i,j}$), which is calculated as follows.

(a) Equation (3.20) is multiplied by the current thickness ($t_{i,j}$), which gives:

$$(\sigma_r t)_{i,j} = -\frac{2}{3}\frac{(\overline{\sigma})_{i,j}}{(\Delta\overline{\varepsilon})_{i,j}}\left(2(\Delta\varepsilon_t)_{i,j} + (\Delta\varepsilon_\theta)_{i,j}\right) t_{i,j}$$

From which:

$$\Delta(\varepsilon_t)_{i,j} = -\frac{1}{2}\left[\frac{3}{2}\left(\frac{\Delta\overline{\varepsilon}}{\overline{\sigma}}\frac{\sigma_r t}{t}\right)_{i,j} + \Delta(\varepsilon_\theta)_{i,j}\right] \tag{a}$$

(b) Then, substituting the value $(\sigma_r t)'_{i,j}$ instead of $(\sigma_r t)_{i,j}$ in equation (a), a new value $\Delta(\varepsilon_t)'_{i,j}$ is obtained, where

$$\Delta(\varepsilon_t)'_{i,j} = -\frac{1}{2}\left[\frac{3}{2}\left(\frac{\Delta\overline{\varepsilon}}{\overline{\sigma}}\frac{(\sigma_r t)'}{t}\right)_{i,j} + \Delta(\varepsilon_\theta)_{i,j}\right] = (\varepsilon_t)'_{i,j} - (\varepsilon_t)_{i-1,j} \tag{3.46}$$

(c) From which,

$$(\varepsilon_t)'_{i,j} = \Delta(\varepsilon_t)'_{i,j} + (\varepsilon_t)_{i-1,j}$$

(d) This gives the new value for the current point thickness, which is used for the next iteration, which is:

$$t'_{i,j} = t_o e^{(\varepsilon_t)'_{i,j}} \tag{3.47}$$

(9) After obtaining a converged value (less than 0.01) for the error function (3.35), calculations continue from one point to the next through the current region. Then, calculations for the current region are terminated when the following region limit end condition is met (depending on the region under consideration):

Region II: the radial position of the current point ($r_{i,j}$) is less than r_c, which is shown in Fig. 3-10.

Region III: the angular position of the current point ($\phi_{i,j}$) is greater than θ_i, where θ_i is the angle of contact between the sheet metal and die profile. The determination of θ_i will be discussed in the next section. This region limit end situation is demonstrated in Fig. 3-11.

Region IV: the radial position of the current point ($r_{i,j}$) is less than r_2, where r_2 is the radial position of boundary (2). The determination of r_2 will be discussed in the next section. This region limit end situation is shown in Fig. 3-12.

Region V: the angular position of the current point ($\phi_{i,j}$) is less than or equal zero, which is shown in Fig. 3-13.

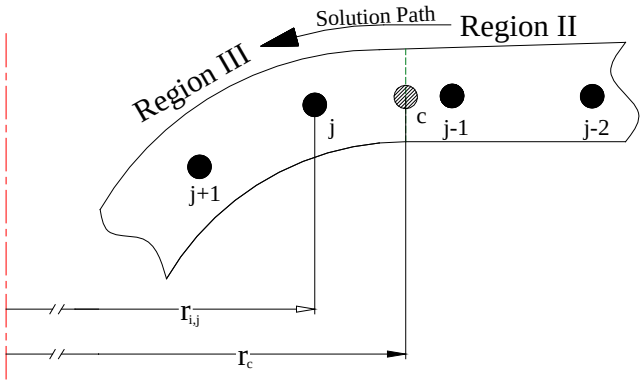

Fig. 3-10: The fixed boundary (c) between regions II and III

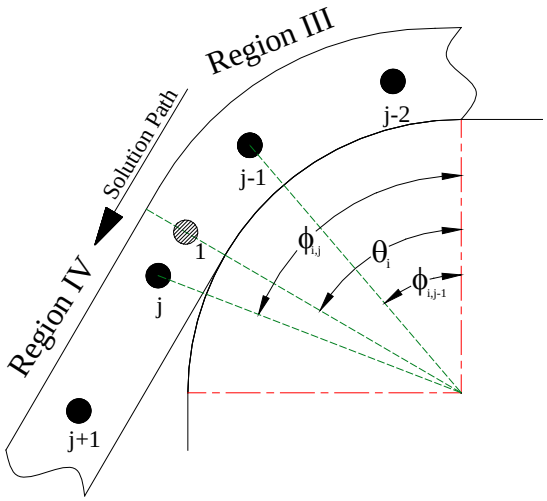

Fig. 3-11: The moving boundary (1) between regions III and IV

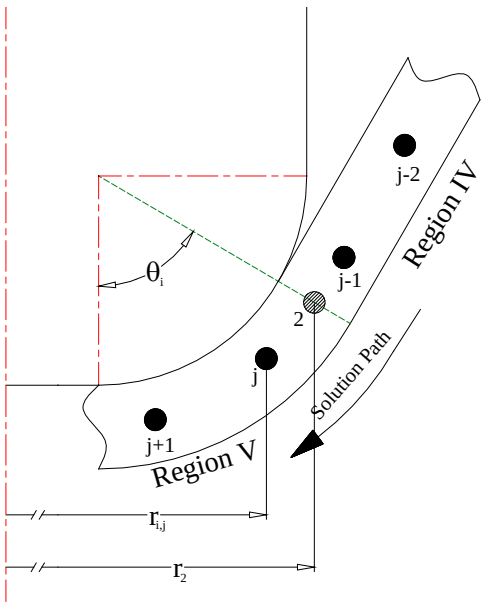

Fig. 3-12: The moving boundary (2) between regions IV and V

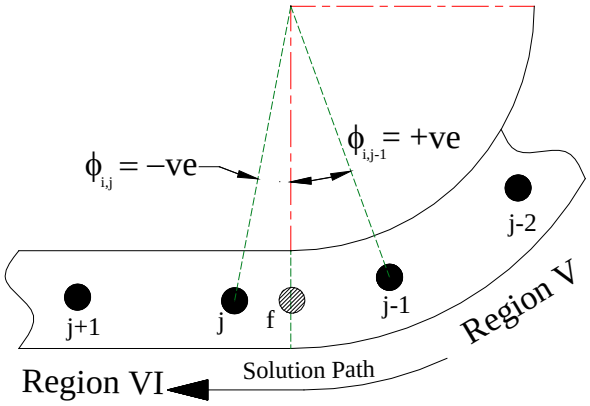

Fig. 3-13: The fixed boundary (f) between regions V and VI

(10) In order to start the next region calculations, the stresses and strains at the boundary point that separates the current region from the next region must be calculated. The current radial positions of the boundary points are known, namely $(r_c)_i$, $(r_1)_i$, $(r_2)_i$, and $(r_f)_i$. However, their initial radial positions $(R_c)_i$, $(R_1)_i$, $(R_2)_i$, and $(R_f)_i$ are unknown *a priori*. So, the continuity equation of each region is used to determine these initial radial positions.

Initial Radial Position for Boundary (c)

From equation (3.24),

$$(R_c)_i = \sqrt{R_{j-1}^2 - \left(r_{i,j-1}^2 - r_c^2\right)\left(\frac{t_{i,j-1} + (t_c)_i}{2t_o}\right)} \tag{3.48}$$

Where, $(t_c)_i$ = thickness at boundary (c) at stage *i*

Initial Radial Position for Boundary (1)

From equation (3.26),

$$(R_1)_i = \sqrt{R_{j-1}^2 - (\rho_d')^2\left[\frac{r_c}{\rho_d'}\left(\theta_i - \phi_{i,j-1}\right) + \left(\cos\theta_i - \cos\phi_{i,j-1}\right)\right]\left(\frac{(t_1)_i + t_{i,j-1}}{t_o}\right)} \tag{3.49}$$

Where, $(t_1)_i$ = thickness at boundary (1) at stage *i*

Initial Radial Position for Boundary (2)

From equation (3.27),

$$(R_2)_i = \sqrt{R_{j-1}^2 - \left(r_{i,j-1}^2 - (r_2)_i^2\right)\left(\frac{t_{i,j-1} + (t_2)_i}{2t_o\cos\theta_i}\right)} \tag{3.50}$$

Where, $(t_2)_i$ = thickness at boundary (2) at stage i

Initial Radial Position for Boundary (f)

At this boundary, $(\phi_f)_i$ = angle of contact between the current sheet point and punch profile = 0 So, from equation (3.29),

$$(R_f)_i = \sqrt{R_{j-1}^2 - (\rho_p')^2 \left[\frac{r_f}{\rho_p'} \phi_{i,j-1} - \cos\phi_{i,j-1} \right] \left(\frac{t_{i,j-1} + (t_f)_i}{t_o} \right)} \tag{3.51}$$

Where, $(t_f)_i$ = thickness at boundary (f) at stage *i*

(11) Once the initial radial position for the boundary point is calculated, same procedure from step (3) to step (7) is used to calculate stresses and strains at the boundary point. Then, the calculations for the current region are terminated when the error function (3.45) is less than or equal 0.01 for the current boundary point.

3.6 Determination of the Moving Boundaries

The Numerical solution presented in the previous section discussed the calculations of stresses and strains at each point in the different regions. Among the four moving boundaries, only two are determined in the numerical solution of region I (section 3.5.1), namely boundaries (a) and (b). The position of the moving boundary (a) at the sheet rim is known. It is determined from the incrementing parameter (Δr) at each stage, where $(r_a)_i = (r_a)_{i-1} - \Delta r$. The second moving boundary (b) is determined when the calculations for region I are accomplished and equation (3.32) is satisfied. However, the other two moving boundaries (1) and (2) are unknown *a priori*. Moving boundary (1) is important to determine the position at which calculations in region III end and those in region IV start. Also, moving boundary (2) determines the point at which calculations in region IV ends and those in region V start. The radial positions $(r_1)_i$ and $(r_2)_i$ of the moving boundaries (1) and (2) can be determined by knowing the value of the contact angle θ which is shown in Fig. 3-14. Since, the cup wall is straight, it forms a tangent line between the die and punch profiles. Thus, the angle of contact between the sheet metal and the die profile or the punch profile has the same value θ.

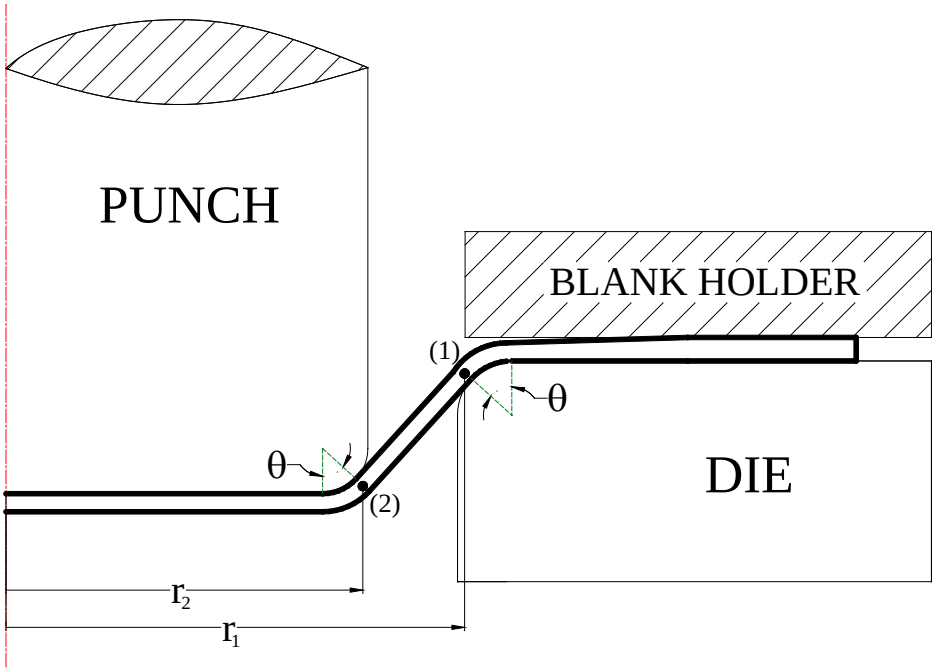

Fig. 3-14: Contact angle θ that determines the position of moving boundaries (1) and (2)

For a given value of θ_i, the radial positions for the two unknown boundaries can be determined with the following equations:

$$(r_1)_i = r_c - (t_1)_i \sin(\theta_i) \tag{3.52}$$

Where, t_1= thickness of point at radius r_1

$$(r_2)_i = r_f + (t_2)_i \sin(\theta_i) \tag{3.53}$$

Where, t_2= thickness of point at radius r_2

However, there is no straightforward method for the determination of the contact angle θ [1], [2], [5], and [7]. Several investigations were carried out to develop a technique for the correct determination of the contact angle θ. This was found to be very crucial on the accuracy and convergence of the results for regions IV to VI.

In the present study, a new technique is developed for the determination of the contact angle θ at each stage of deformation. This technique follows a prediction/correction strategy. In the prediction stage, a modification of Swift's approach [1] is adopted to obtain an approximate guess of the angle θ. Then, an optimization search method is adopted to determine a corrected (improved) value of the angle θ.

3.6.1 Determination of the Contact Angle θ

Step 1: Prediction

Fig. 3-15 shows the geometry of the deforming cup at various stages. Three unknowns are encountered, namely θ, T, and H. These unknowns can be determined by the simultaneous solution of the following three nonlinear equations (see Appendix A2 for details).

$$t_W \cos(\theta)T^2 + 2t_W[r_f + \rho_p^{'} \sin(\theta)]T + [2\rho_p^{'} t_P r_f + 2r_d \rho_d^{'} t_D + 2\rho_d \rho_d^{'} t_D]\theta$$
$$-[2\rho_p^{'2} t_P - 2\rho_d^{'2} t_D]\cos(\theta) - R_a^2 t_0 + r_f^2 t_B + 2\rho_p^{'2} t_P - 2\rho_d^{'2} t_D + [r_b^2 - r_c^2]t_F$$
$$+[r_a^2 - r_b^2]t_a = 0 \tag{3.54}$$

$$H^2 - [2N\cos(\theta)]H + [K^2 + N^2 - 2NK\sin(\theta) - T^2] = 0 \tag{3.55}$$

$$\theta = \frac{1}{2}\pi - \left[\tan^{-1}\left(\frac{H}{K}\right) + \tan^{-1}\left(\frac{T}{N}\right)\right] \tag{3.56}$$

Where,

t_F = Mean thickness of the deformed sheet in region II

t_D = Mean thickness of the deformed sheet in region III

t_W = Mean thickness of the deformed sheet in region IV

t_P = Mean thickness of the deformed sheet in region V

t_B = Mean thickness of the deformed sheet in region VI

T = length of the sheet centerline tangent between the die and the punch profiles

H = Vertical distance between the die profile center and the punch profile center

N = Distance between the die profile center and the punch profile center normal to the tangent line (T)

K = Horizontal distance between the die profile center and the punch profile center

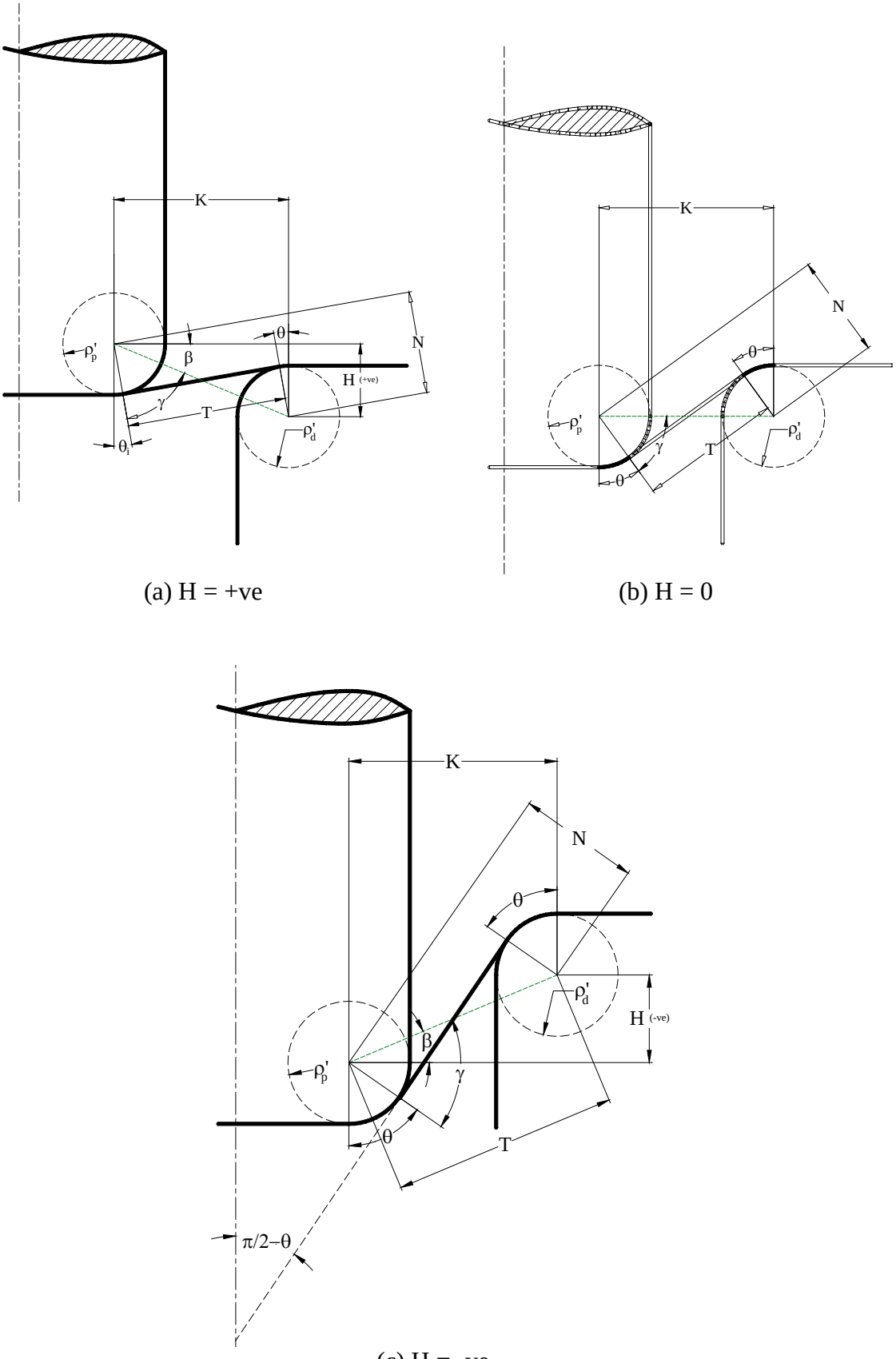

(a) H = +ve

(b) H = 0

(c) H = -ve

Fig. 3-15: Geometrical relations in deep drawing at various stages of deformation

Calculations on these three equations start after the termination of region II calculations in the following manner.

(1) Start by assuming values for θ and the regions mean thicknesses t_F, t_D, t_W, t_P, and t_B to be equal to those of the previous stage. For the case of *i=1*, assume θ is equal to zero and the mean thicknesses are equal to the sheet initial thickness.
(2) Equation (3.54) is solved for the tangent length (T).
(3) The obtained T is substituted into equation (3.55), where H can be obtained.
(4) Then, by having T and H equation (3.56) is solved for a new value of θ denoted by θ_{new}.
(5) An error function is checked for convergence of θ, which is given by:

$$\theta_{error} = \left| \frac{\theta - \theta_{new}}{\theta_{new}} \right| \times 100 \tag{3.57}$$

If equation (3.57) gives a value greater than 0.01, calculations are repeated from step (2) to step (5) with $\theta = \theta_{new}$. Else, calculations on θ are terminated.

The value of θ obtained from these equations is an approximate value since the average volume at each region is used. The finite difference solution marches from region I to region V by satisfying equilibrium and continuity conditions for each point in the deforming sheet. As will be shown in chapter 5, if a value in one point is inaccurate, error will accumulate over subsequent points. Since, the value of θ calculated is considered approximate, error accumulates starting from region IV at moving boundary (1) until end of region V at boundary (f) and over the number of stages of solution. So, a slight change in θ deviates the solution from the start of region IV until it reaches its maximum deviation below the punch at region VI. The effect of change in θ on the thickness strain and radial stress is shown in Fig. 3-16 and Fig. 3-17 respectively. The shown distribution is for the first stage of deformation at a punch travel of 5mm for the cup described in section 3.9.2.

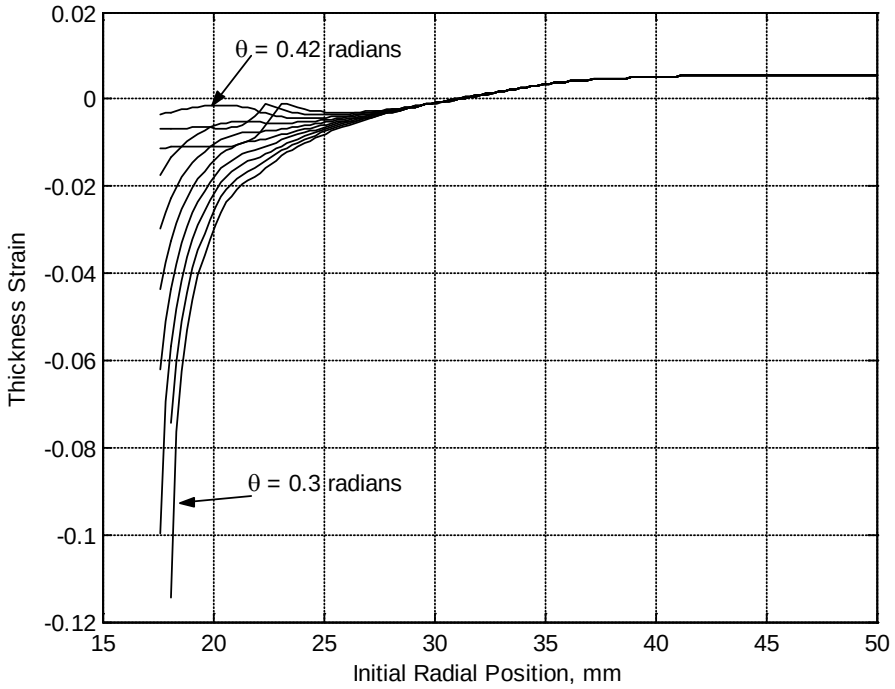

Fig. 3-16: Thickness strain distribution for different values of θ

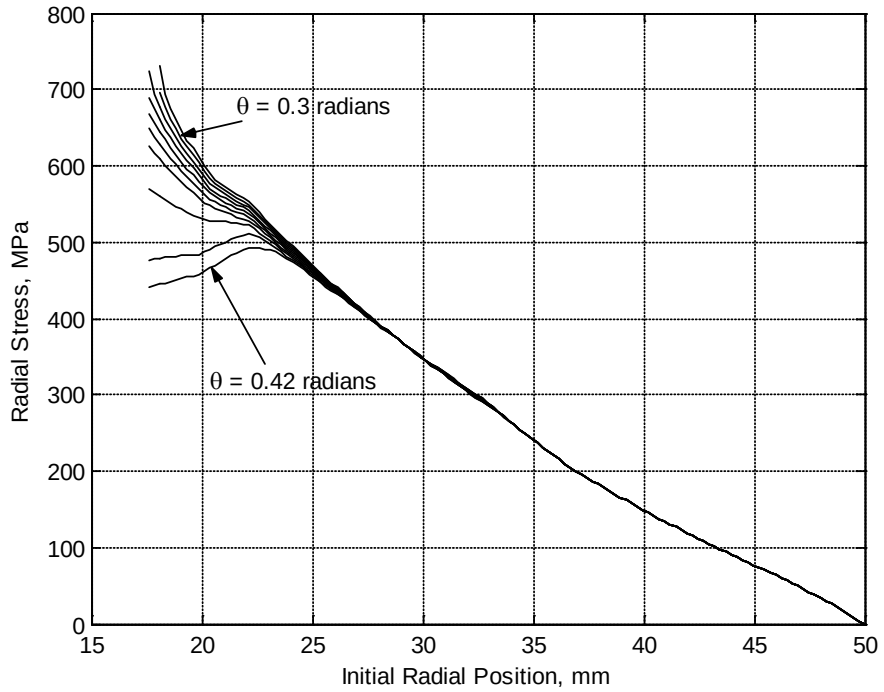

Fig. 3-17: Radial stress distribution for different values of θ

Step 2: Correction

The experimental analysis carried out on the cup drawing process shows that circumferential and radial strains are usually equal at the punch bottom [1], [24], and [43]. The analytical solution developed by Woo [4] suggested that for certain moving boundaries (1) and (2) locations, the monotonic solution from rim to boundary (f) is satisfactory if it gives $(\varepsilon_\theta = \varepsilon_r)_f$ at boundary (f). In the present study, the solution for $(\varepsilon_\theta = \varepsilon_r)_f$ is formulated as a minimization problem which searches for the angle θ that minimizes $(\varepsilon_\theta - \varepsilon_r)_f$. Therefore, once the initial guess of the contact angle θ is calculated from the prediction step, the following objective function is minimized by varying the value of θ:

$$\Delta\varepsilon_f = (\varepsilon_\theta - \varepsilon_r)_f \tag{3.58}$$

At each new search value for θ, evaluation of stresses and strains are performed for regions III to V to determine the value of the strains at radius r_f to satisfy equation (3.58). One-dimensional search methods and Nelder-Mead local search method are used interchangeably in this problem, which terminates the search at a function tolerance of $1x10^{-6}$. First, one-dimensional search methods are used for the minimization. If no solution is obtained using the one-dimensional search methods, Nelder-Mead method is used, which is a multivariable search method. It is based on evaluating the objective function at the vertices of a geometric figure called "simplex". Then, it iteratively shrinks the simplex as better points are found until the desired function tolerance is obtained [56]. This solution approach for the determination of the contact angle was applied to several cups and was found to be successful for solving over all stages until a complete cup is formed.

3.7 Punch Force and Travel Calculation

The variation of the punch force during the deep drawing process is important in predicting the amount of stresses in the deforming sheet. Thus, for larger punch force values, more stresses are induced into the sheet. The usual representation of the punch force is through determining its variation with the punch travel. Following is the calculations of the punch force and punch travel in the cup drawing process.

3.7.1 Punch Force

The radial (meridional) force (F_r) acting on the wall of the cup at stage *i* is shown in Fig. 3-18, and is given by:

$$\left(F_r\right)_i = 2\pi\left[r_1 t_1 (\sigma_r)_1\right]_i$$

Where, the subscript (1) indicates values at radius r_1 at boundary (1)

Resolving this radial force in the vertical direction, the punch force $(F_p)_i$ at stage *i* can be obtained as:

$$\left(F_P\right)_i = 2\pi\left[r_1 t_1 (\sigma_r)_1 \sin\theta\right]_i \tag{3.59}$$

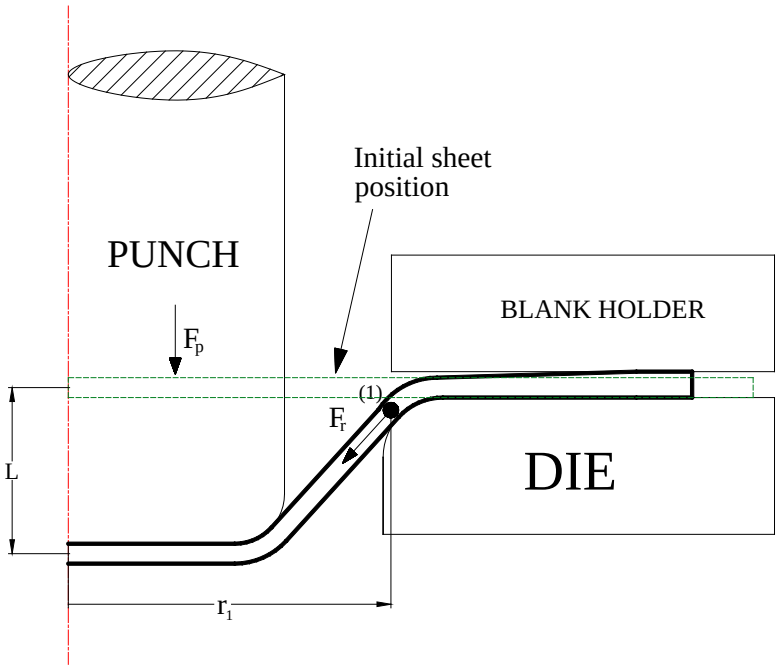

Fig. 3-18: Punch force and punch travel in deep drawing

3.7.2 Punch Travel

The punch travel (L_i) at any stage *i* can be determined from [3] (see Fig. 3-18):

$$L_i = \left[\rho_d^{'}(1-\cos\theta) + (r_1 - r_2)\tan\theta + \rho_p^{'}(1-\cos\theta)\right]_i \tag{3.60}$$

Where, $\left(\rho_d^{'}\right)_i$ is calculated at boundary (1) = $\rho_d + \dfrac{(t_1)_i}{2}$

$\left(\rho_p^{'}\right)_i$ is calculated at boundary (2) = $\rho_p + \dfrac{(t_2)_i}{2}$

3.8 The Computer Code for the Analysis of the Cup Drawing Process

A computer code is developed and run using MATLAB 6.5 to analyze the cup drawing process based on the process theory and numerical solution discussed in the previous sections. The developed model computer code is made up of a main program called "Cup" that interacts with other sub-functions. Each sub-function is built to perform a different operation. The interaction of these sub-functions with the main program is shown in the block diagram in Fig. 3-19.

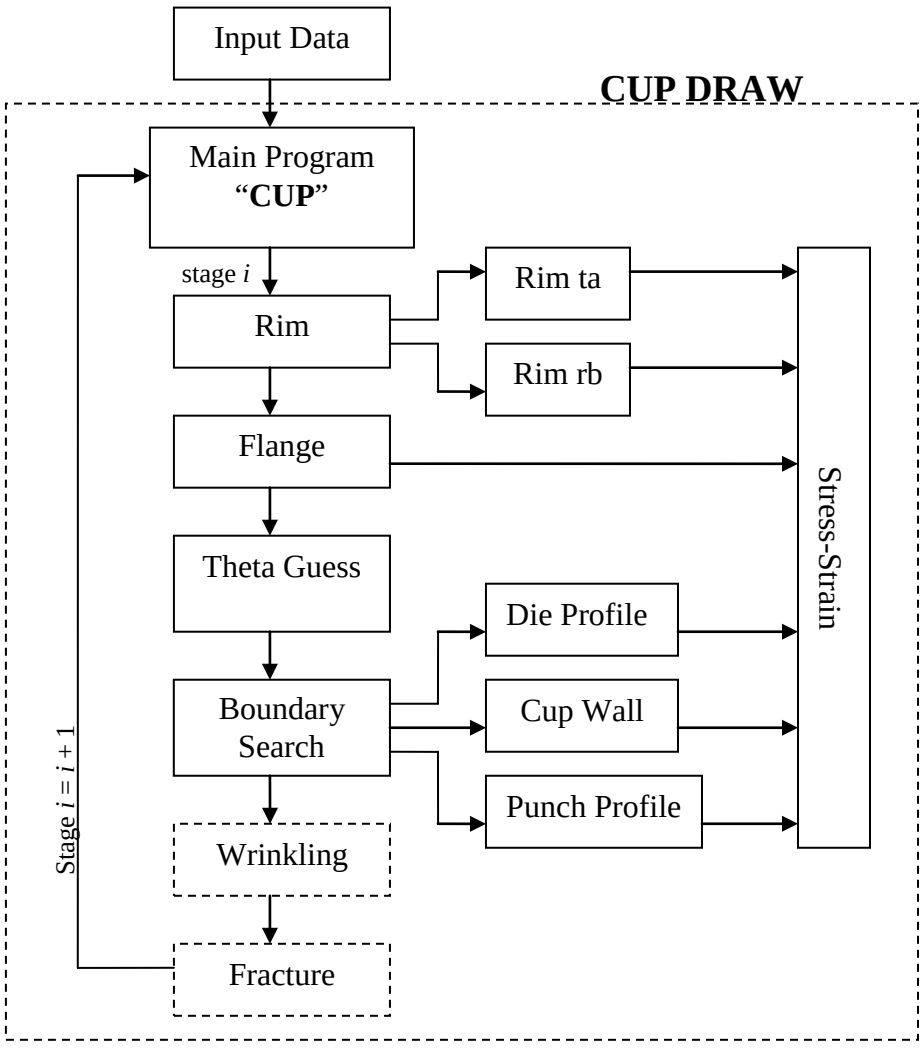

Fig. 3-19: Block diagram of the main program and sub-functions in cup drawing process

Each block represents a sub-function with its name written inside it. The arrows represent the flow of calculations in the program. The main program "*CUP*"

controls the flow of data to and from the sub-functions. The procedure starts with calling the *Input Data* sub-function, which contains data necessary for the analysis. *Input data* includes the cup geometry, sheet metal blank material properties, loading conditions, and finite difference discretization. Then, *CUP* starts the calculations for region I by calling the sub-function *Rim*, which calls two other subfunctions *Rim ta*, and *Rim rb*. *Rim ta* calculates the stresses and strains in region I, then *Rim rb* determines the position of the moving boundary (2) at radius r_b. Once calculations for region I are terminated, *CUP* calls the sub-function *Flange* to proceed with region II calculations.

After the termination of the calculations in region II, the sub-function *Theta Guess* is called to calculate an initial guess (prediction) for the contact angle θ as discussed in section 3.6.1. Once, a guess for θ is obtained, the angle θ correction step is perform by calling the *Boundary Search* sub-function. Then, *Boundary Search* calls other sub-functions, namely *Die Profile, Cup Wall*, and *Punch Profile* to perform the stresses and strains calculations in regions III, IV, and V respectively in order to determine the value of $(\varepsilon_\theta - \varepsilon_r)_f$ as given by equation (3.58). The sub-function *Stress-Strain* is called by *Rim ta, Rim rb, Flange, Die Profile, Cup Wall*, and *Punch Profile* to calculate the strains and stresses at each point in the deforming sheet using the plasticity relations discussed in section 3.2.

The sub-functions *Wrinkling* and *Fracture* are called by *CUP* to check if the process will fail by either flange wrinkling or cup wall fracture. The wrinkling and fracture criteria used in these sub-functions are discussed in the next chapter. They are only activated when it is required to check for the process limits; otherwise, they are inactive. If no wrinkling or fracture occurred, the current stage of deformation (i) is terminated and the next step ($i+1$) is started.

The functions included within the dashed line represent the computer code "CUP DRAW" which will be used in the optimization of the BHF in the next chapter. More details on the computer code are given in Appendix B, which provides the pseudo–code for the main program and its sub-functions.

3.9 Cases Investigated

The developed analytical model is applied in the analysis of two different cup models. The first cup is used for the verification of the analytical model against experimental results from the literature. The second cup is used in a comparison with a developed finite element model. Also, a parametric study was conducted on the second cup to determine the effect of the different parameters on the results. Following are descriptions of the cases that are investigated, while the results are given in chapter 5.

3.9.1 Analytical Model Verification

The developed analytical model is verified by comparing its results with those of the experimental investigation carried out by Saran et al. [24]. The details of the compared cup geometry, material properties, and loading conditions are shown in Fig. 3-20. The comparison is made for the following:

- Punch Travel vs. flange radius reduction
- Punch Travel vs. Punch Force
- Circumferential, radial and thickness strains

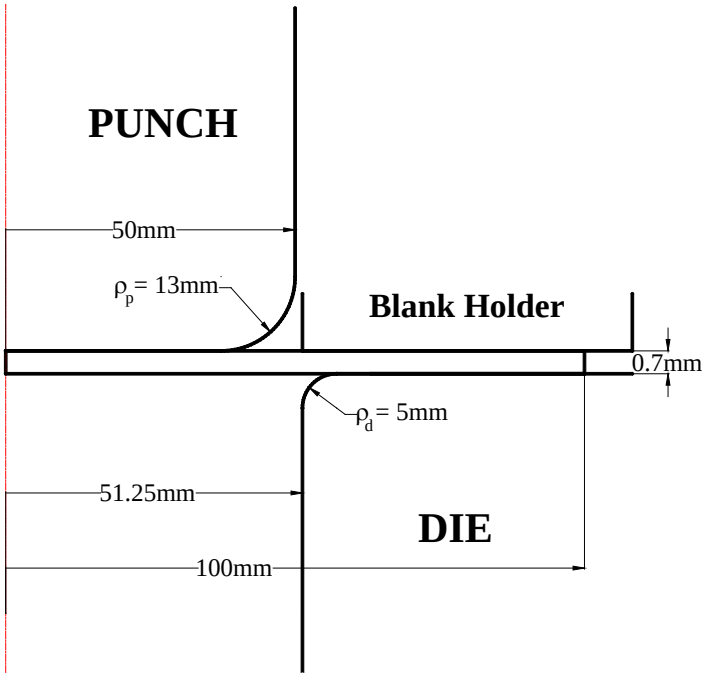

Geometry
to = 0.7*mm*
R_a = 100*mm*
ρ_d = 5*mm*
ρ_p = 13*mm*
r_d = 51.25*mm*
r_e = 50*mm*
Material: 70/30 Brass
C = 895*MPa*
n = 0.42
E = 110*GPa*
ν = 0.34
Density = 8470 Kg/m^3
Loading
F_{BH} = 100kN
$\mu_{BH} = \mu_{DP} = \mu_{PP}$ 0.06

Fig. 3-20: Cup used in the analytical model verification

3.9.2 Comparison between the Analytical Model and a Developed Finite Element Model

A comparison between the developed analytical model and a finite element model is carried out in order to determine the points of strength and weakness in both models. The comparison is carried out on the cup shown in Fig. 3-21. The material of the sheet metal blank used in this model is aluminum alloy AL7075-T6 which is known for its high strength and is widely used in the aircraft industry. The material is selected as part of an on going research at AUC on the deep drawing process using this material [52].

Due to the nonlinearity in geometry, material, loading conditions, and other complexities in the deep drawing process, ABAQUS finite element package was selected to run the finite element analysis. ABAQUS has two analysis modules; Standard and Explicit. ABASUS/Standard is a general purpose analysis module suitable for a large number of linear and nonlinear problems. On the other hands, ABAQUS/Explicit is a special-purpose analysis module which uses explicit dynamic finite element formulation. ABAQUS/Explicit is capable of solving highly nonlinear quasi-static problems more efficiently than ABAQUS/Standard. Deep-drawing is considered a quasi-static problem which involves large membrane deformations, wrinkling and complex frictional contact conditions. Thus, ABAQUS/Explicit was selected for the finite element analysis of the problem. The following is a brief overview of the finite element model. Details of the model including the ABAQUS input files are given in Appendix D.

Geometry: The geometry of the cup modeled on ABAQUS is shown in Fig. 3-21.

Material properties: The material used in the analysis is aluminum alloy AL7075 with properties shown in Fig. 3-21. The material follows the Ludwik-Hollomon flow rule given in equation (3.18).

Meshing: The drawing tools including die, punch and blank holder are modeled using analytical rigid surfaces, while the sheet is modeled using solid axisymmetric elements. The sheet is meshed with 4 elements across the thickness and 200 elements over the sheet radius to give a total of 800 elements.

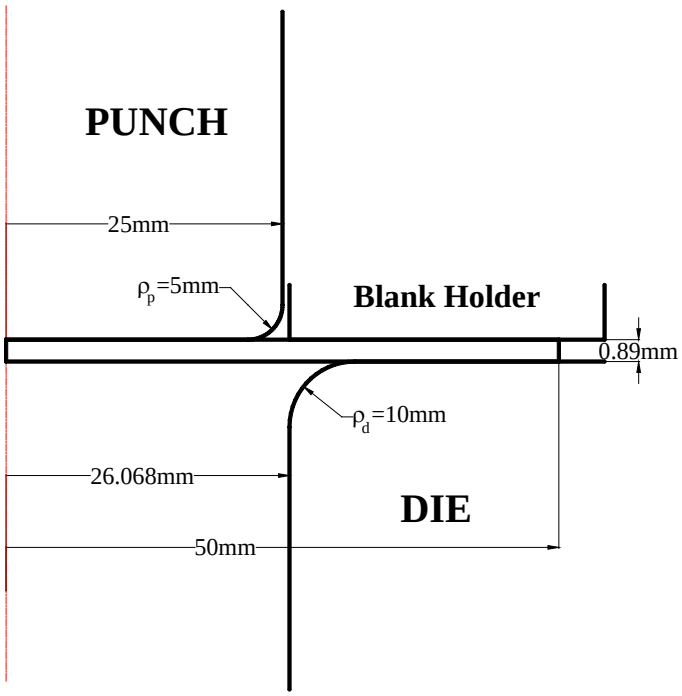

Geometry
to = 0.89*mm*
R_a = 50*mm*
ρ_d = 10*mm*
ρ_p = 5*mm*
r_d = 26.068*mm*
r_e = 25*mm*
Material: AL7075-T6
C = 756.6*MPa*
n = 0.0782
E = 65*GPa*
ν = 0.33
Density = 2796 Kg/m^3
Loading
F_{BH} = 17KN
$\mu_{BH} = \mu_{DP} = \mu_{PP} = 0.13$

Fig. 3-21: Cup used in the comparison with the finite element model

Friction coefficient: A constant coulomb friction with a coefficient of 0.13 is used between all contacting surfaces including punch-sheet, die-sheet and blank holder–sheet.

Blank Holder Force: The BHF is applied as a concentrated load on the reference node of the blank holder.

Punch velocity: As indicated in references [53] and [54], in order to determine the velocity of the punch during the process, a frequency analysis needs to be carried out to determine the time period of the event. The first modal frequency of the sheet is found to be 402.66 Hz. This gives a time period of 2.483×10^{-3} seconds, which is taken as the step time. The total punch stroke is taken to be 30mm. Then, the required constant velocity to give the total punch stroke is $30/(2.483 \times 10^{-3})$ = 12,082mm/s (12.082m/s). This velocity may seem high compared to the punch velocity in the physical process, which is in the order of 1m/s. The computer time used in the solution of the problem using explicit analysis is directly proportional to the time period of the event. Thus, it is desirable to decrease the time period, which consequently increases the velocity. However, if the velocity is very high, inertial effects will dominate and the results will not correspond to the physical low-speed problem. The maximum velocity above which inertial effects will dominate is found

to be 1% of the wave speed of the material. For metals, the wave speed is in the range of 5000m/s. This gives an upper bound for the punch velocity of around 50m/s.

The comparison between the analytical model and the finite element model is carried out for the following:

- Punch Travel vs. flange radius reduction
- Punch Travel vs. Punch Force
- Thickness, radial and circumferential strains distribution
- Radial, Circumferential, and Von Mises stresses distribution
- Strains and stresses history at the punch bottom

3.9.3 Parametric Study

The analytical model is used to analyze the cup shown in Fig. 3-21, for different die design and process parameters. Each parameter is varied over 5 values to study its effect on the punch force and thickness strain. These parameters are given in Table 3-2.

The coefficient of friction between the sheet and the blank holder and the die surface (μ_{BH}) and that between the sheet and the die profile (μ_{DP}) usually have the same value in the physical process of cup drawing. This is due to the use of the same lubricant on the die surface including the part in contact with the flange area and the die profile. As a result, they are considered in the parametric study as the same coefficient of friction and are named the die coefficient of friction (μ_D), such that $\mu_D = \mu_{BH} = \mu_{DP}$.

Table 3-2: Parameters used in the parametric study

Parameter	Values considered
Die profile radius (ρ_d)	6,8,10,12, and 14mm
Punch profile radius (ρ_p)	5,6.5,8,10, and 12mm
Blank holder force (F_{BH})	5,17,30,45, and 60kN
Coefficient of friction with the die surface (μ_D)	0.045,0.06,0.08,0.1, and 0.13
Drawing ratio (B_0)	1.9,1.95,2.0,2.1, and 2.2

CHAPTER 4

OPTIMIZATION OF BLANK HOLDER FORCE SCHEME

4.1 Introduction

Blank holder force (BHF) is an important parameter in the deep drawing process. It is used to suppress the formation of wrinkles that can appear in the flange of the drawn part. Wrinkling is associated with compressive instability. It occurs due to the increase in the compressive circumferential stress (σ_θ) in the flange which reaches to a limit that causes buckling or wrinkling of the sheet metal. When increasing the BHF, thickness stress increases which restrains any formation of wrinkles. Wrinkling formation is shown in Fig. 4-1.

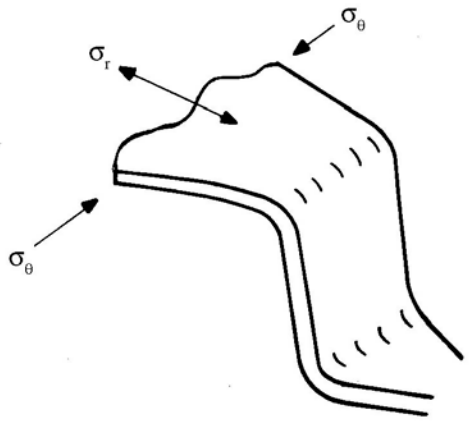

Fig. 4-1: Flange Wrinkling [58]

However, the large value of the BHF will restrain the blank material from flowing into the die profile and throat. As a result, the material in the wall and at the punch profile will be stretched and fracture would occur. So, the BHF must be set to a value that avoids both process limits of wrinkling and fracture. The range of suitable values is called the process window which can be shown in Fig. 4-2. To explain the concept of the process window, consider two cases. In case I, the cup drawing process has the limits (bold lines) for wrinkling and tearing away from each other. Thus, there is a large range of values for the BHF that gives a complete cup without hitting any of

the two limits. However, in case II, the two process limits (dashed lines) overlap. This results in limiting the maximum possible punch stroke above which wrinkling and/or tearing would occur, which is shown by the dotted horizontal line.

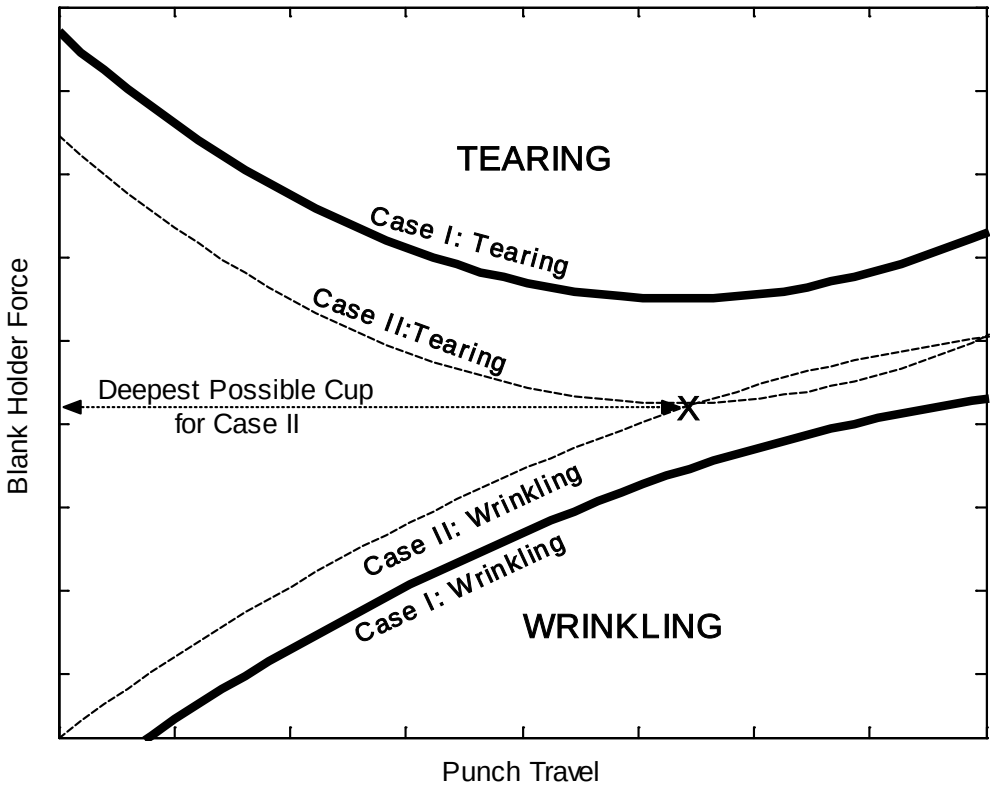

Fig. 4-2: Forming Process Window

For a certain cup, the range of values for a suitable BHF gets smaller depending on many parameters. One of these is the sheet metal properties where some materials are known to have good formability like steels and copper alloys. On the other hand, aluminum alloys are less formable which limit the range of suitable values of the BHF for the same drawing ratio. Also, Die design and process parameters affect the process window. For example, for a small die profile radius and large friction coefficient, the range gets smaller. Another parameter that affects the process window is the drawing ratio. If it increases, a higher BHF will be required to suppress wrinkling due to the increase in the compressive stress in the flange. This will cause the wrinkling limit to move closer to the tearing limit. Thus, the possible suitable range for the BHF gets smaller.

Besides avoiding both process limits (wrinkling and tearing), it is desirable to have a deep drawn component with uniform thickness, which means less thinning. A

direct link to the sheet thinning is the punch force. For higher values of the punch force, more thinning is expected. This is due to the fact that the punch force is directly related to the radial stress in the sheet as was shown by equation (3.59) for the punch force calculation. Therefore, in order to have less thinning in the drawn part, the maximum punch force must be reduced. This can be achieved by controlling the value of the BHF through out the process.

4.2 Approach for Optimizing the Blank Holder Force

The BHF can be varied with punch travel either linearly or non-linearly. The objective of the present study is to develop an optimization strategy for determining the optimum BHF scheme for a certain cup model that minimizes the maximum punch force without causing wrinkling or tearing in the cup material. This objective is applied to the linear BHF scheme. So, the objective can be formulated as an optimization problem in the following manner:

- Objective function: Minimize the maximum punch force in the cup deep drawing process. The maximum punch force, $(F_P)_{max}$, is determined as the maximum value obtained from equation (3.59), i.e. $(F_P)_{max} = \max(F_P)$
- Variables:
  - Initial value (intercept) of the BHF function (u_0)
  - Slope of the BHF function (u_1) (either positive or negative slope)

  Such that the function is:

  $$F_{BH} = u_0 + u_1 D_a \quad (4.1)$$

  Where,

  F_{BH} = Blank holder force

  D_a = Flange radius reduction = $R_a - r_a$
- Constraints: Avoid wrinkling and tearing using equations (4.4) and (4.5) respectively which are given in the next sections.

The objective function is evaluated using the developed analytical model. The numerical solution discussed in the previous chapter in section 3.5.1 uses the sheet rim displacement (flange radius reduction) as the incremental parameter for the stages of deformation. Thus, the BHF function is entered to the analytical model in terms of

the flange radius reduction (D_a). However, in industry, the punch travel is the controlling parameter. Thus, it is useful to obtain the BHF function in terms of the punch travel instead of the flange radius reduction. By investigating the relation between the punch travel and the flange radius reduction it is found to be nearly linear, except at the early stages of deformation. This relation for three cases of different cup geometries and sheet material properties is shown in Fig. 4-3 with their properties given in Table 4-1.

Table 4-1: Different cases of cup geometries and sheet materials

Parameter	**Case I**	**Case II**	**Case III**
t_0, mm	0.89	0.7	1
R_a, mm	50	73.5	101.6
ρ_d, mm	10	5	6.35
ρ_p, mm	5	13	6.35
r_e, mm	25	35	50.8
r_d, mm	26.068	36.25	52.09
Material	AL7075-T6 C=756.6MPa, n=0.0782	Brass 70/30 C=895MPa, n=0.42	Mild Steel C=661.8MPa, n=0.23
$\mu_{BH}=\mu_{DP}=\mu_{PP}$	0.13	0.06	0.06
F_{BH}, kN	17	50	68

The relation between the punch travel and the flange radius reduction can be assumed linear and has the following relation:

$$D_a = q_0 + q_1 L$$

Where, q_0 and q_1 are the intercept and slope of the relation respectively

By substituting this relation into equation (4.1), a relation between the BHF and punch travel is obtained as:

$$F_{BH} = v_0 + v_1 L \qquad (4.2)$$

Where,

v_0 = Initial value (intercept) of the BHF function = $u_0 + u_1 q_0$

v_1 = Slope of the BHF function = $u_1 q_1$

L = Punch travel

A comparison between the optimized linear BHF function given by equation (4.2) and the actual optimized BHF scheme is shown in Fig. 4-4 for case III that is given in Table 4-1. The linear relation given by equation (4.2) is considered an approximation to the actual linear relation in terms of the flange radius reduction as given by equation (4.1). However, by comparing the maximum punch force for the linearized scheme given by equation (4.2) with the actual scheme given by equation (4.1), it is found that the difference in the maximum punch force is not greater than 0.2%. Thus, the assumption of a linear relation between the punch travel and the flange radius reduction is considered acceptable.

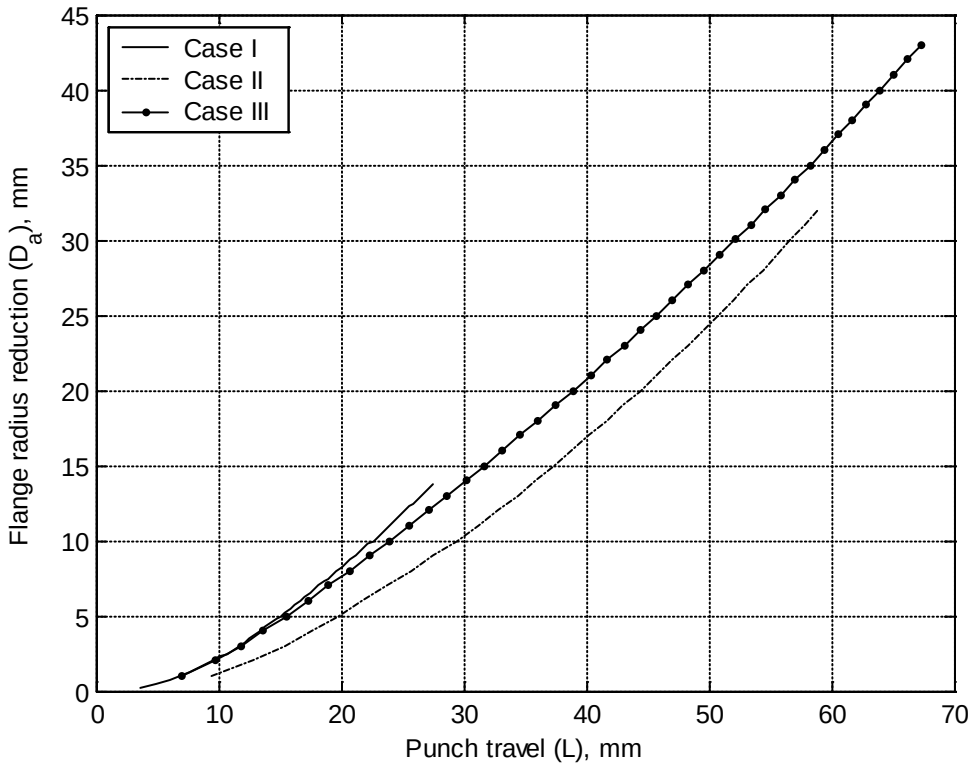

Fig. 4-3: Relation between rim displacement and punch travel for different cases

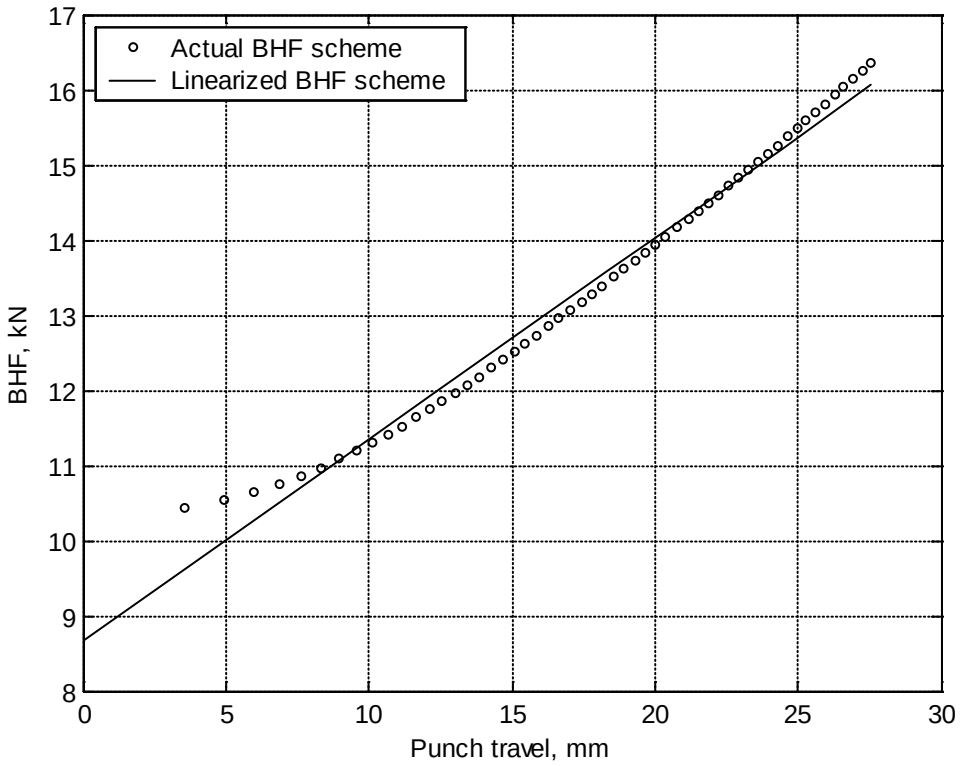

Fig. 4-4: Linearized BHF scheme

4.3 Wrinkling Criterion

The wrinkling criterion used in this analysis is based on a semi-empirical work carried out by Kawai [29]. His work is found to be simple to apply to the analytical solution in the present study. Wrinkling criteria by other investigators requires sophisticated analysis including bifurcation analysis or geometrical analysis by measuring the wrinkle dimensions. Kawai's wrinkling criterion is applicable to a large range of materials including copper, brass, aluminum, and mild steel. He provided a formula for the critical blank holding pressure that would suppress wrinkling, which is given by:

$$p_{cr} = E_o \left[\frac{\omega_{cr} \dfrac{3.82\beta_c^2 \delta B_o}{\left(B_o^2 - \beta_c^2\right)\alpha_B \alpha_H} \left[\left(\dfrac{\sigma_c}{E_o} \right)^2 - \dfrac{4.77\alpha_B \alpha_D}{\beta_c^2 \delta^4} \right]}{1 + \omega_{cr} \mu_{BH} \left(3.82\beta_c^2 \delta^2 B_o\right) \dfrac{1}{\alpha_H} \left(\dfrac{\sigma_c}{E_o} \right)} \right] \tag{4.3}$$

Where,

ω_{cr} =Critical specific wave amplitude for local wrinkling which is taken to be equal $0.17x10^{-3}$

β_c $=r_c/r_d$

β_o $= r_a/r_d$ (current drawing ratio)

B_o $= R_a/r_d$

δ $= 2r_d/t_o$ (specific hole diameter)

α_B $=(\beta_o-\beta_c)/(\beta_o\beta_c)$

α_H $=\beta_o+\beta_c$

α_D $=(\beta_o+\beta_c)^2/(\beta_o-\beta_c)^3$

σ_c =radial stress at radial position r_c

$$=1.1\sigma_{eq}\ln\left(\beta_o/\beta_c\right)$$

where, $\sigma_{eq}=\bar{\sigma}_o+\bar{\varepsilon}_{eq}^2$

$$\bar{\varepsilon}_{eq}=\frac{2}{3}\ln\frac{B_o^2-\beta_o^2+\{(\beta_o+\beta_i)/2\}^2}{\{(\beta_o+\beta_c)/2\}^2}$$

E_o $=\dfrac{4EF_o}{\left(\sqrt{E}+\sqrt{F_o}\right)^2}$ (plastic buckling modulus)

E = young's modulus of the sheet metal

$F_o=nA\bar{\varepsilon}_{flange}^{n-1}$ tangent modulus of buckling of the sheet metal

$\bar{\varepsilon}_{flange}=\dfrac{3}{4}\bar{\varepsilon}_{eq}$ (average equivalent strain in the flange)

Then, the critical blank holding force below which wrinkling will occur can be determined from:

$$\left(F_{BH}\right)_{cr}=\pi\left(R_a^2-r_c^2\right)p_{cr} \tag{4.4}$$

4.4 Fracture Criterion

The fracture criterion used in the present analysis is based on the notion that necking is assumed to occur at the point where uniaxial stress occurs in the material. This point is usually located at the punch nose, i.e. at radial position r_2. This criterion was discussed by Marciniak [39] and applied by Ahmetoglu et al [40].

For a material following the Holloman's flow rule:

$$\bar{\sigma} = C\bar{\varepsilon}^{n} \tag{3.10}$$

Fracture occurs at a uniaxial state of stress when the equivalent strain $\bar{\varepsilon} = n$. So, the critical radial stress which initiates necking is:

$$(\sigma_r)_{cr} = Cn^n$$

Then the radial force (see Fig. 4-5), which initiates necking,

$$\begin{aligned}(F_r)_{cr} &= 2\pi r_2 t_2 (\sigma_r)_{cr} \\ &= 2\pi r_2 t_2 (Cn^n)\end{aligned}$$

This can be given in terms of a critical punch force at the current stage as follows:

$$(F_P)_{cr} = 2\pi r_2 t_2 (Cn^n)\sin\theta \tag{4.5}$$

The actual current punch force is calculated from equation (3.59). If the actual current punch force is higher than the critical punch force calculated from equation (4.5), then fracture is expected to occur.

For other material flow curves, $d\bar{\sigma}/d\bar{\varepsilon}$ should be calculated at the point of uniaxial state of stress (boundary (2)) at each stage of deformation. If this value is less than σ_r at this point, then necking is expected to occur.

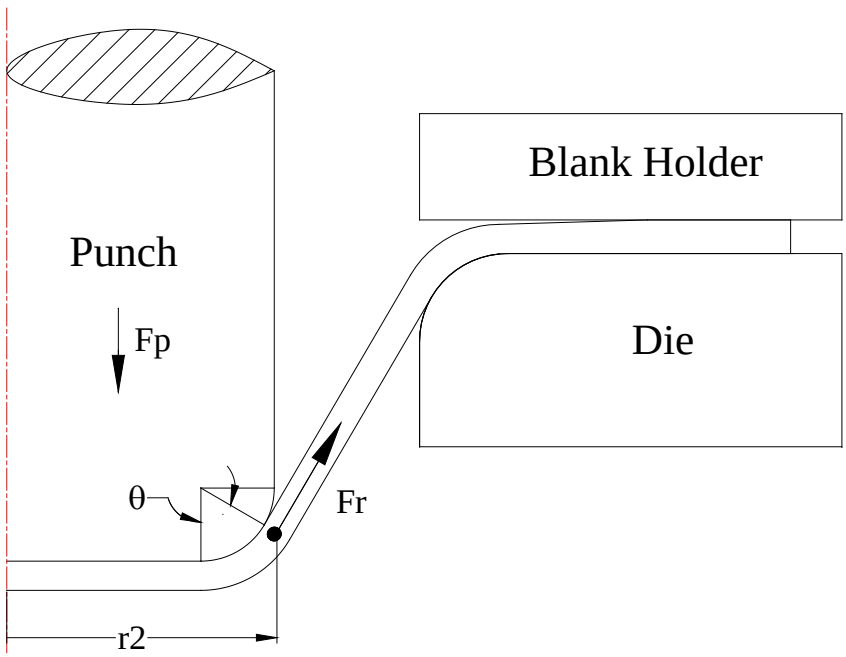

Fig. 4-5: Radial force at the critical point

4.5 Optimization Search Method

In order to achieve the optimization objective, genetic algorithms (GAs) are used. This global search method is found to be most suitable due to the multi-modal nature of the objective function at hand. Functions with multi-modal nature are those that have more than one local minimum for a minimization problem. In the case of the present objective function, these local minima are due to the approximations in the numerical solution of the analytical model. If a local search method is used, it usually fails to find the global minimum of the function by falling into a local minimum. Genetic algorithms are known to be able to search through all of the function space, thus it can detect the global minimum of the function. GAs operates by using initial random points (chromosomes) spread throughout the whole search space. Then, at each iteration (generation), these random points are refined using different operators to spread over more search space to look for the optimum function value. The search ends when a specified number of iterations are completed. An elaboration on the GAs is presented in Appendix C.

4.6 The Computer Code for the BHF Optimization

The computer code for the optimization of the BHF is based on the analytical model computer code that was described in chapter 3, but with a slight modification. The main program *CUP DRAW* is called by the genetic algorithm function (*GAs*). *GAs* will keep calling *CUP DRAW* by sending different BHF function coefficients (u_0 and u_1) and getting the maximum punch force $(F_p)_{max}$ corresponding to these coefficients. Thus, it searches the space of the BHF function to determine the coefficients that give the minimum $(F_p)_{max}$. The sub-function *Input Data* is called by *GAs* which sends the necessary data to *CUP DRAW* at each time it calls it. A block diagram of the computer code is shown in Fig. 4-6. The pseudo-code of the GAs is given in Appendix C.

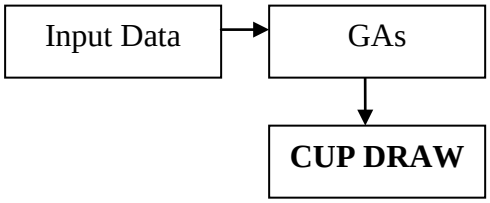

Fig. 4-6: Block diagram of the computer code for the BHF optimization

4.7 Cases Investigated

Optimization of the BHF scheme is carried out on two cup models. The first is used to compare the optimized BHF scheme with the constant scheme, while the second is used to analyze the nature of the optimized BHF scheme. The following is a description of the two cases investigated.

4.7.1 Cup Drawing with Constant BHF versus Optimized BHF Scheme

The first model is the one given in Fig. 3-20, which has a constant BHF. The optimized BHF is compared with the given constant BHF to determine the improvement on the results. This comparison, which is given in the next chapter, is carried out using the analytical model and a developed finite element model. The finite element model is developed on the same basics of the model stated in the previous chapter and described in detail in Appendix D. The following is a brief overview of the model.

Geometry: The geometry of the modeled cup is shown in Fig. 3-20.

Material properties: The material used in the analysis is 70/30 brass with properties shown in Fig. 3-20. The material follows the Ludwik-Hollomon flow rule given in equation (3.18).

Meshing: The die, punch, and blank holder are defined as analytical rigid surfaces. The sheet is meshed using solid axisymmetric elements with 4 elements across the thickness and 300 elements over the sheet radius to give a total of 1200 elements.

Friction coefficient: A constant coulomb friction with a coefficient of 0.06 is used between all contacting surfaces including punch-sheet, die-sheet and blank holder-sheet.

Blank Holder Force: The BHF is applied as a concentrated load on the reference node of the blank holder. In the case of the optimized linear BHF, the load is defined as a variable load with respect to the process or step time.

Punch velocity: The first modal frequency of the sheet is found to be 58.057 Hz, which gives a time period of 1.722×10^{-3} seconds. The total punch stroke is taken to be

80mm. Then, the required constant velocity to give the total punch stroke is 4644.56mm/s (4.64m/s).

4.7.2 Nature of the Optimized BHF Scheme

The second cup model that is optimized is the one shown previously in Fig. 3-21. Optimization is carried out on this cup for five different drawing ratios, where each is optimized for four die coefficients of friction to give a total of 20 cases. The drawing ratios investigated are 1.9, 1.95, 2.0, 2.1, and 2.2, while the die coefficients of friction are 0.045, 0.06, 0.1 and 0.13. These cases are optimized to determine the nature of the optimum BHF scheme as will be shown in the next chapter.

CHAPTER 5

RESULTS AND DISCUSSION

5.1 Verification of the Analytical Model

The developed analytical model is verified by comparing its results with the experimental investigation carried out by Saran et al. [24] for the 70/30 brass cup shown in Fig. 3-20. The comparisons between analytical and experimental results are made for the following:

- Punch Travel vs. flange radius reduction
- Punch Travel vs. Punch Force
- Circumferential, radial and thickness strains

5.1.1 Punch Travel vs. Flange radius reduction

There are only two experimental data points for the relation between the punch travel and the flange radius reduction as shown in Fig. 5-1. However, the analytical model shows good agreement with the experimental results. At the early stages of deformation, the analytical model shows a slow increase in the flange radius reduction. Then, in the later stages the relation between the punch travel and the flange radius reduction is nearly linear.

5.1.2 Punch Travel vs. Punch Force

The experimental results for the punch travel versus punch force show the relation up to a punch travel of 40mm as shown in Fig. 5-2. The comparison with the analytical model shows very good correlation. A small deviation of about 5% from the experimental results is shown at the maximum punch force at a punch travel of 40mm. This comparison confirms the ability of the analytical model in predicting the punch force with very good accuracy.

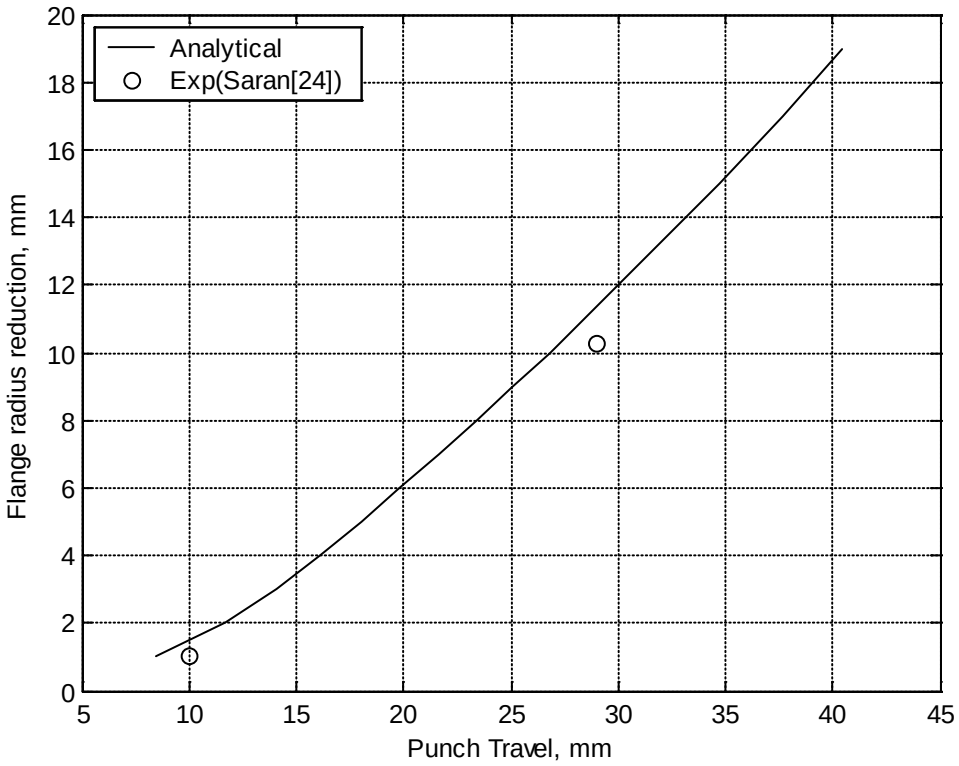

Fig. 5-1: Punch travel vs. flange radius reduction

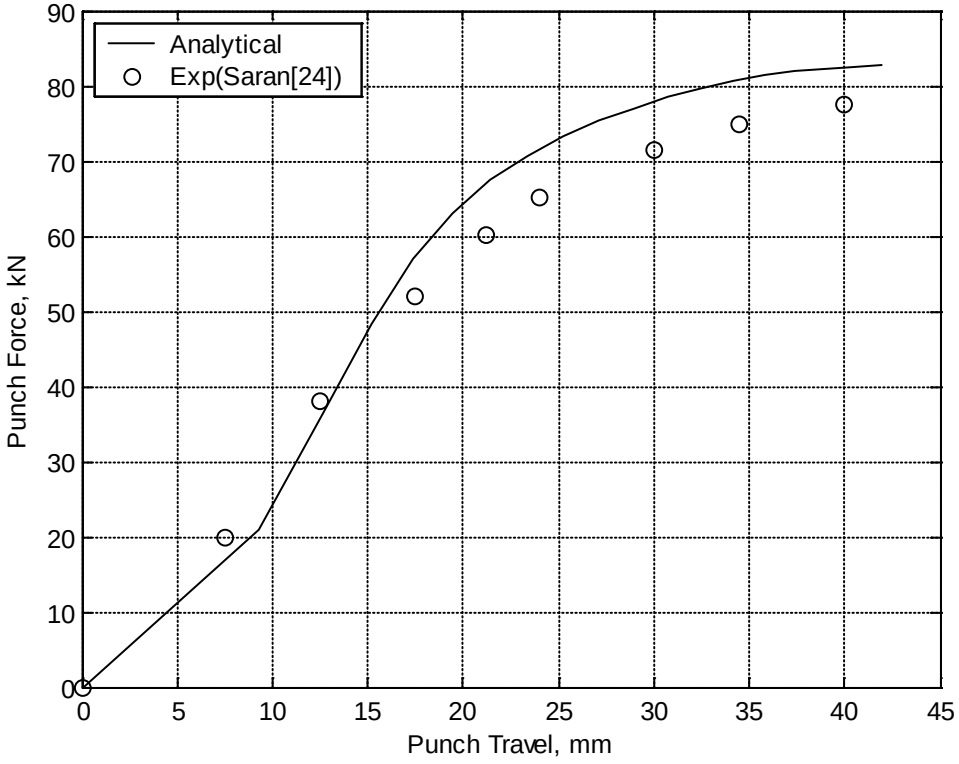

Fig. 5-2: Punch travel vs. punch force

5.1.3 Strains

The circumferential, radial and thickness strains distributions are compared at a punch travel of 30mm. Both experimental and analytical results show good correlation and same trends. The following is a description of the strains distributions.

The circumferential strain is constant with a positive value over the punch bottom which is located at an initial radial position of 0 to 37mm as shown in Fig. 5-3. The same is noticed for the radial strain in Fig. 5-4 which is equal to the circumferential strain at the punch bottom. Also, thickness strain in Fig. 5-5 shows a constant trend at the punch bottom, but with a negative value.

Over the punch profile, from an initial radial position of 37mm to 50mm, the circumferential strain starts decreasing to negative values. On the other hand, radial strain gradually increases and thickness strain slightly decreases suggesting a possible formation of a neck.

Over, the cup wall from an initial radial position of 50mm to around 70mm, the circumferential strain decreases until it reaches a maximum negative value of around -0.25 at the die profile. Also, the radial strain increases to a maximum peak of around 0.22 at the die profile. On the other hand, thickness strain transforms from negative values to positive values, which implies slight thickening at the die profile.

In the flange region, circumferential strain starts increasing again up to around -0.15 at the rim, while radial strain decreases to 0.06. As for the thickness strain it increases up to its maximum value of around 0.075 at the area under the blank holder force. The good agreement between the analytical model and the experimental results verifies the developed model and validate the assumptions made.

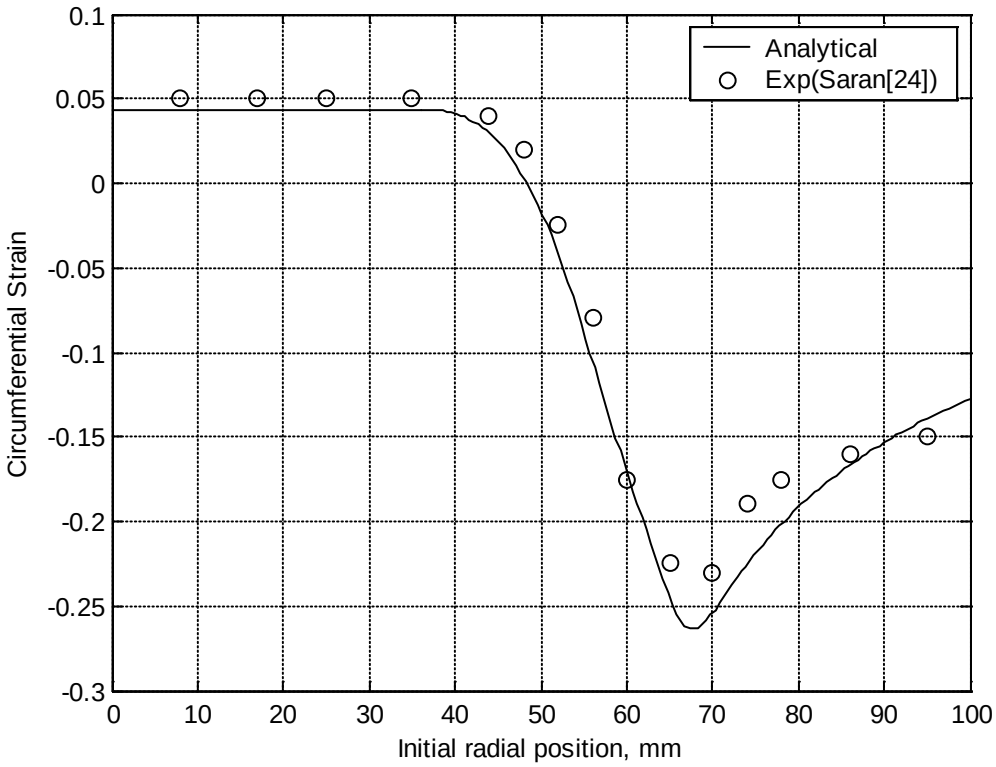

Fig. 5-3: Circumferential strain distribution at a punch travel of 30mm

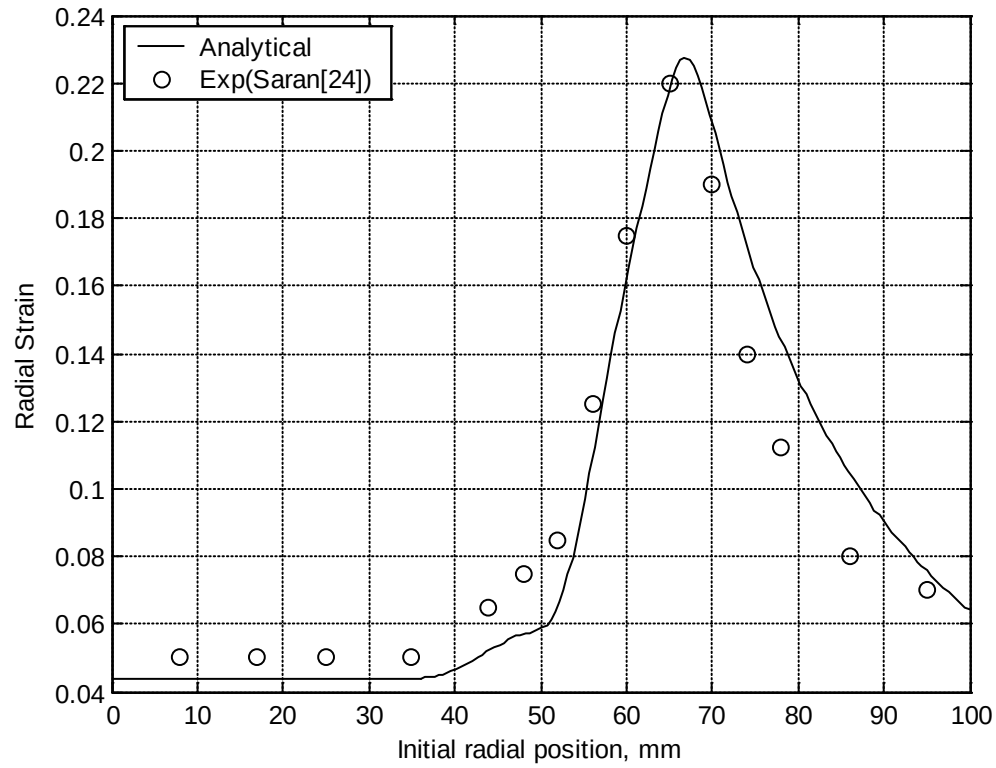

Fig. 5-4: Radial strain distribution at a punch travel of 30mm

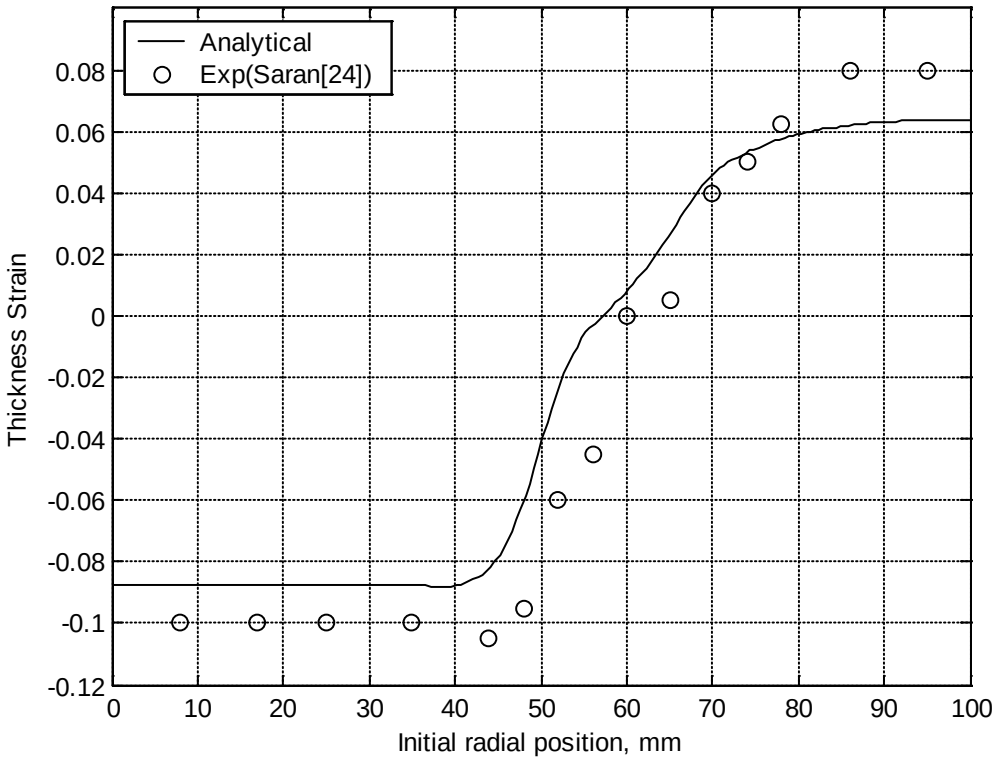

Fig. 5-5: Thickness strain distribution at a punch travel of 30mm

5.2 Comparison between the Analytical Model and a Finite Element Model

A comparison between the results of the developed analytical model and those of the finite elements is carried out on the cup shown in Fig. 3-21 to examine the points of strength and weakness in both models. The comparison is made for the following results:

- Punch Travel vs. flange radius reduction
- Punch Travel vs. Punch Force
- Thickness, circumferential, and radial strains distribution
- Radial, circumferential and Von Mises stresses distribution

In the finite element model, the stresses and strains distributions are calculated by taking the average stresses and strains of the four elements across the thickness.

5.2.1 Punch Travel vs. Flange radius reduction

Fig. 5-6 shows the comparison between the punch travel and flange radius reduction for both the analytical model and the finite element model. The difference between the two models is negligible at the early stages, but increases at later stages reaching around 5% at the final stage, which is acceptable.

5.2.2 Punch Travel vs. Punch Force

The comparison of the punch force for the two models shows excellent agreement as shown in Fig. 5-7. However, there is a slight deviation after the maximum punch force. This deviation increases up to the final stage, where the punch force given by the finite element model differs by around 12% from the analytical model. This small deviation might be due to the different way of calculation of the punch force in the two models. In the analytical model, the punch force is calculated using equation (3.59). On the other hand, the finite element model calculates the punch force from the normal force induced due to the contact of the punch with the deforming sheet. Yet, the two models give nearly the same maximum punch force value, which is the usual main concern in the analysis of the process.

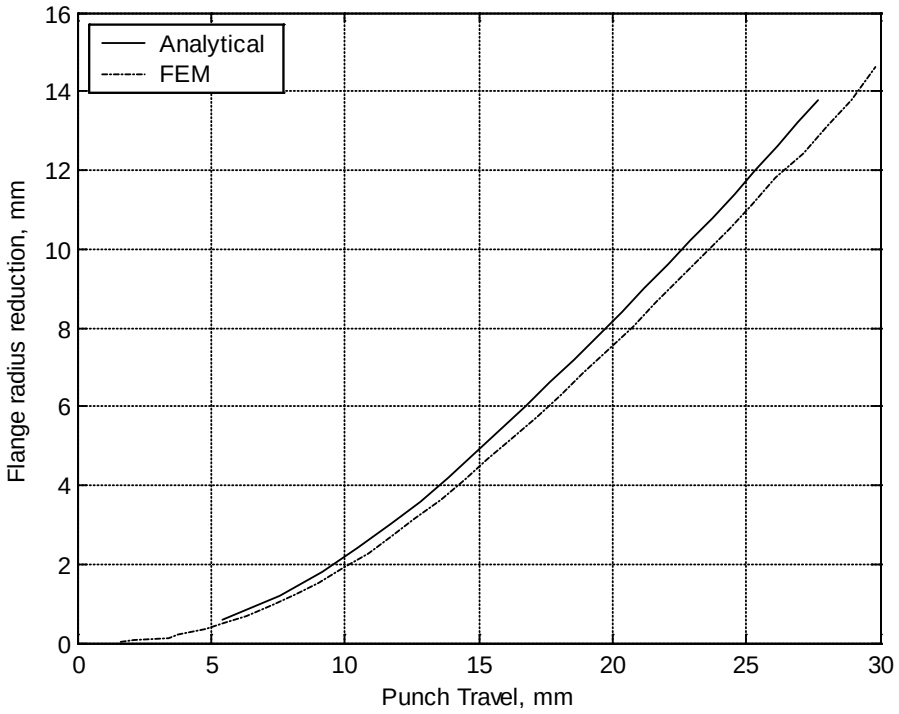

Fig. 5-6: Punch travel vs. Reduction of flange radius

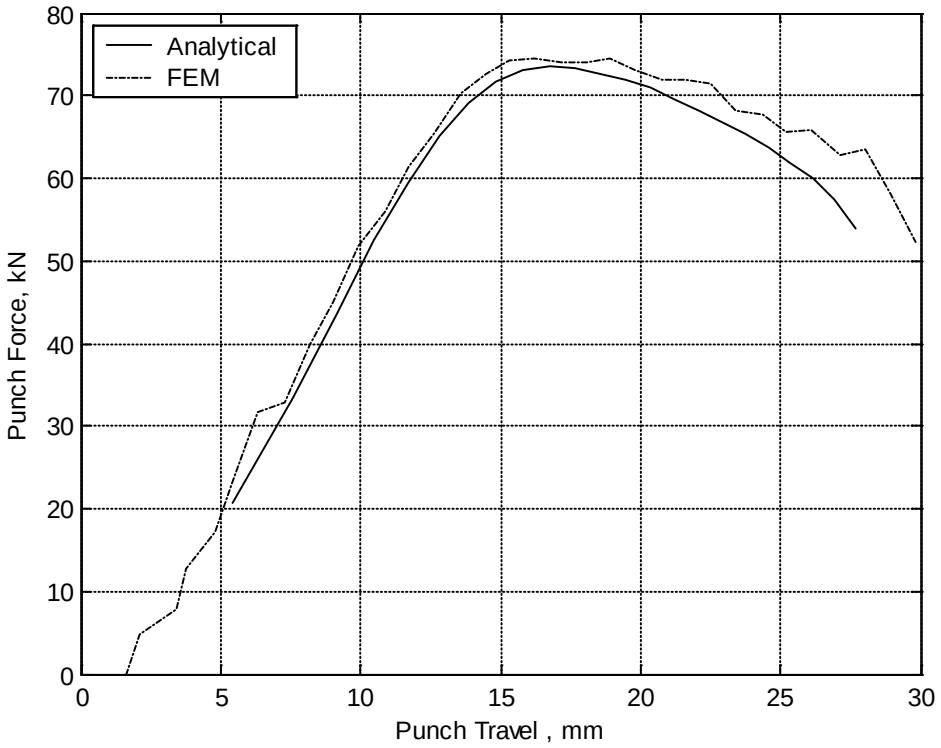

Fig. 5-7: Punch Travel vs. Punch force

5.2.3 Thickness, Radial and Circumferential Strains Distribution

The radial, circumferential and thickness strains are analyzed at two different stages of deformation. The first position is at a punch travel of 16mm and the second is at 27.5mm, which corresponds to the final stage of deformation. The thickness strain distribution for the first position is shown in Fig. 5-8. Both the analytical model and the finite element model show good agreement in all regions except at the punch and die profiles. The punch profile extends from an initial radial position of 19.5mm to 27mm, while the die profile extends from an initial radial position of 30mm to 42mm.

In the punch profile region, the analytical model does not predict the potential neck suggested by the finite element model which has a thickness strain of around -0.07. Similar results are noticed in the work of Al-Makky and Woo [5] where their analytical model showed significant difference compared to their experimental results for the thickness strain near the punch region. Consequently, one would expect that the results at the punch region are not accurate enough.

In the die profile region, the difference between the two models is nearly constant at a thickness strain of 0.015. The same difference between the two models at the punch and die profiles can be recognized in the radial strain in Fig. 5-9.

Apart from these differences, the results seem to be comparing well, especially the circumferential strain shown in Fig. 5-10, which shows very good match between the analytical model and the finite element model.

At the second position, where the punch travel reaches 27.5mm the flange region disappears. The thickness, radial, and circumferential strains at this position are shown in Fig. 5-11, Fig. 5-12, and Fig. 5-13 respectively. The difference between the analytical model results and those of the finite element model are nearly the same as the strains distributions at a punch position of 16mm.

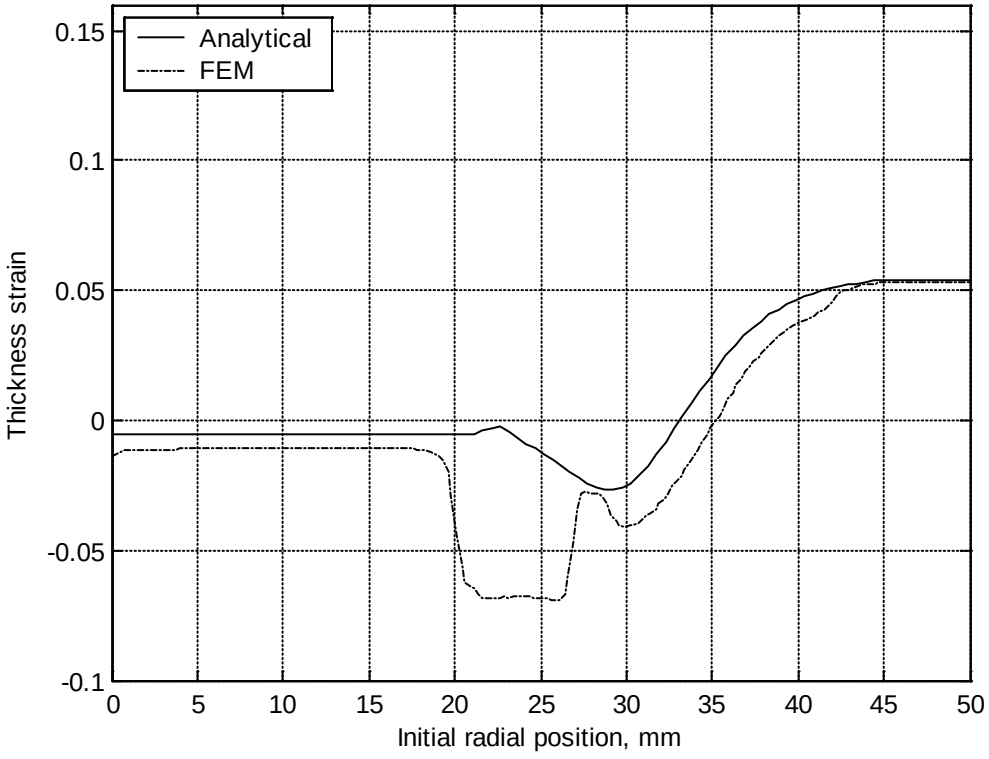

Fig. 5-8: Thickness strain distribution at a punch travel of 16mm

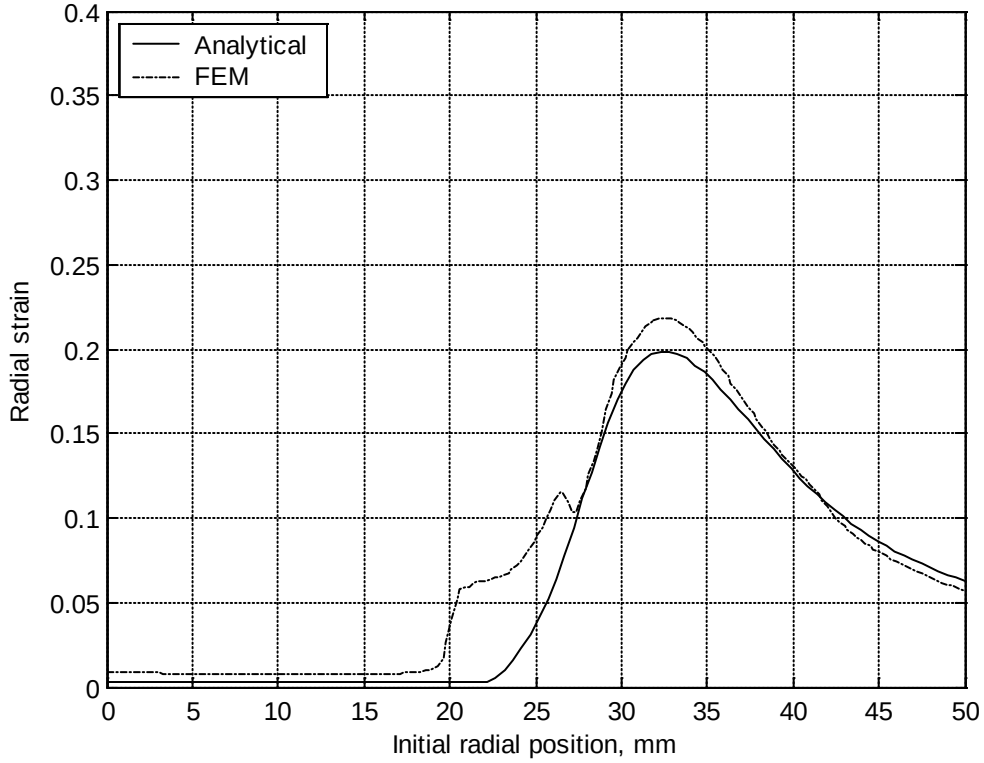

Fig. 5-9: Radial strain distribution at a punch travel of 16mm

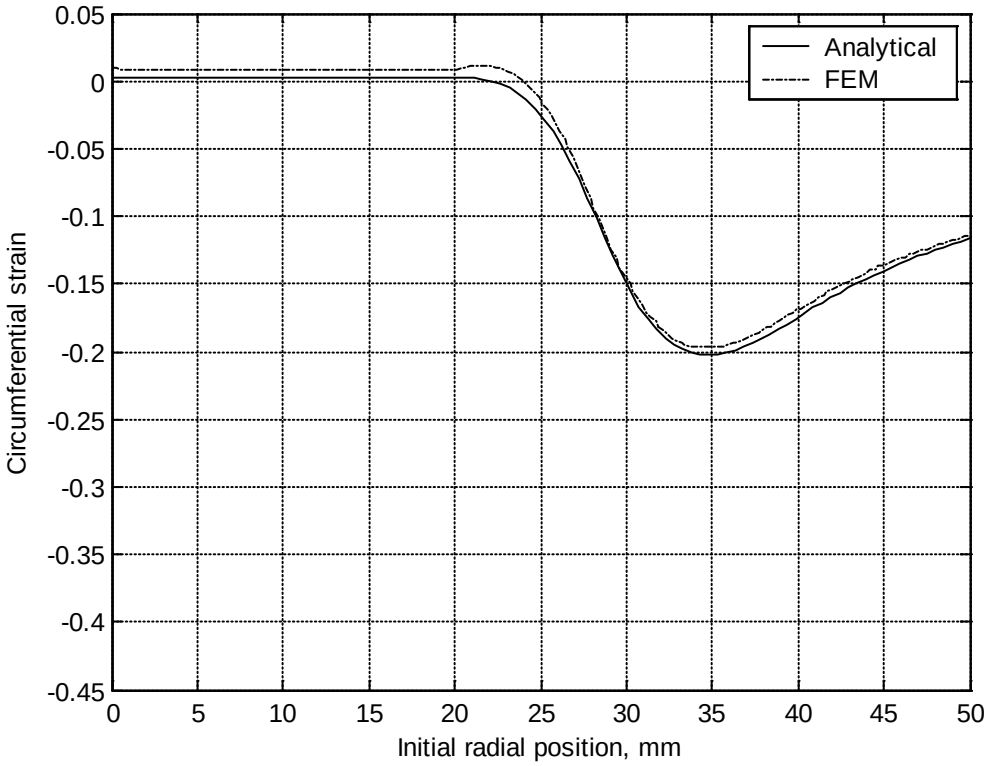

Fig. 5-10: Circumferential strain distribution at a punch travel of 16mm

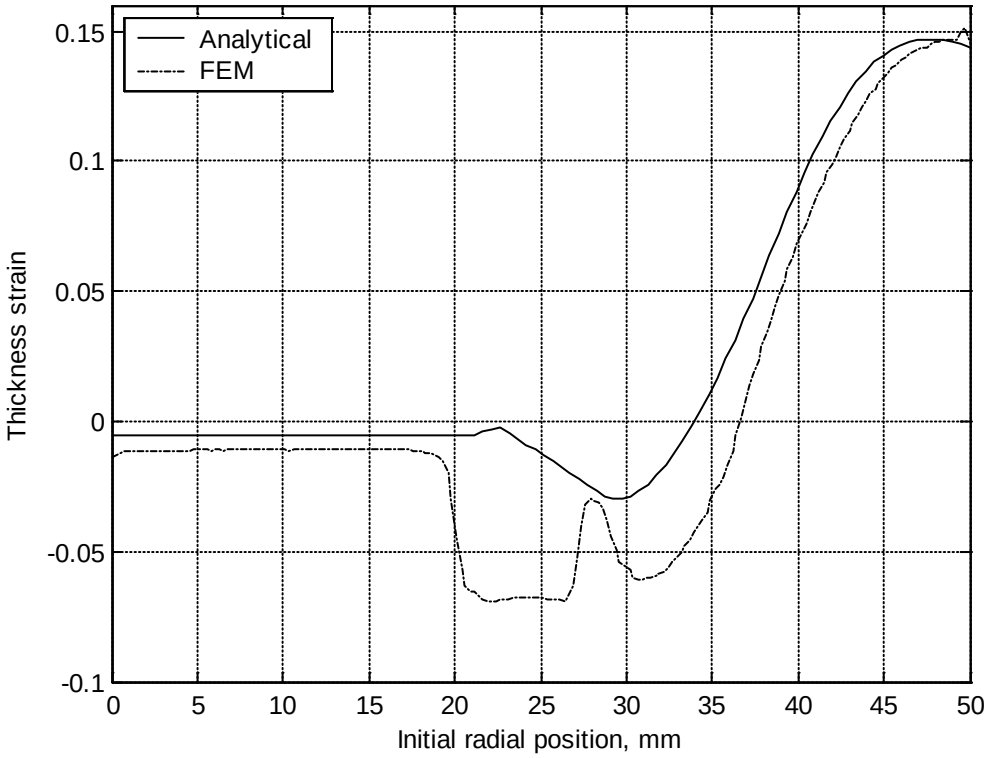

Fig. 5-11: Thickness strain distribution at a punch travel of 27.5mm

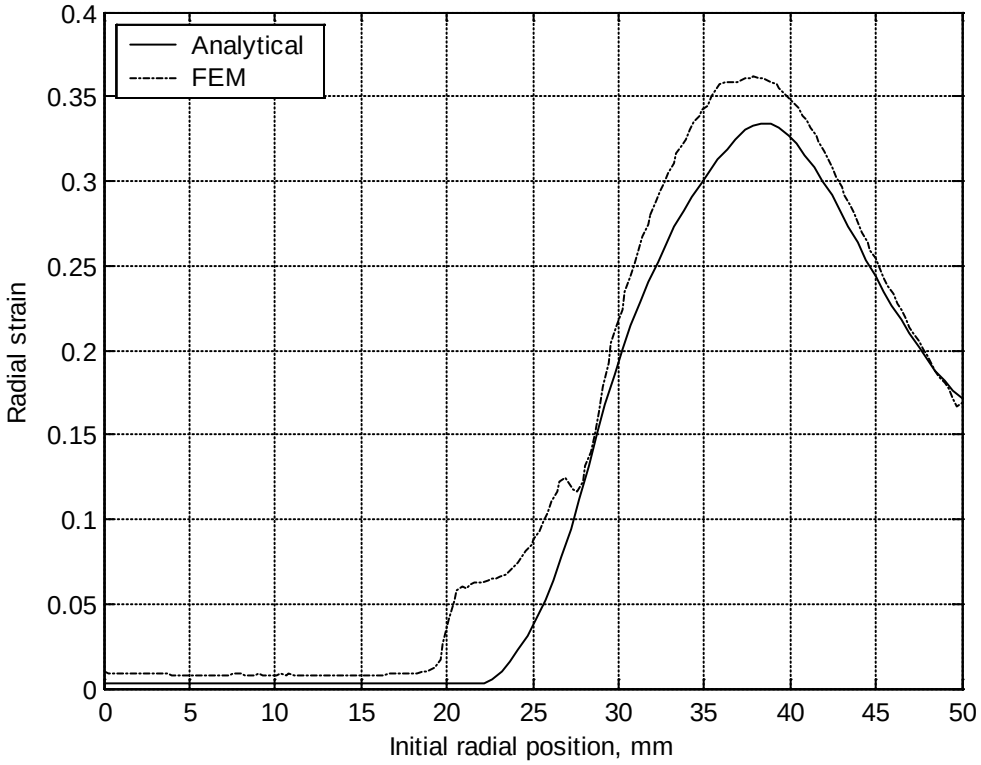

Fig. 5-12: Radial strain distribution at a punch travel of 27.5mm

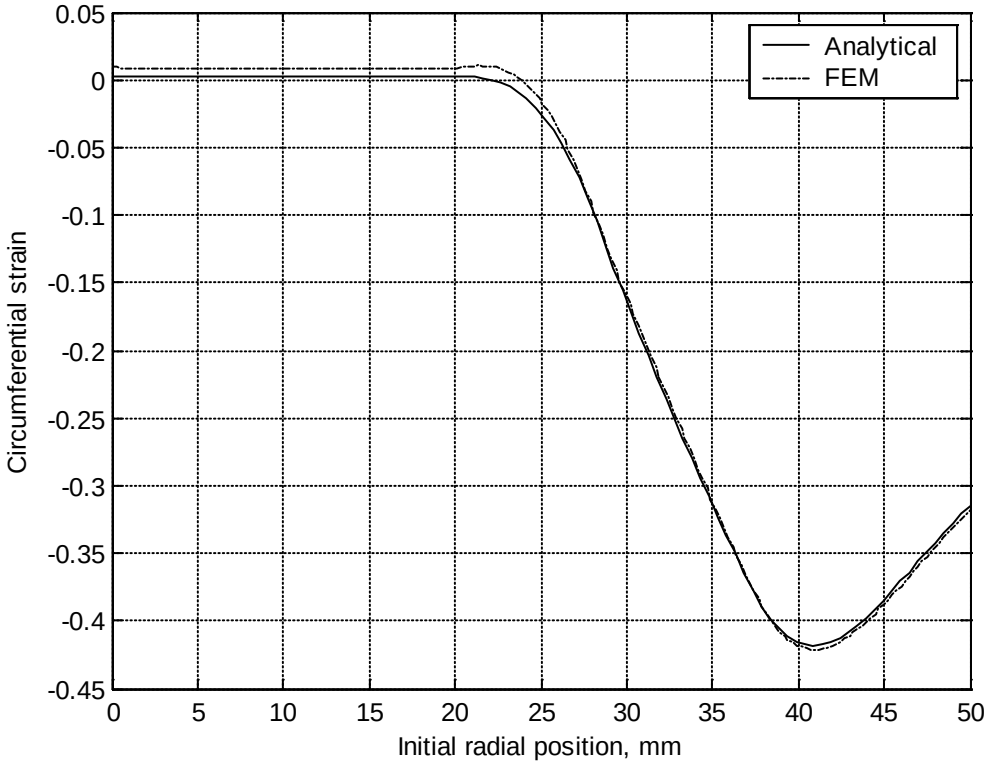

Fig. 5-13: Circumferential strain distribution at a punch travel of 27.5mm

5.2.4 Radial, Circumferential and Von Mises Stresses Distribution

The distribution for the radial, circumferential, and Von Mises stresses are compared with the finite element model at two punch travels of 16mm and 27.5mm. The radial stress at the punch travel of 16mm is shown in Fig. 5-14. The curves for the two models matches accurately in all regions except at the punch profile and punch bottom regions. The radial stress from the analytical model at these two regions shows the same trend as that of the finite element model, but with a less magnitude which reaches about 20% difference. The same correlation between the analytical model and finite element model results is shown in the circumferential stress in Fig. 5-15 and Von Mises stress in Fig. 5-16. The difference at the punch bottom reaches around 10% in the case of the circumferential stress and about 5% in the case of the Von Mises stress. Again, it is observed that there is a large variation in the circumferential and Von Mises stresses at the punch profile regions.

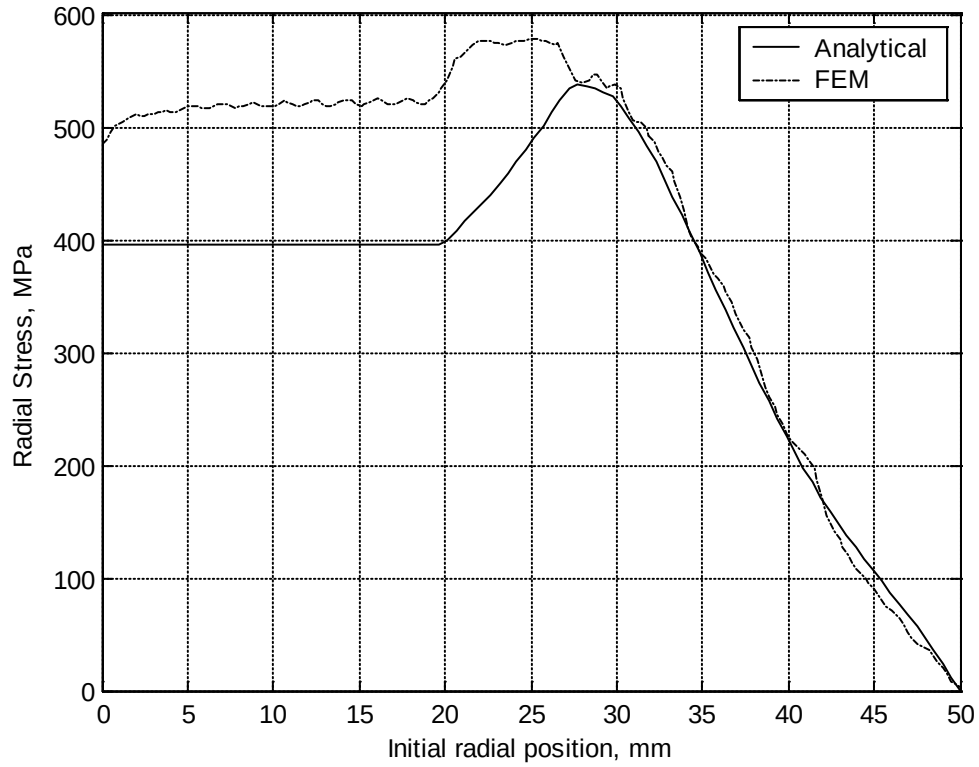

Fig. 5-14: Radial stress distribution at a punch travel of 16mm

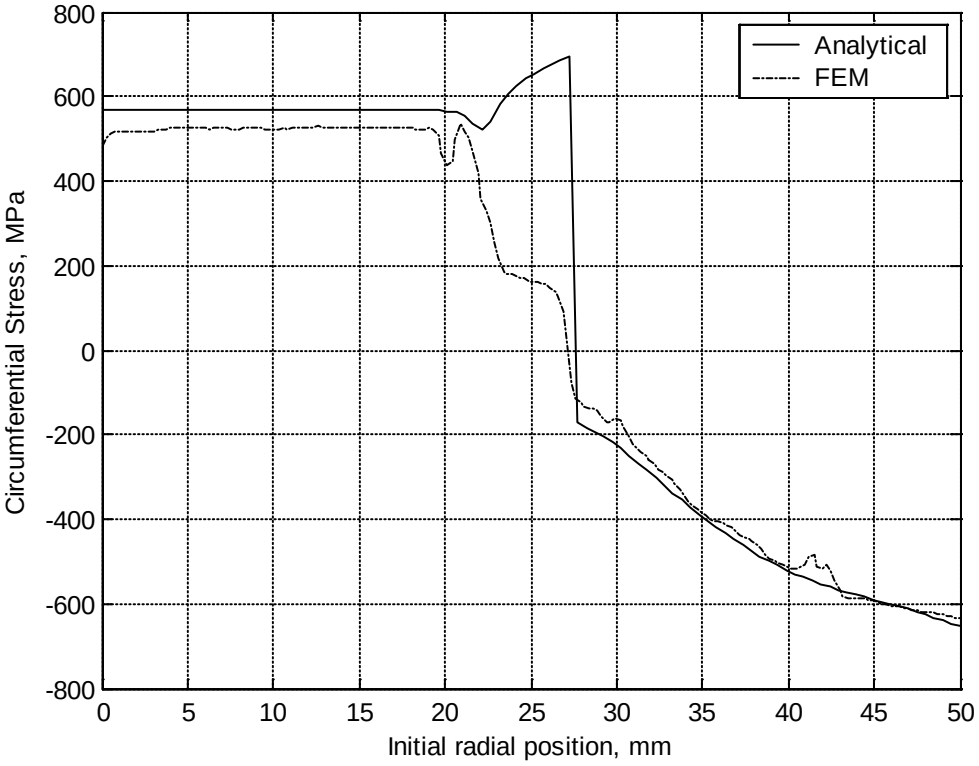

Fig. 5-15: Circumferential stress distribution at a punch travel of 16mm

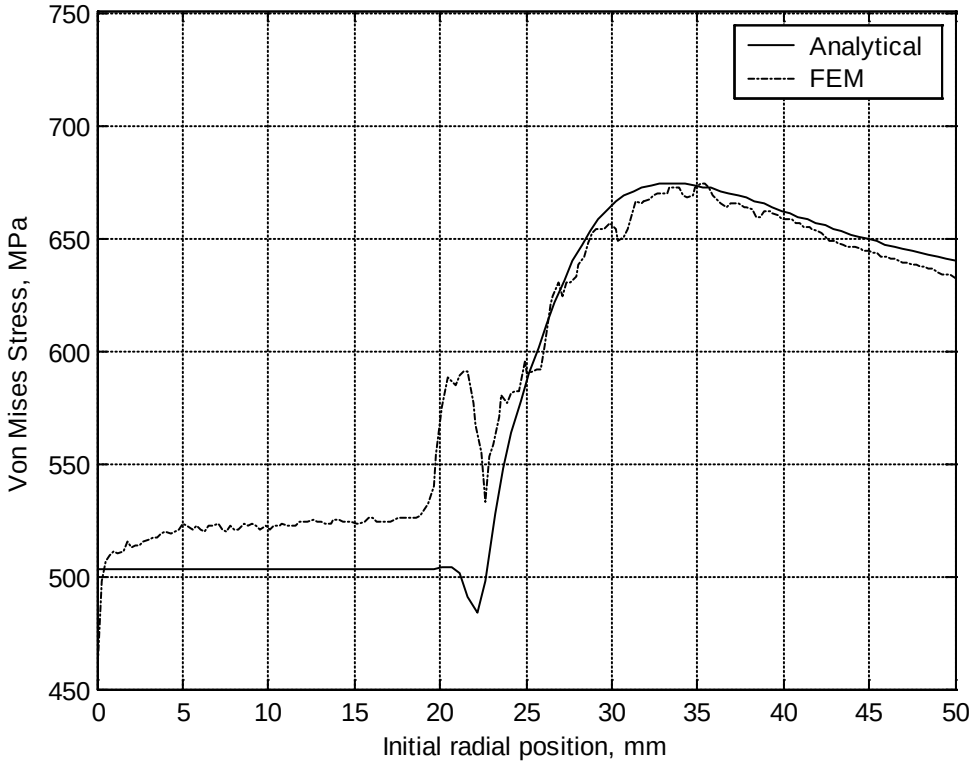

Fig. 5-16: Von Mises stress distribution at a punch travel of 16mm

The radial stress at the final stage of deformation for a punch travel of 27.5mm is shown in Fig. 5-17. There is a small difference but still acceptable between the two models in the die profile region. This difference in the radial stress increases in the cup wall to around 10%. Then, there is a very large difference between the results of the two models in the punch profile and punch bottom regions.

For the case of the circumferential stress shown in Fig. 5-18, there is a small difference of around 10% at the punch bottom. Also, the Von Mises stress shows a small difference at the punch bottom region which is around 5% as shown in Fig. 5-19. However, at the punch profile both the circumferential and Von Mises stresses obtained from the analytical model show large differences compared to those of the finite element model.

The differences between the analytical and finite element model for the strains and stresses at the punch profile and punch bottom imply that the analytical model suffers from numerical sensitivity. Thus, it can not accurately predict the results at these two regions. It is to be noted that most of the published work was limited to

show results up to the end of the cup wall. This suggests that similar differences in strains and stresses were encountered with other investigators.

The condition of the uniaxial stress at boundary (2) at the intersection between the cup wall and punch profile can be recognized from the circumferential stress distributions. At punch travel of 16mm, the circumferential stress shown in Fig. 5-15 has a zero value at an initial radius of around 27mm, which corresponds to boundary (2). The same occurs at punch travel of 27.5mm as shown in Fig. 5-18, where the circumferential stress is zero at an initial radial position of around 28mm. This condition of zero circumferential stress indicates a state of uniaxial stress ($\overline{\sigma} = \sigma_r$) at which necking is expected to initiate ([39] and [40]).

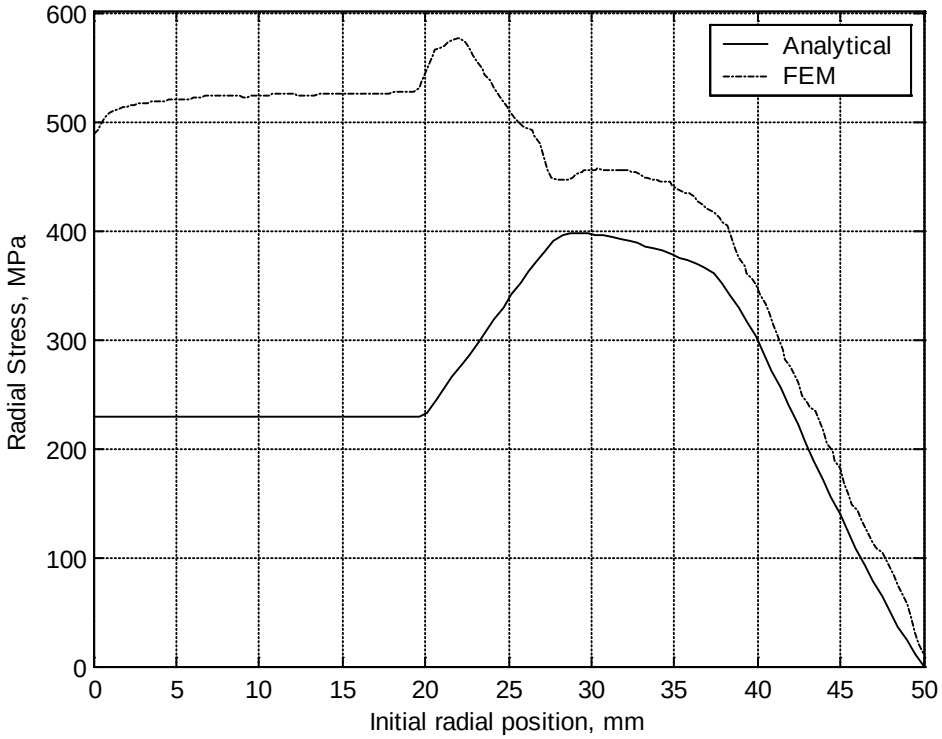

Fig. 5-17: Radial stress distribution at a punch travel of 27.5mm

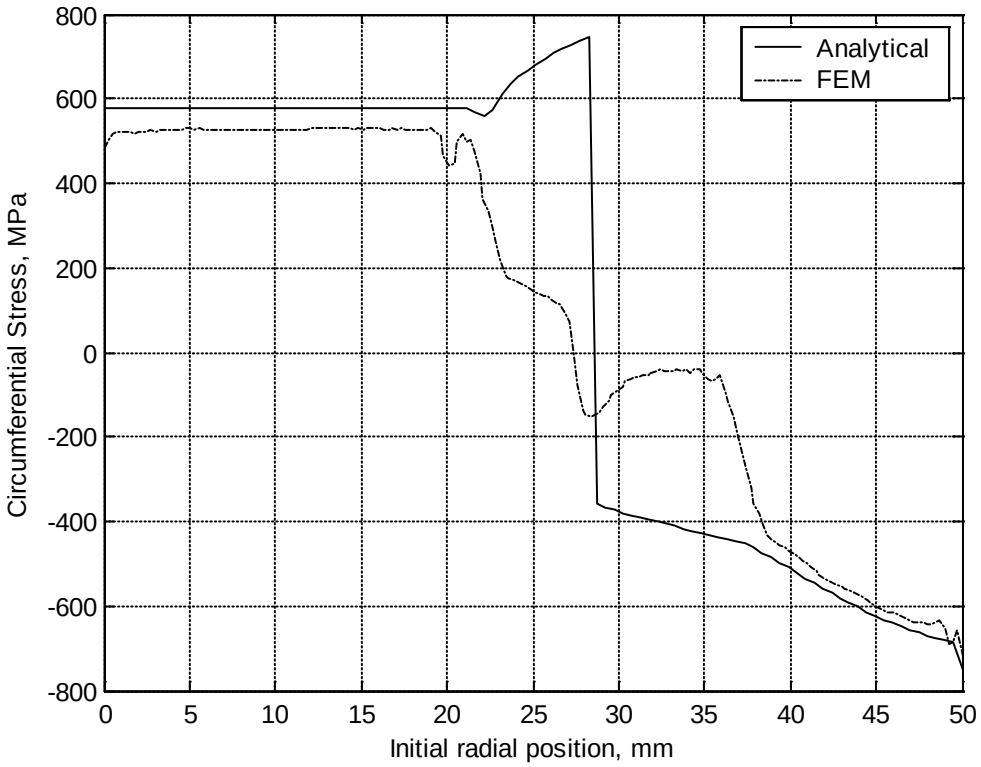

Fig. 5-18: Circumferential stress distribution at a punch travel of 27.5mm

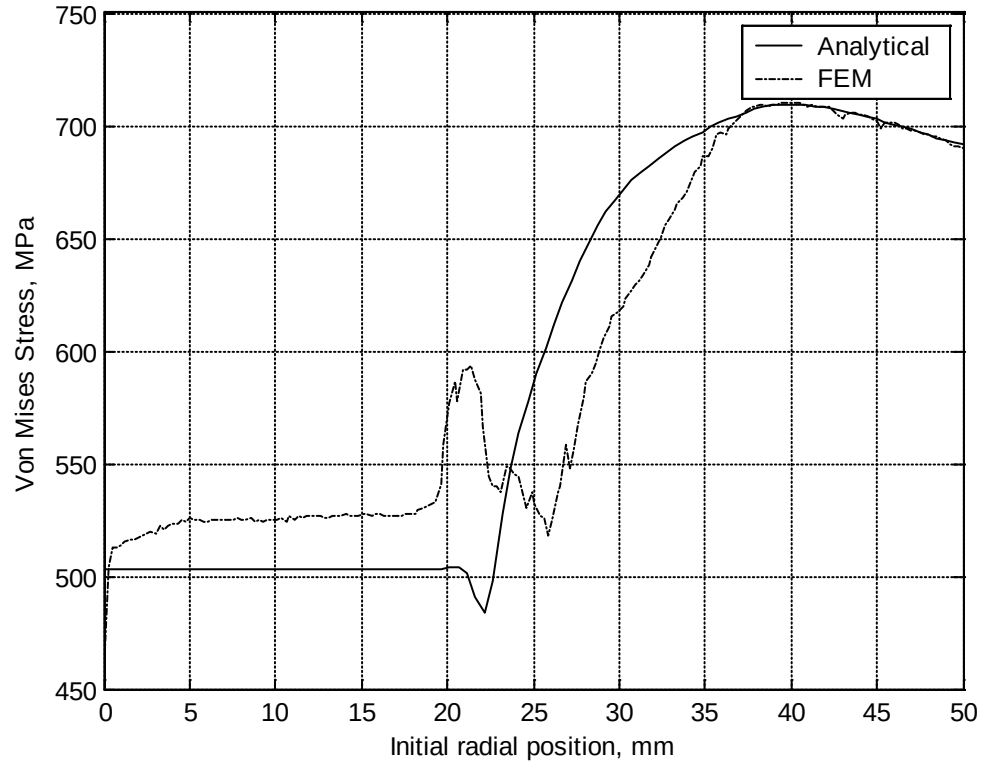

Fig. 5-19: Von Mises stress distribution at a punch travel of 27.5mm

5.2.5 Limitations and Advantages of the Analytical Model

As discussed in the previous section the apparent numerical sensitivity of the analytical solution near the punch profile and punch bottom indicates that the results there for strains and stresses might not be accurate enough. However, the results of both the analytical and finite element models in the flange, die profile, and cup wall show good agreement. Thus, the results of the analytical model can be used with confidence in these three regions. Fortunately the punch force is based on the radial stress at the die profile exist (boundary (1)) as indicated by equation (3.59). This is important since the BHF optimization objective is to minimize the maximum punch force.

Although the analytical model has some limitations, it is a very useful tool for the analysis of the cup drawing process. The main strengths of the analytical model are described in the following points.

1. The model can be useful in conducting parametric studies on the different parameters affecting the process including die design, process and material parameters. Compared to the finite element model, the analytical model requires less calculation time. The calculation time in the analytical model depends on the size of the cup, where the calculation time is directly proportional to the initial blank diameter. In fact, the cup considered in the previous analysis required 30 seconds on a 2.5GHz processor to solve up to the final stage. On the other hand, the calculation time for the finite element model was 10minutes on the same computer. Thus, the analytical model requires only 5% of the time taken in the finite element analysis. This relatively less computation time means that one can carry out several runs for different parameters in less time than the finite element model.
2. The value of the suitable blank holder force (BHF) is usually unknown before hand. Experimental testing is performed to determine the appropriate BHF that avoids process limits of wrinkling and tearing, which requires time and money. On the other hand, since optimization of the BHF requires hundreds of runs, it would probably require a month to determine the optimum BHF using finite elements. The analytical model can be useful in this respect, where it can be used as the analysis tool in the optimization process as will be shown in the results of

section 5.4. Also, the integration of an optimization search algorithm with a finite element package like ABAQUS is tedious since ABAQUS is a standalone program. However, the analytical model can be easily integrated with an optimization algorithm as suggested in chapter 4. Moreover, the effort for the input data in the analytical model is trivial compared to the finite elements. Of course, the finite element method has the edge on the analytical model whenever the interest is on the details of strains and stresses distributions especially for the thickness strain.

3. The analytical model is useful as an analysis tool in the design of any cup drawing process. It can be used as a server to perform a preliminary analysis to predict the stresses and strains induced in the deforming cup and determine the suitable parameters that give the least strains. Then, a more accurate finite element analysis can be carried out for the cup with these suitable parameters. This can be followed by a full scale experimental work to verify the numerical results.

5.3 Parametric Study

The developed analytical model is useful in predicting the effect of any of the die, process and material parameters on the stresses and strains induced into the deforming sheet. In order to find out the capability of the model, a parametric study is performed on the AL7075-T6 cup shown in Fig. 3-21 with the variation of the following parameters:

- Die profile radius (ρ_d)
- Punch profile radius (ρ_p)
- Drawing ratio (B_0)
- Coefficient of friction with the die surface (μ_D)
- Blank holder force (F_{BH})

5.3.1 Effect of the Die Profile Radius

The die profile radius is investigated at values of 6, 8, 10, 12, and 14mm. The effect of the die profile on the punch travel - punch force curve is shown in Fig. 5-20. For the early stages of deformation, the punch travel-punch force curve shifts to the right with the increase in the die profile radius. After reaching the maximum punch

force, the punch travel – punch force curve corresponding to a certain die profile radius coincides with curves of smaller die profile radii. The maximum punch force at each case decreases as die profile radius increases. This is shown in Fig. 5-21, where the die profile radius vs. maximum punch force relation shows a nearly linear relation. This relation can be approximated with the following linear equation:

$$\left(F_p\right)_{\max} = k_0 + k_1\rho_d \tag{5.1}$$

Where, k_0 and k_1 are constants that differ according to the cup geometry, loading and material properties. For the AL7075-T6 cup used in the present study, the equation is:

$$\left(F_p\right)_{\max} = 80.22 - 0.7\rho_d \quad \text{(kN)} \tag{5.2}$$

This equation can be useful in predicting the maximum punch force for any value of the die profile radius. This finding confirms the work of Moshksar and Zamanian [48], who carried out experimental work, but on a different cup and found that the relation between the die profile radius and maximum punch force is nearly linear for different drawing ratios.

The decrease in the die profile radius induces more radial stress in the die profile region, which propagates to the cup wall and punch profile regions. Thus, it is expected to have more thinning in the deforming sheet due to the decrease in the die profile radius. This is shown in the thickness strain distribution for different die profile radii in Fig. 5-22. The maximum thinning is around 3.5% at ρ_d = 6mm and decreases to around 2.6% at ρ_d = 14mm as shown in Fig. 5-23. Chung and Swift [1] performed experimental testing on different cups and noticed the same effect of the die profile radius.

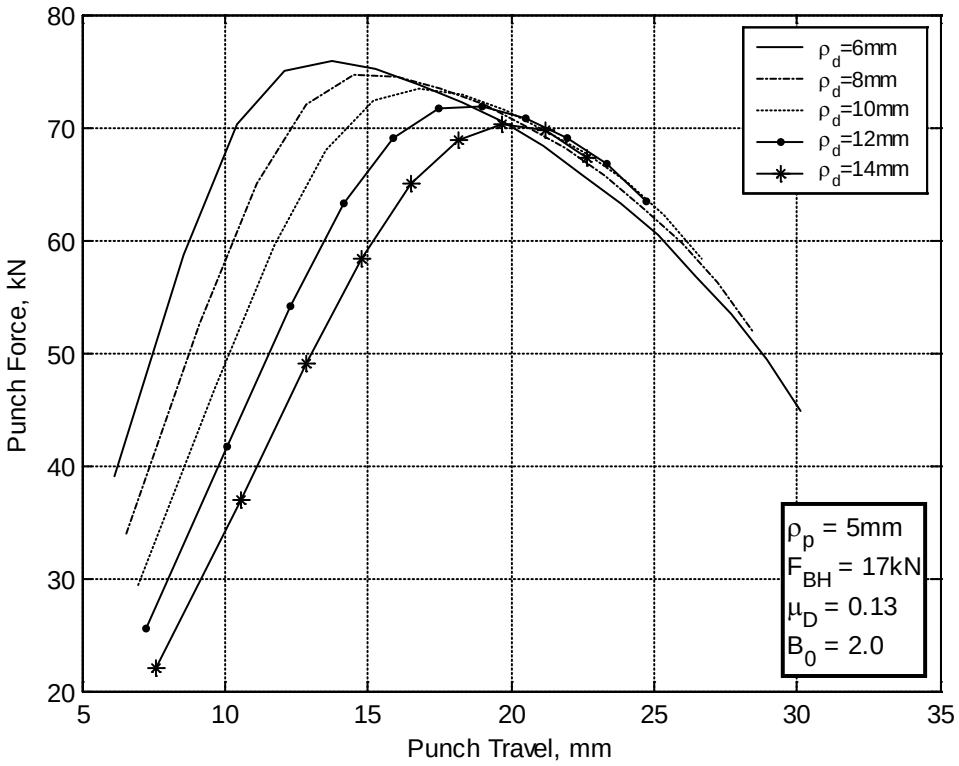

Fig. 5-20: Effect of the die profile radius on the punch force

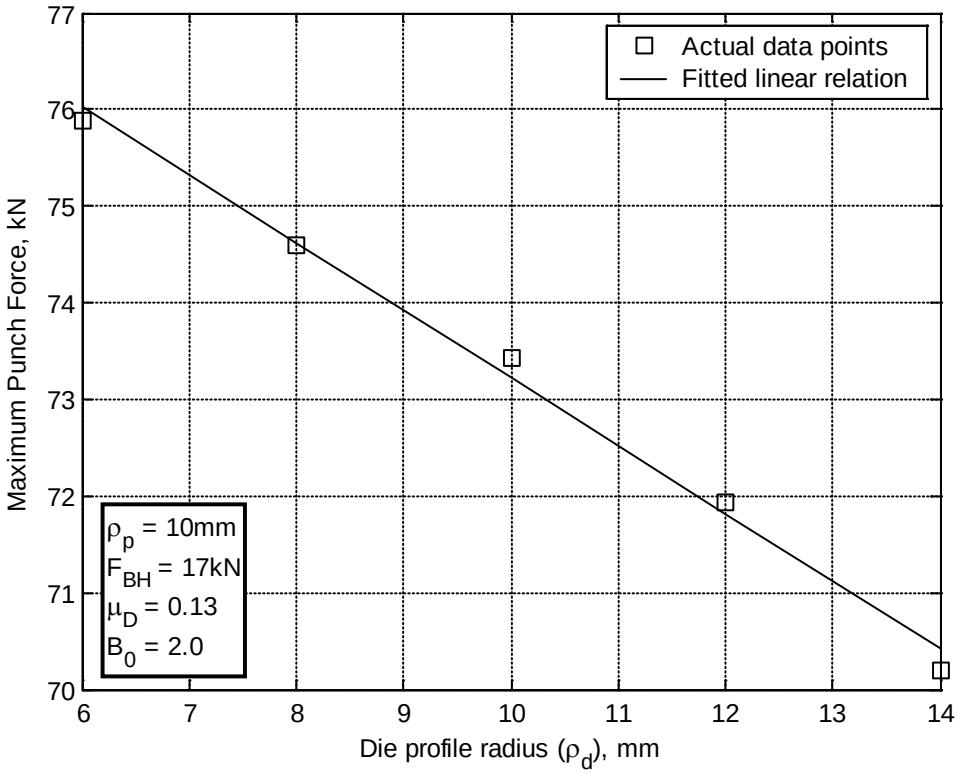

Fig. 5-21: Effect of the die profile radius on the maximum punch force

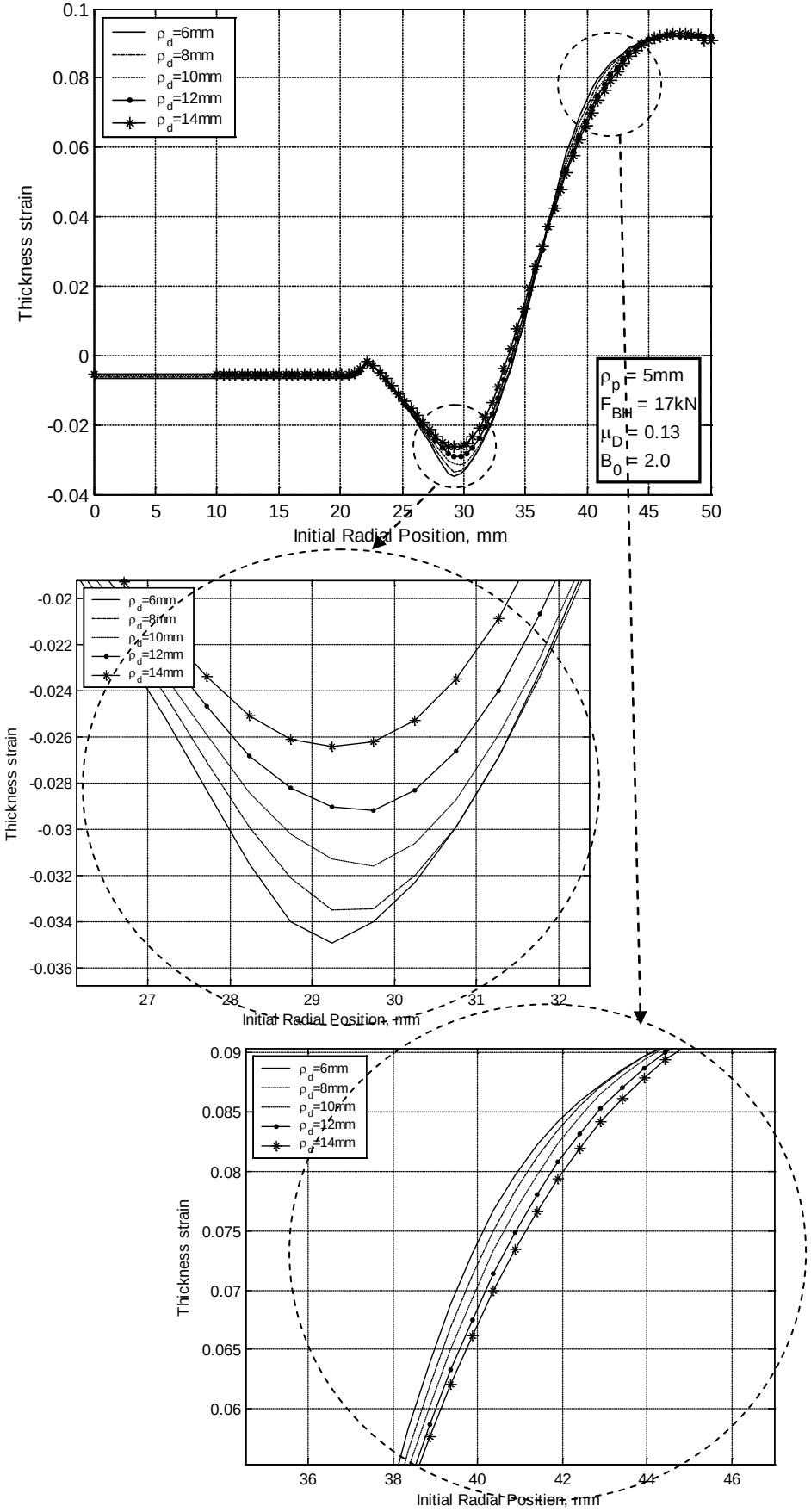

Fig. 5-22: Effect of the die profile radius on the thickness strain distribution

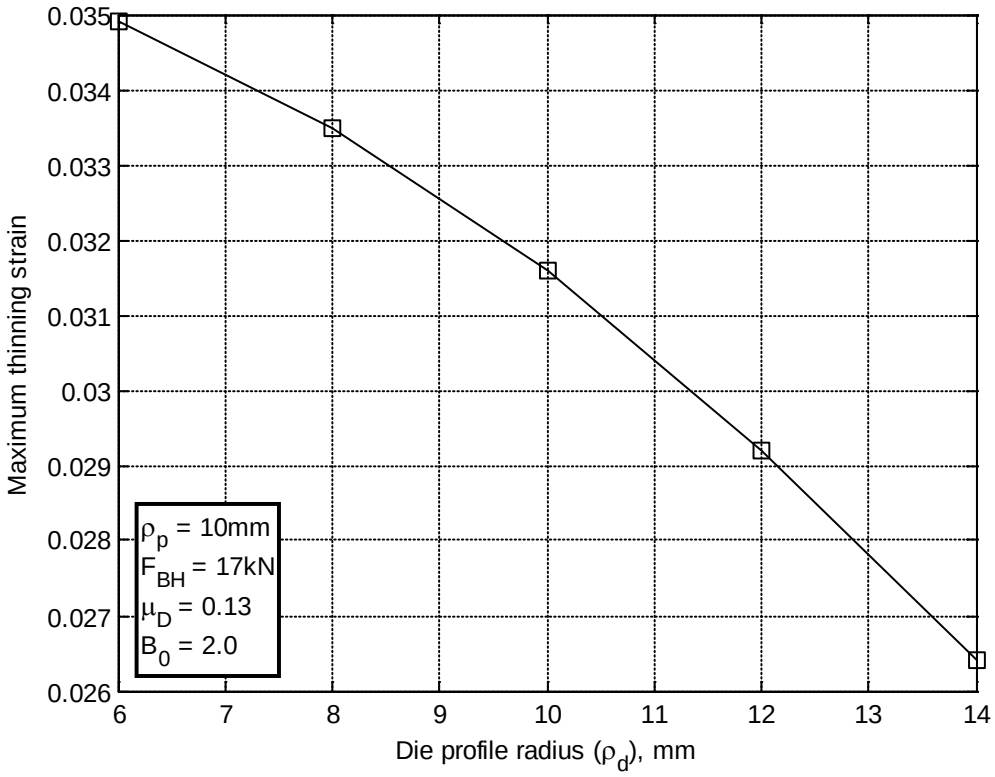

Fig. 5-23: Effect of the die profile radius on the maximum thinning strain

5.3.2 Effect of the Punch Profile Radius

The punch travel – punch force curve is shown in Fig. 5-24 for different punch profile radii. By increasing the punch profile radius, the curve shifts to the right with a more gradual rise and longer punch stroke. However, the maximum punch force slightly decreases by increasing the punch profile radius as shown in Fig. 5-25. This agrees well with the investigations carried out by Chung and Swift [1] and Moshksar and Zamanian [48].

As for the thickness strain, it is shown in Fig. 5-26, that more thinning occurs at the punch bottom as the punch profile radius increases. This agrees well with Chung and Swift [1] investigations. According to their studies, the maximum thinning strain decreases with increasing punch profile radius until a point at which thinning starts increasing again. Considering Fig. 5-27, it can be noticed that the maximum thinning strain decreases from ρ_p=5mm to ρ_p=8mm and then increases back with the increase in the punch profile radius.

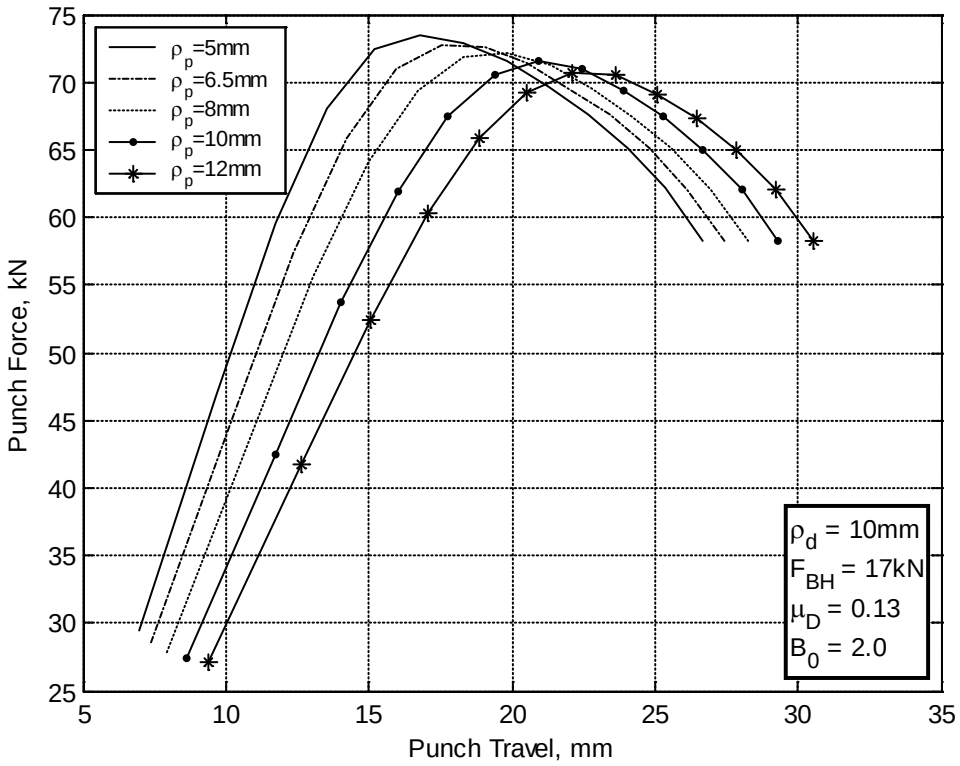

Fig. 5-24: Effect of the punch profile radius on the punch force

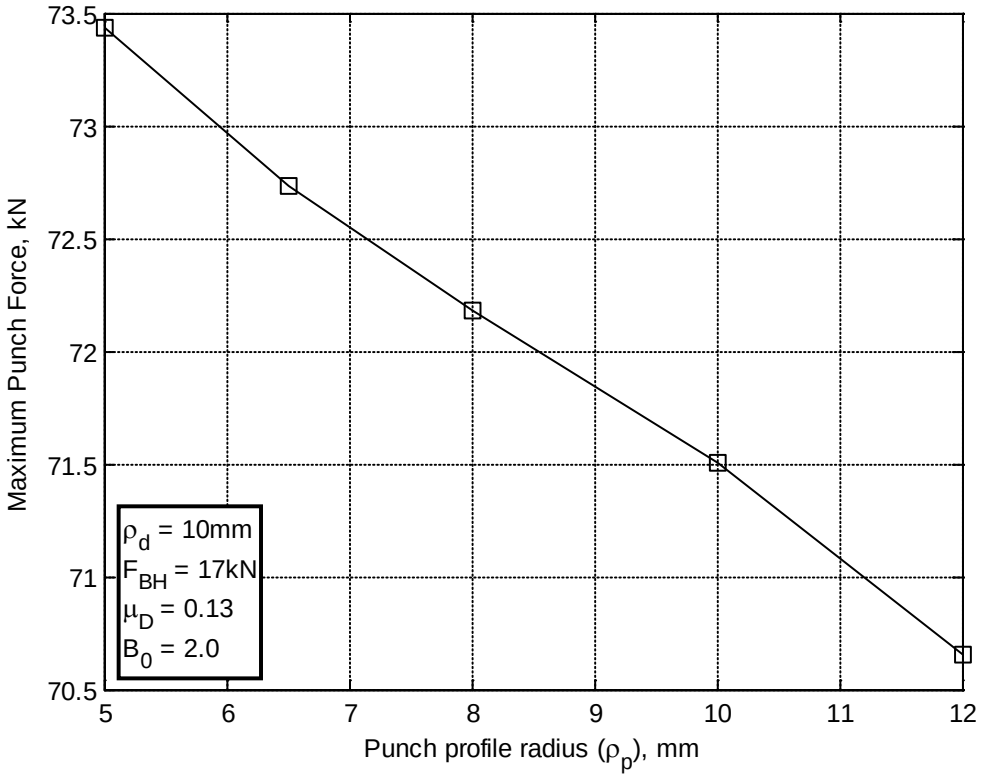

Fig. 5-25: Effect of the punch profile radius on the maximum punch force

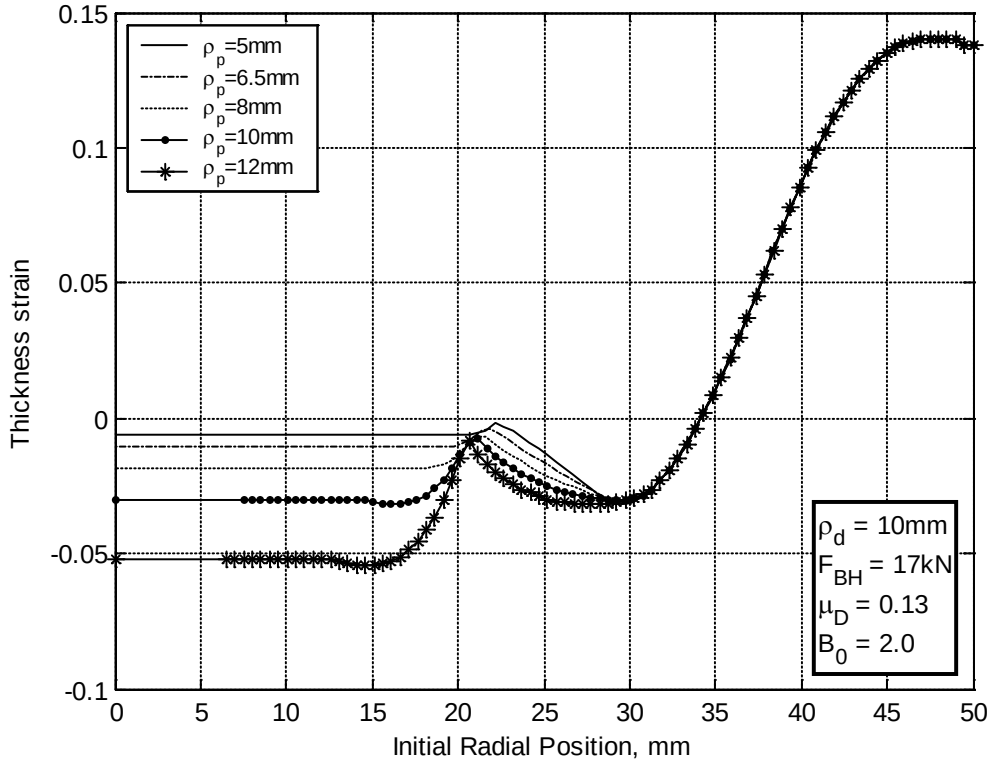

Fig. 5-26: Effect of the punch profile radius on the thickness strain distribution

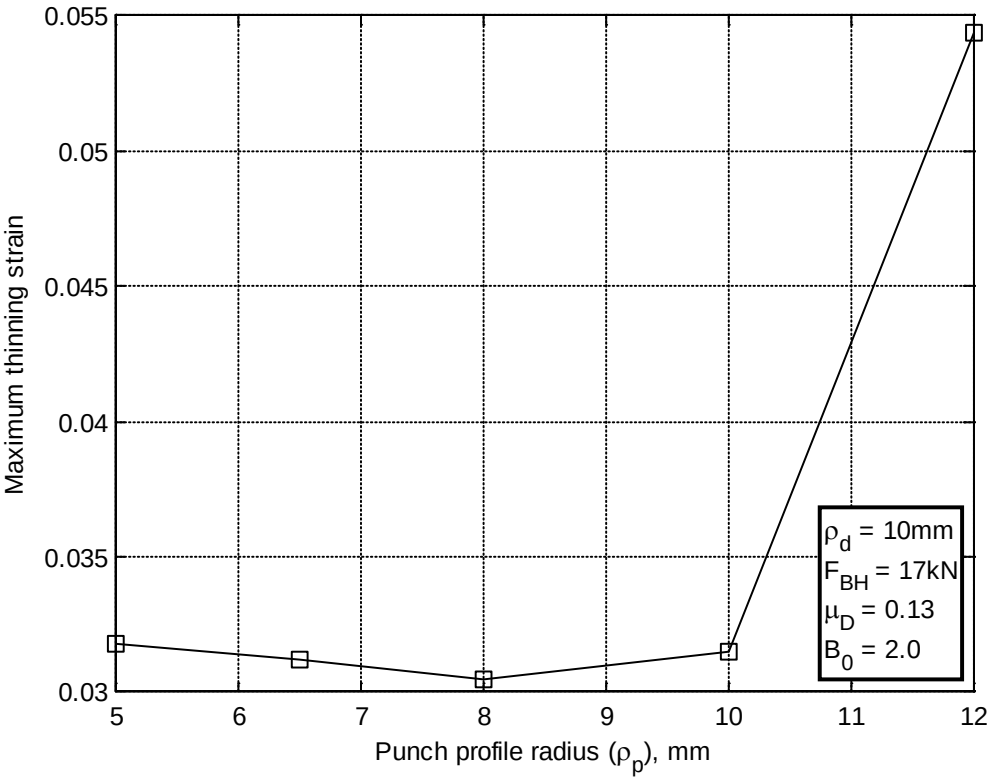

Fig. 5-27: Effect of the punch profile radius on the maximum thinning strain

5.3.3 Effect of the Blank Holder Force

The blank holder force is investigated at values of 5, 17, 30, 45, and 60kN. Punch force is proportional to the radial stress in the flange. By increasing the blank holder force, radial stress increases, thus increasing punch force. The punch travel – punch force curve shifts upward as the BHF increases as shown in Fig. 5-28. Thus, the maximum punch force increases from 71kN at F_{BH} = 5kN to around 82kN at F_{BH} = 60kN which is shown in Fig. 5-29.

The increase in the radial stress in the material due to the increase in the BHF causes more thinning at the cup wall and punch bottom as shown in Fig. 5-30. Also, less thickening in the flange occurs since the normal BHF acting on the flange restrains its thickening. The relation between the BHF and the maximum thinning strain shows a linear trend up to 30kN as shown in Fig. 5-31. Then, the slope changes slightly after that, which suggests that the rate of thinning increases as the BHF increases.

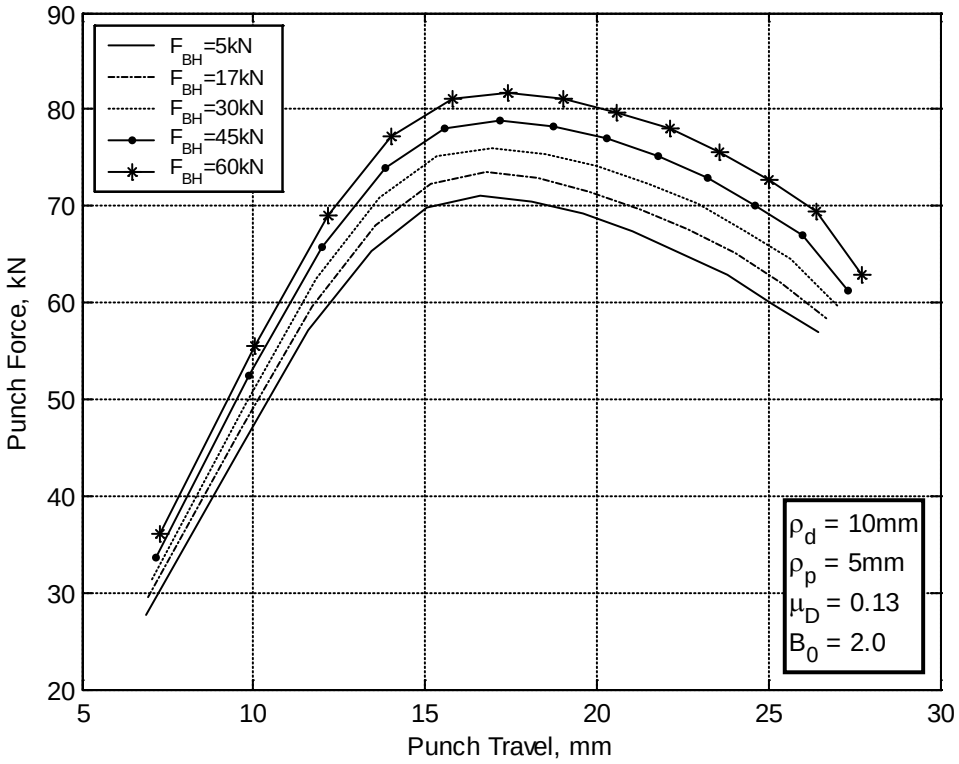

Fig. 5-28: Effect of the blank holder force on the punch force

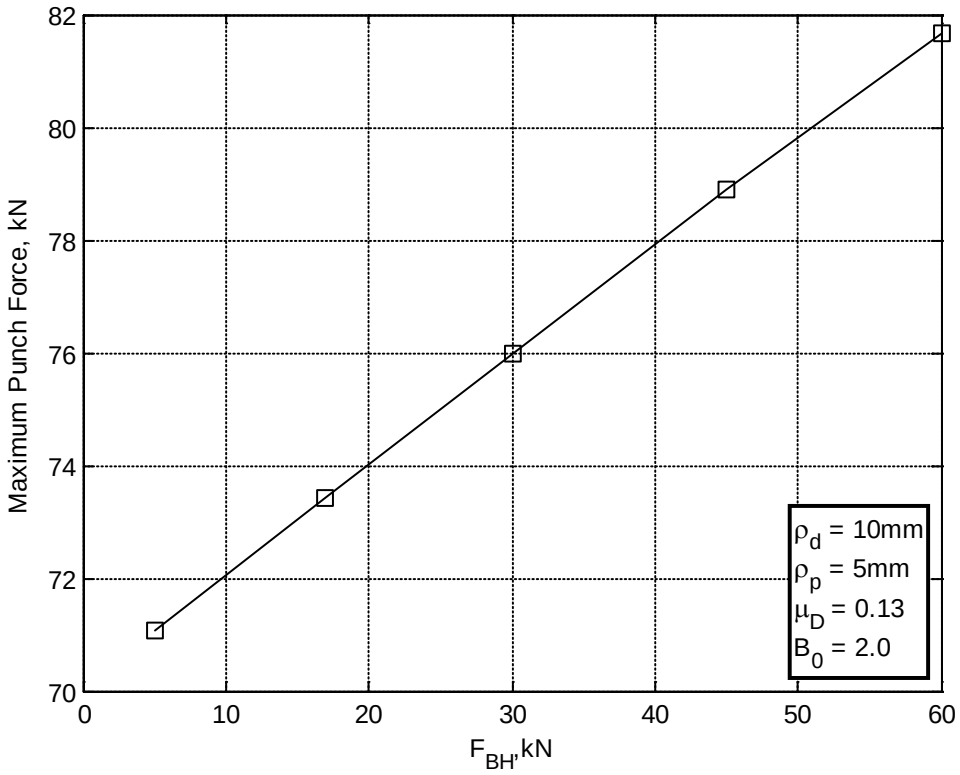

Fig. 5-29: Effect of the blank holder force on the maximum punch force

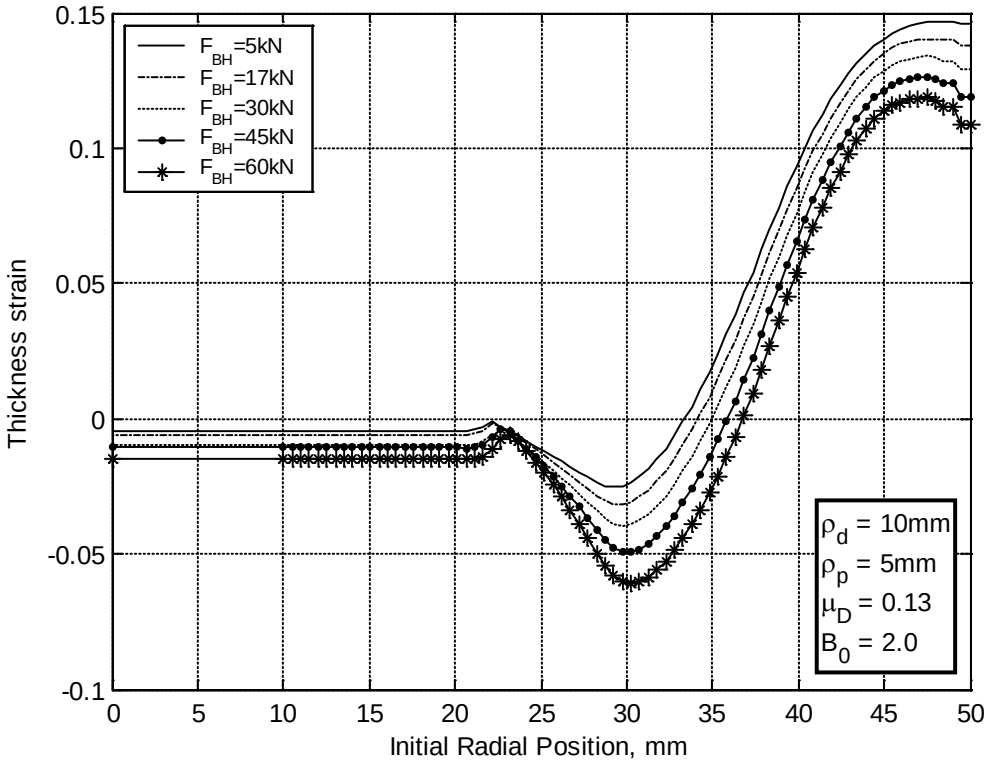

Fig. 5-30: Effect of the blank holder force on thickness strain distribution

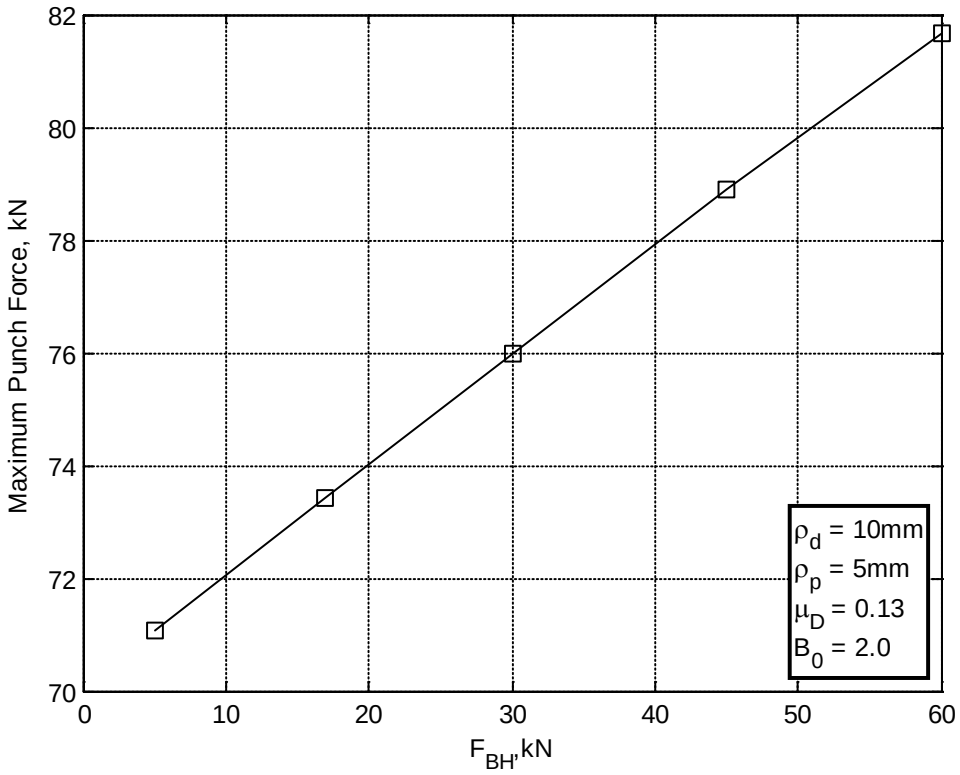

Fig. 5-31: Effect of the blank holder force on maximum thinning strain

5.3.4 Effect of the Die Coefficient of Friction

The die coefficient of friction (μ_D) effect is investigated at values of 0.045, 0.06, 0.08, 0.1, and 0.13. The die coefficient of friction has direct impact on the punch force. It is shown in Fig. 5-32 that by increasing the coefficient of friction, the punch travel – punch force curve is shifted upwards at the later stages of deformation. However, at the early stages, up to a punch travel of 10mm, little difference is noticed. The relation between the die coefficient of friction and the maximum punch force is investigated for the drawing ratios of 1.9, 1.95, 2.0, 2.1, and 2.2 as shown in Fig. 5-33. The relation shows a linear trend with nearly the same increasing slope for all drawing ratios. Thus, it is possible to fit linear functions for those relations which take the following form:

$$(F_p)_{max} = a_0 + a_1 \mu_D \quad (kN)$$

Where, a_0 and a_1 are the intercept and slope of the maximum punch force function in terms of the die coefficient of friction (μ_D)

The fitted linear relations for each drawing ratio are shown in

Table 5-1.

Table 5-1: Linear relations for the die coefficient of friction vs. punch force

Drawing ratio (B_0)	**Maximum punch force relation with the die coefficient of friction**
1.9	$(F_p)_{max} = 51.7 + 108\ \mu_D$
1.95	$(F_p)_{max} = 55.2 + 111.1\ \mu_D$
2.0	$(F_p)_{max} = 58.5 + 114.4\ \mu_D$
2.1	$(F_p)_{max} = 64.7 + 120.8\ \mu_D$
2.2	$(F_p)_{max} = 70.5 + 123.9\ \mu_D$

An average slope of these five relations is found to be 115.6. The intercept (a_0) is found to have a nearly linear relation with the drawing ratio as shown in Fig. 5-34. Thus, a linear function can be deduced to describe the relation between the drawing ratio and the intercept (a_0) as follows:

$$a_0 = -66.7 + 62.5\ B_0$$

Therefore, the previous five linear relations can be written as one approximate function as follows:

$$(F_p)_{max} = -66.7 + 62.5\ B_0 + 115.6\ \mu_D \quad (5.3)$$

The thickness strain distributions for the different die coefficients of friction are shown in Fig. 5-35. By increasing the coefficient of friction, more thinning occurs at the cup wall. As for the maximum thinning strain relation with the die coefficient of friction, it is shown in Fig. 5-36 that the relation is nearly linear for different drawing ratios. However, it tends to have a higher rate of increase as the coefficient of friction increases.

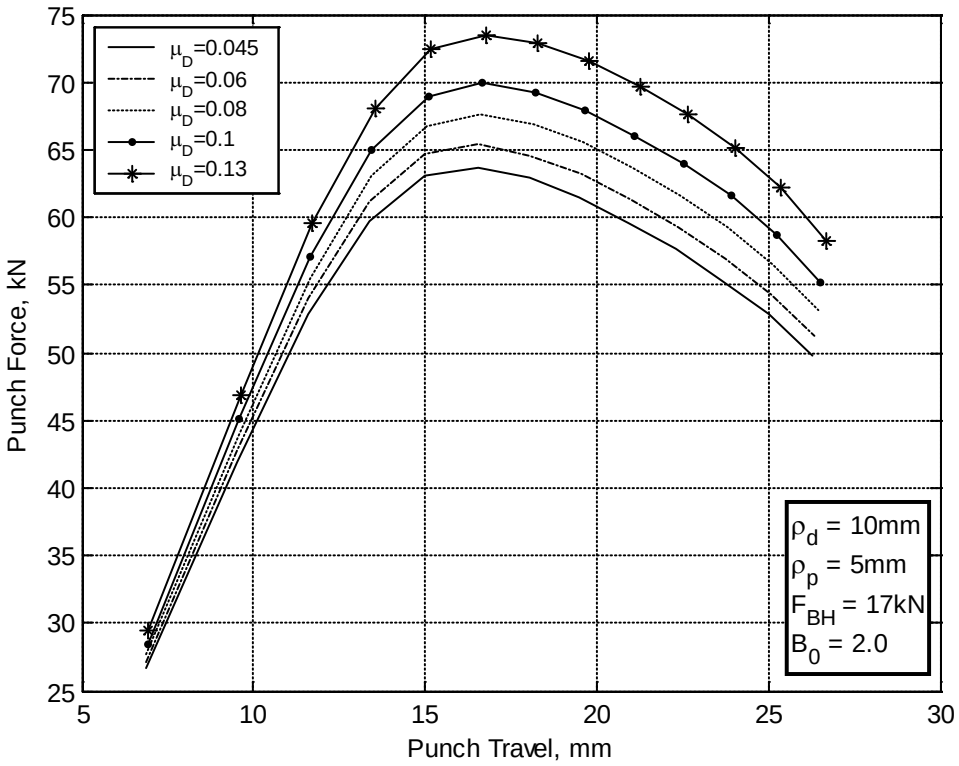

Fig. 5-32:Effect of the die coefficient of friction on the punch force

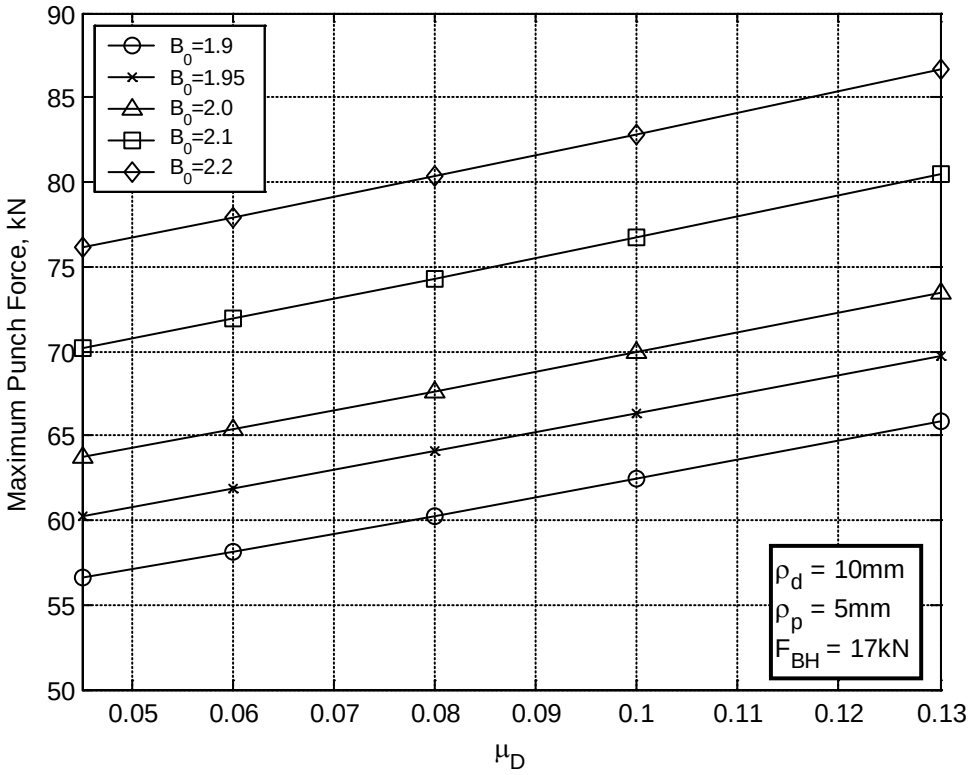

Fig. 5-33: Effect of the die coefficient of friction on the maximum punch force

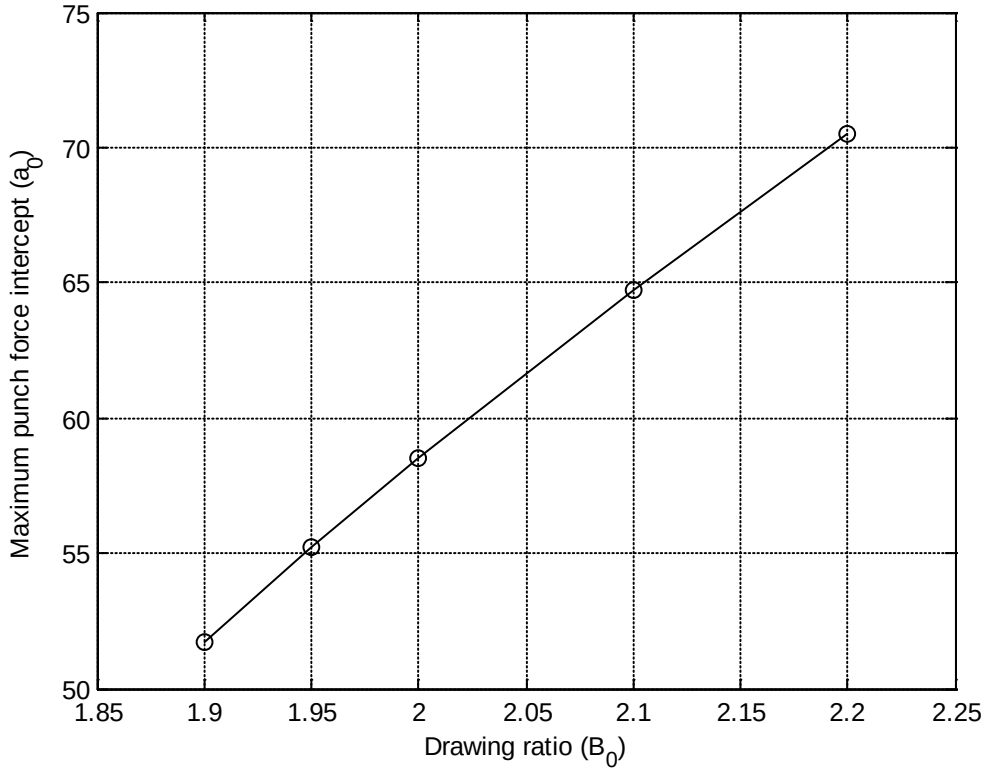

Fig. 5-34: Relation between drawing ratio and maximum punch force intercept

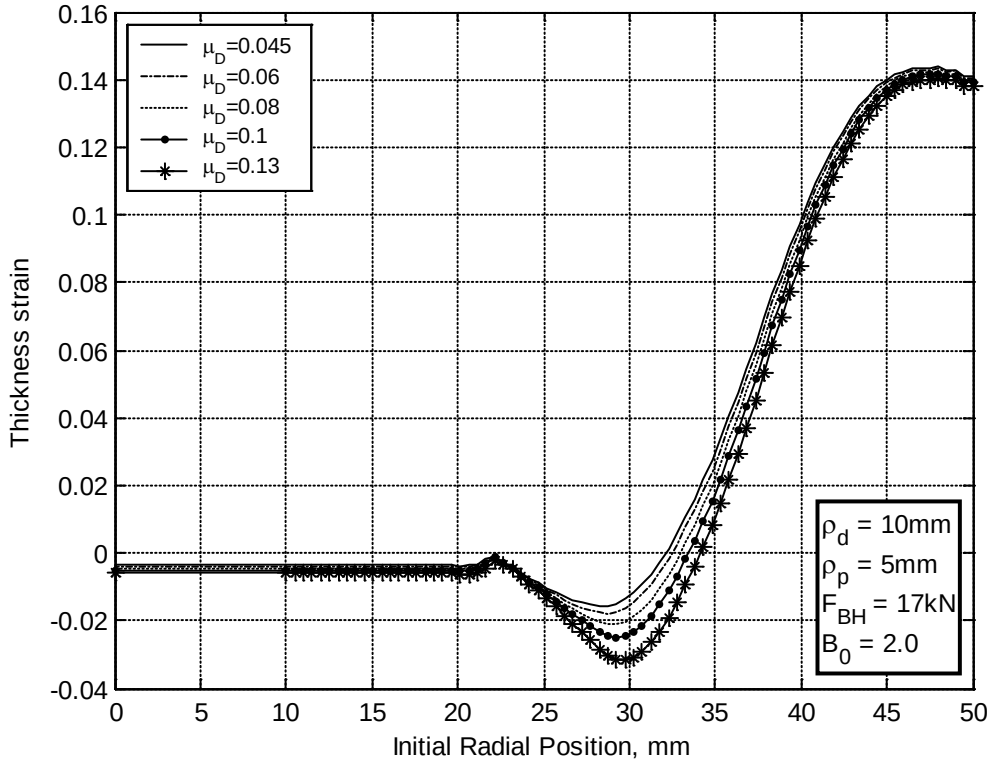

Fig. 5-35: Effect of the die coefficient of friction on the thickness distribution

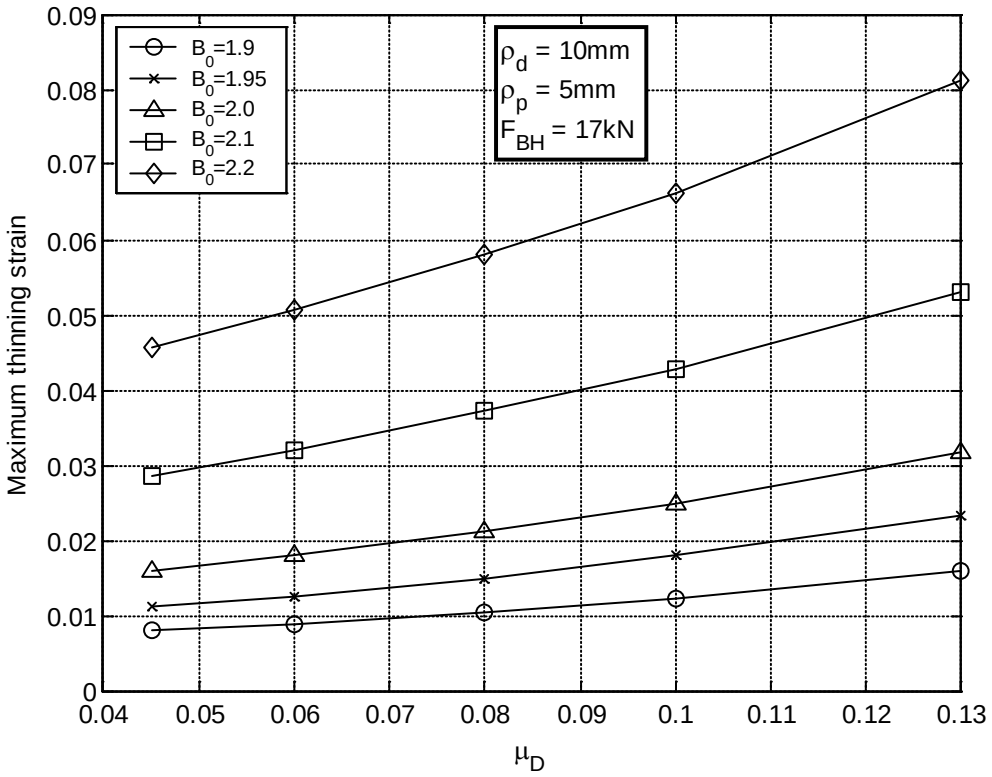

Fig. 5-36: Effect of the die coefficient of friction on the maximum thinning strain

5.3.5 Effect of the Drawing Ratio

Deep drawing blanks with larger diameters induce larger stresses in the sheet, therefore limiting the zone through which an acceptable BHF can operate. The increase in the radial stress in the cup wall increases the punch force and the punch stroke as shown in the Fig. 5-37. Also, the large drawing ratio increases the punch travel in a linear trend as shown in Fig. 5-38 for different die coefficient of friction. This confirms the investigation of Korhonen **[51]** who mentioned, based on experimental testing, that the ratio between the drawing forces to blank diameter is very close to being linear. Also, Chung and Swift [1] found that for any given drawing conditions, the punch load increases with the drawing ratio in an approximately linear manner over the whole useful range with a slight tendency to drop near the limiting drawing ratio, which can be recognized from Fig. 5-38. The relation can still be approximated with equation (5.3).

The thickness strain is found to increase for either thinning or thickening as the drawing ratio increases, which is shown in Fig. 5-39. The rate of increase of the maximum thinning strain with the drawing ratio is nearly polynomial as shown in Fig.

5-40. Also, this rate of increase is higher for larger values of the die coefficient of friction.

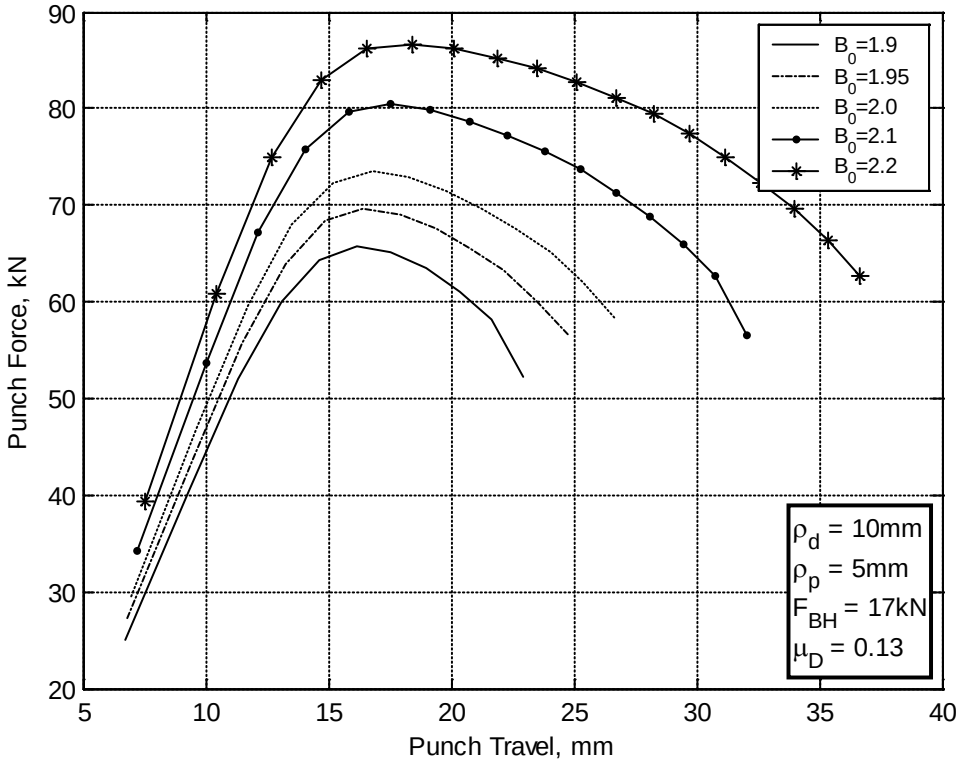

Fig. 5-37: Effect of the drawing ratio on the punch force

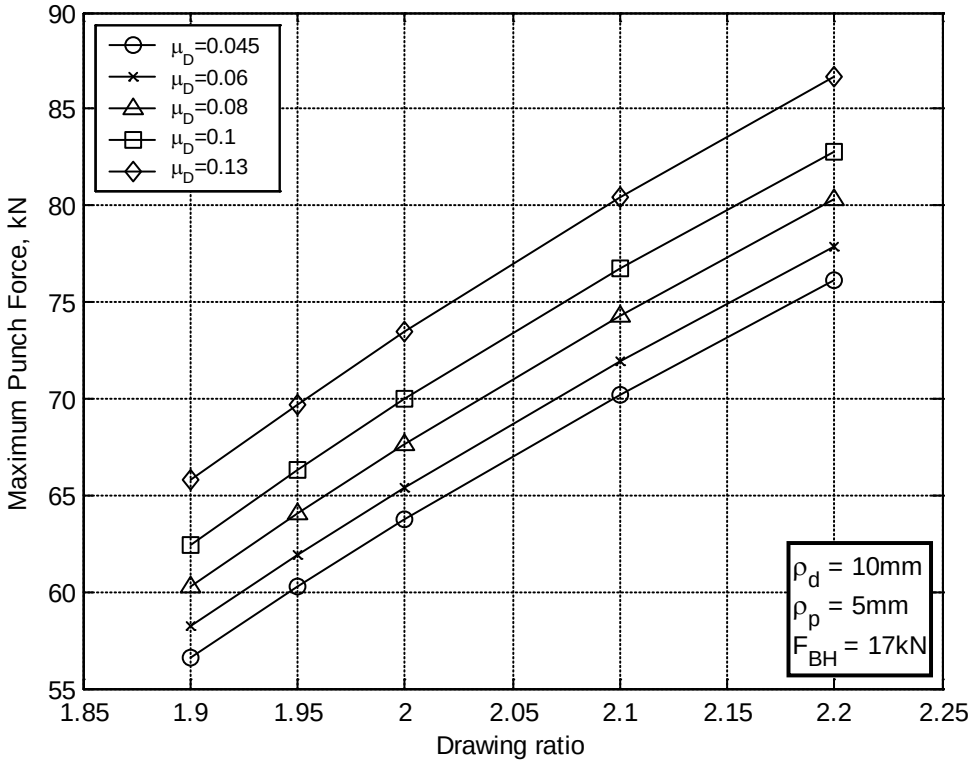

Fig. 5-38: Effect of the drawing ratio on the maximum punch force

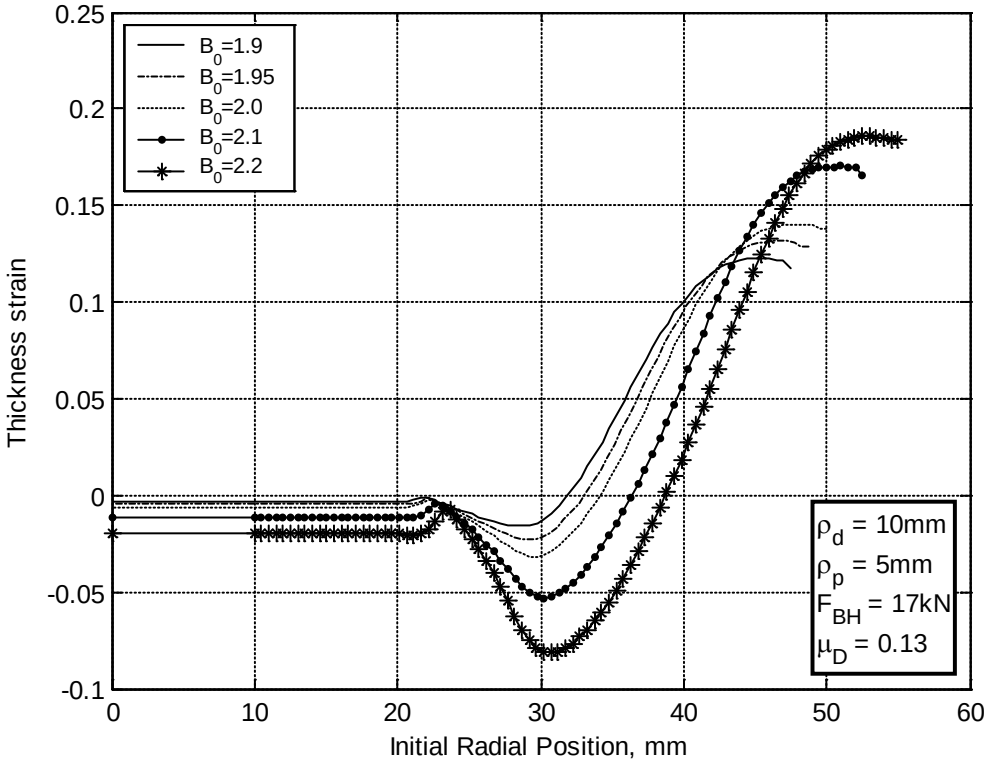

Fig. 5-39: Effect of the drawing ratio on the thickness strain distribution

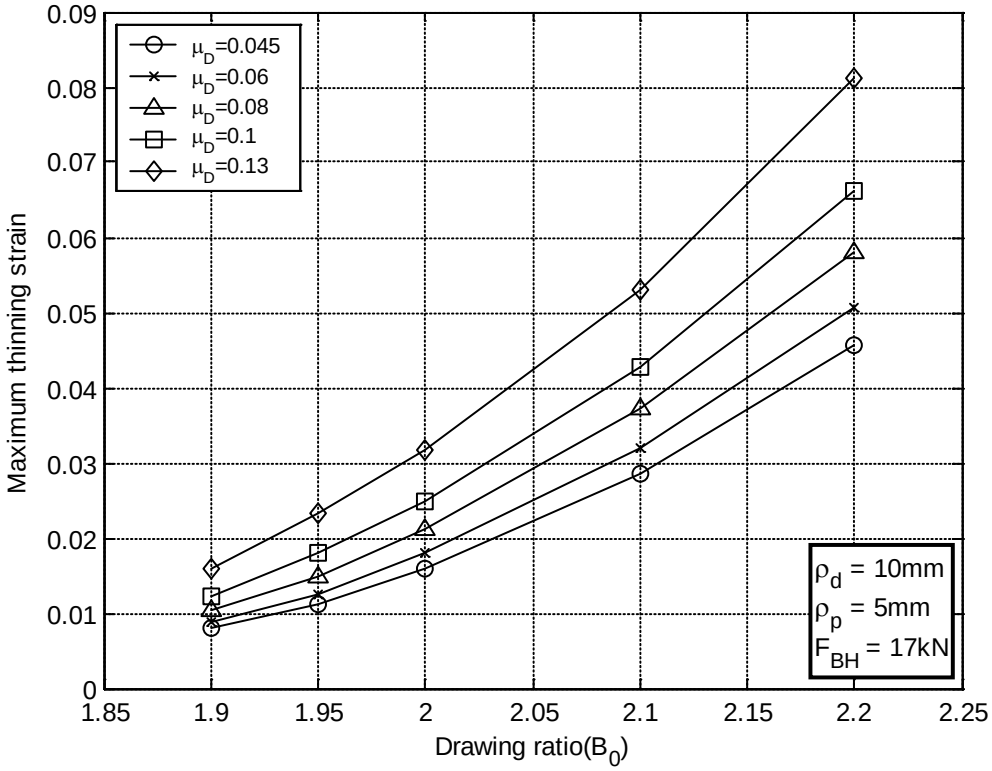

Fig. 5-40: Effect of the drawing ratio on the maximum thinning strain

To conclude this section, it is evident that the developed analytical model is capable of investigating the process of cup forming in an acceptable manner that agrees with known observations and investigations. This is an encouraging result which indicates that the model can be used in the optimization process as will be shown in the next section.

5.4 Modeling with Optimized Blank Holder Force Scheme

The objective of the optimization process, as mentioned in chapter 4, is to find the suitable BHF linear function that gives the least maximum punch force, while avoiding the process limits.

5.4.1 Cup Drawing with Constant BHF versus Linear BHF Scheme

The cup used in the verification of the analytical model in section 5.1 is now considered for the BHF scheme optimization. The optimized scheme is compared with the constant 100kN BHF given by the experimental results of Saran et al. [24]. The optimum BHF scheme for this cup is shown in Fig. 5-41, which has the following relation:

$F_{BH} = 4.64 + 1.09\ L$ (kN) , L in mm

The comparison between the constant BHF and the linear BHF schemes is shown in Fig. 5-42 using the analytical model. It can be recognized that the use of the linear BHF scheme decreased the punch force over all stages. At the maximum value of the punch force at a punch travel of around 42mm, the punch force decreased from 82.6kN to 77.9kN (5.78%). Similar decrease was also indicated by the results from the finite element model of the same problem as shown in Fig. 5-43. The maximum punch force decreased from 84.7kN to 81kN (4.37%).

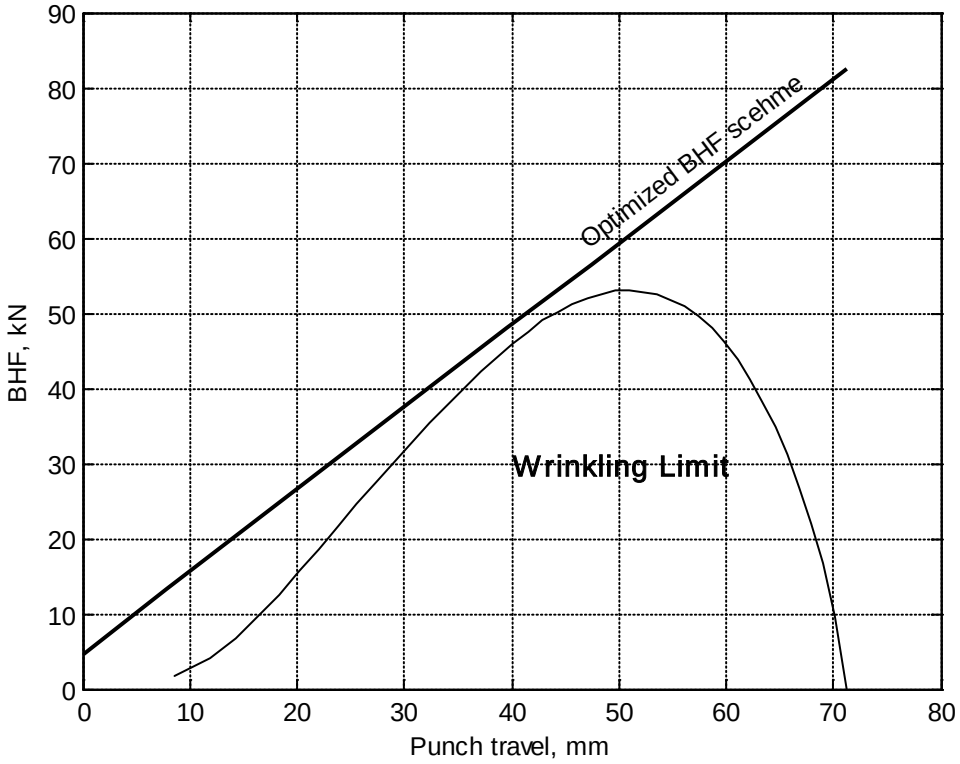

Fig. 5-41: BHF scheme for the experimental cup

The thickness strain distribution for the two cases of constant and linear BHF schemes is shown in Fig. 5-44 using the analytical model. It is evident that the maximum thinning has decreased by using the optimized linear BHF scheme. It decreased from a value of -0.158 to -0.123 (21.97%). The same is true with the finite element model results shown in Fig. 5-45 where the maximum thinning strain decreased from a value of -0.231 to -0.178 (22.94%). This decrease in thickness strain provides a more uniform thickness at the punch bottom which is a major requirement in the cup forming process. Table 5-2 shows the reduction in the punch force and the thinning strain due to the use of the linear BHF.

Table 5-2: Reduction in punch force and maximum thinning strain

Output parameter	**Analytical Model**	**FEM**
Percentage decrease in the Punch Force	5.78	4.37
Percentage decrease in the maximum thinning strain	21.97	22.94

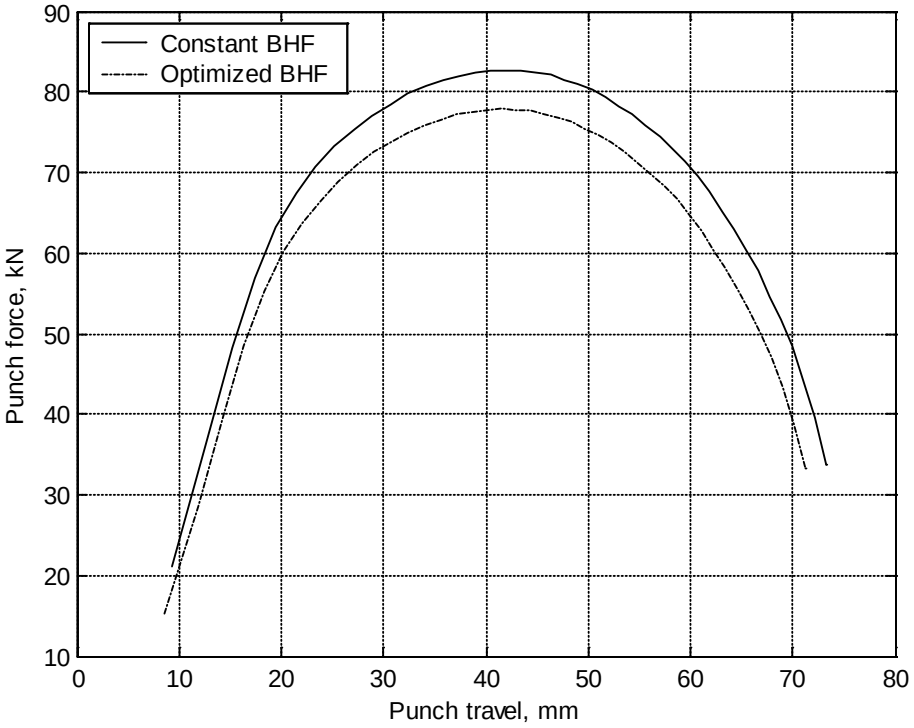

Fig. 5-42: Punch travel vs. punch force in the analytical model

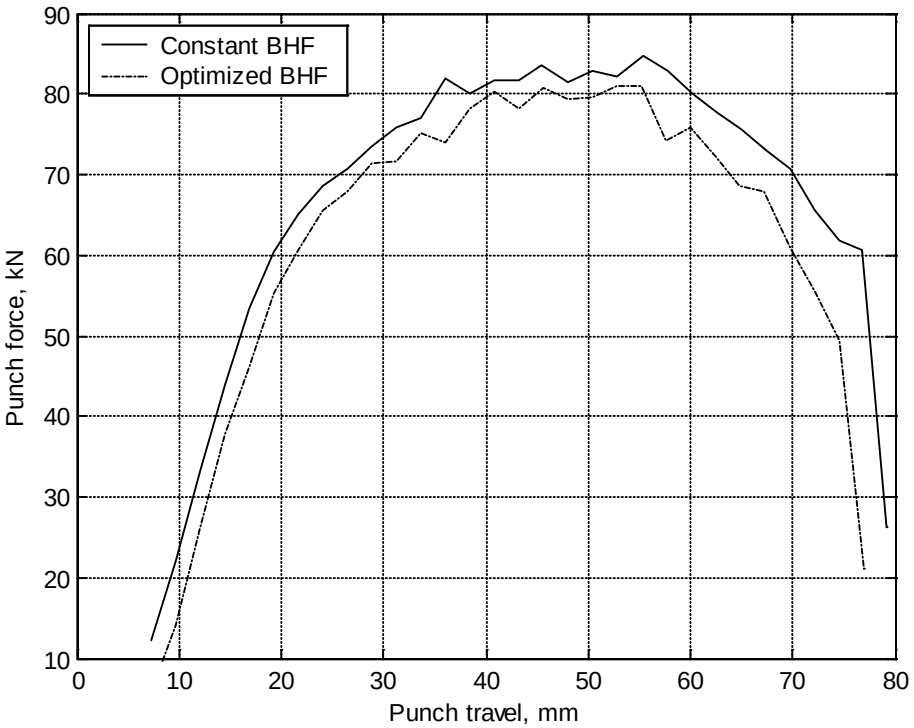

Fig. 5-43: Punch travel vs. punch force in the finite element model

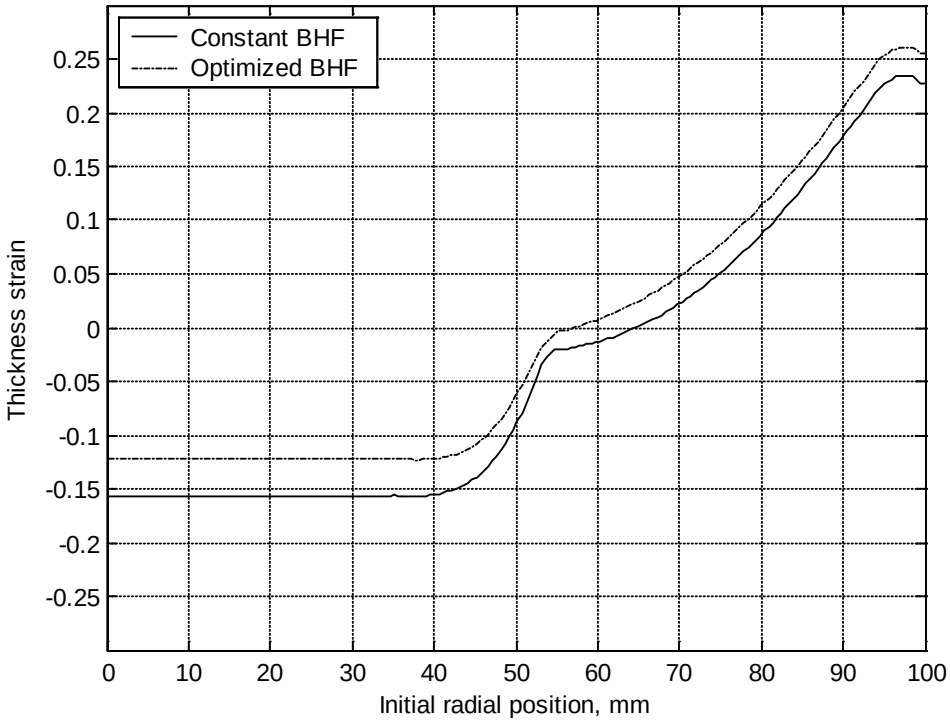

Fig. 5-44: Thickness strain distribution in the analytical model

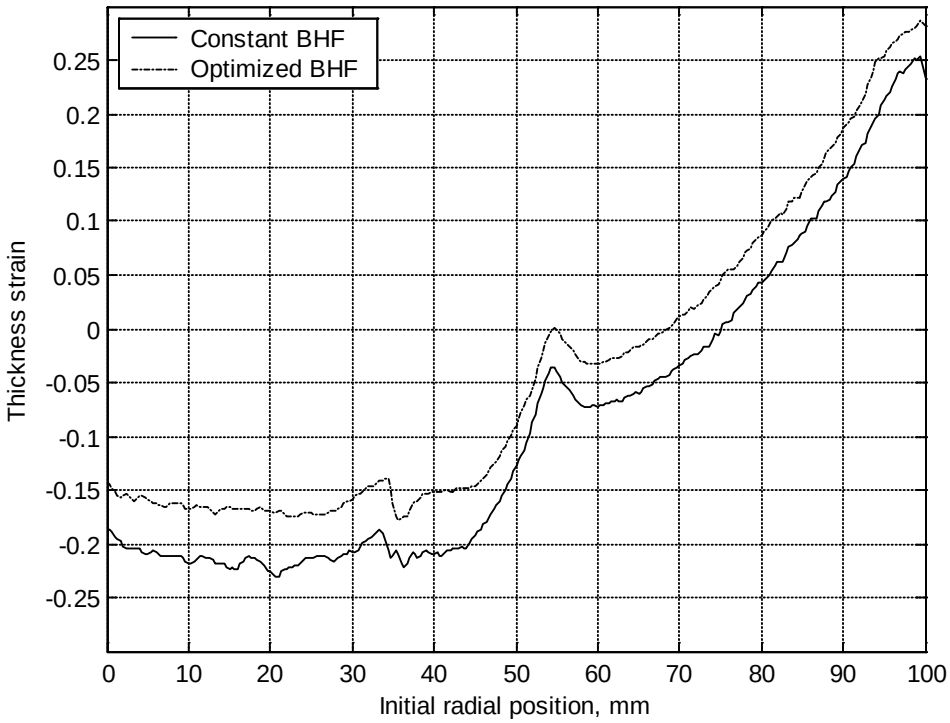

Fig. 5-45: Thickness strain distribution in the finite element model

5.4.2 Nature of the Optimized BHF Scheme

It is of interest to investigate the nature of the optimized BHF scheme and how it is affected by varying the process and die parameters. Two parameters seem to be most influential here mainly the drawing ration (B_0) and the die coefficient of friction (μ_D). Five drawing ratios are investigated with B_0 equals 1.9, 1.95, 2.0, 2.1, and 2.2. For each drawing ratio, four die coefficients of friction (0.045, 0.06, 0.1, and 0.13) are considered. The optimized BHF schemes are shown for each case in Fig. 5-46 to Fig. 5-50. The optimized BHF functions for the 20 cases are shown in Table 5-3, where the optimized BHF function is represented by:

$$F_{BH} = v_0 + v_1 L \tag{4.2}$$

All BHF schemes for the different drawing ratios are passing just above the wrinkling limit. This is expected since the optimization objective is to minimize the maximum punch force, which is directly proportional with the BHF as was discovered in the parametric study in section 5.3.3. Thus, the minimum possible BHF, which passes just above the wrinkling limit, corresponds to the minimum maximum punch force.

The process window for the small drawing ratios is very large that the fracture limit was excluded from the diagrams of B_0 equals 1.9, 1.95, and 2.0 to be able to view the BHF schemes as shown in Fig. 5-46, Fig. 5-47, and Fig. 5-48 respectively. Starting from B_0 equals 2.1 with a friction coefficient of 0.13, the fracture limit gets closer to the wrinkling limit as shown in Fig. 5-49. However, there is still a large space from 18.5kN to 34kN of acceptable BHF values that avoid both process limits. In the case of B_0 equals 2.2, there is no possible solution for the cases with friction coefficients of 0.1 and 0.13 as shown in Fig. 5-50. The two limits of wrinkling and fracture overlap, thus making it impossible to draw a full cup.

For the low drawing ratio of 1.9 which is shown in Fig. 5-46, the optimum BHF scheme has a negative slope. However, for the larger drawing ratios (2.0 – 2.2), the slope is positive. On the other hand, a drawing ratio of 1.95 has a nearly constant BHF scheme as shown in Fig. 5-47. This shows that there exists a break point at which the optimum BHF scheme shifts from a negative slope to a positive slope.

Also, this suggests that no general recommendation can be declared about which slope is better. In other words, the slope depends on the drawing ratio, where negative slope can be favorable for some drawing ratios and the positive be favorable for others.

Table 5-3: Optimized BHF functions

Case	Drawing ratio (B_0)	Die coefficient of friction (μ_D)	BHF function intercept (v_0)	BHF function slope (v_1)
1	1.9	0.045	12.010	-0.178
2	1.9	0.06	12.530	-0.215
3	1.9	0.1	11.349	-0.147
4	1.9	0.13	11.669	-0.170
5	1.95	0.045	10.289	0.056
6	1.95	0.06	11.258	-0.005
7	1.95	0.1	11.180	-0.008
8	1.95	0.13	11.964	-0.055
9	2.0	0.045	9.988	0.212
10	2.0	0.06	10.011	0.208
11	2.0	0.1	9.322	0.237
12	2.0	0.13	8.662	0.268
13	2.1	0.045	6.737	0.669
14	2.1	0.06	4.943	0.756
15	2.1	0.1	5.137	0.722
16	2.1	0.13	4.965	0.714
17	2.2	0.045	3.122	1.075
18	2.2	0.06	4.207	1.002
19	2.2	0.1	No solution	
20	2.2	0.13		

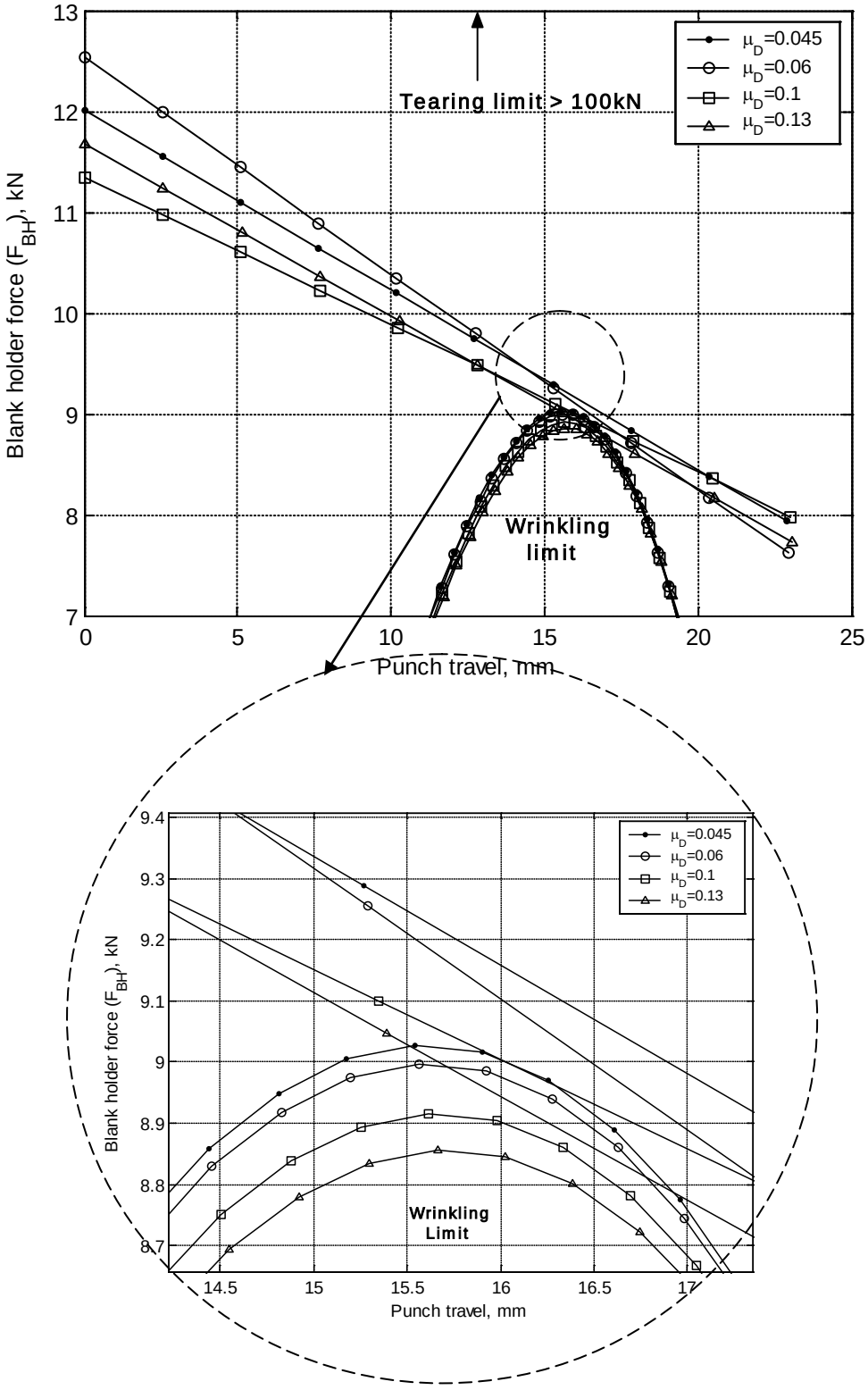

Fig. 5-46: BHF scheme for a drawing ratio of 1.9

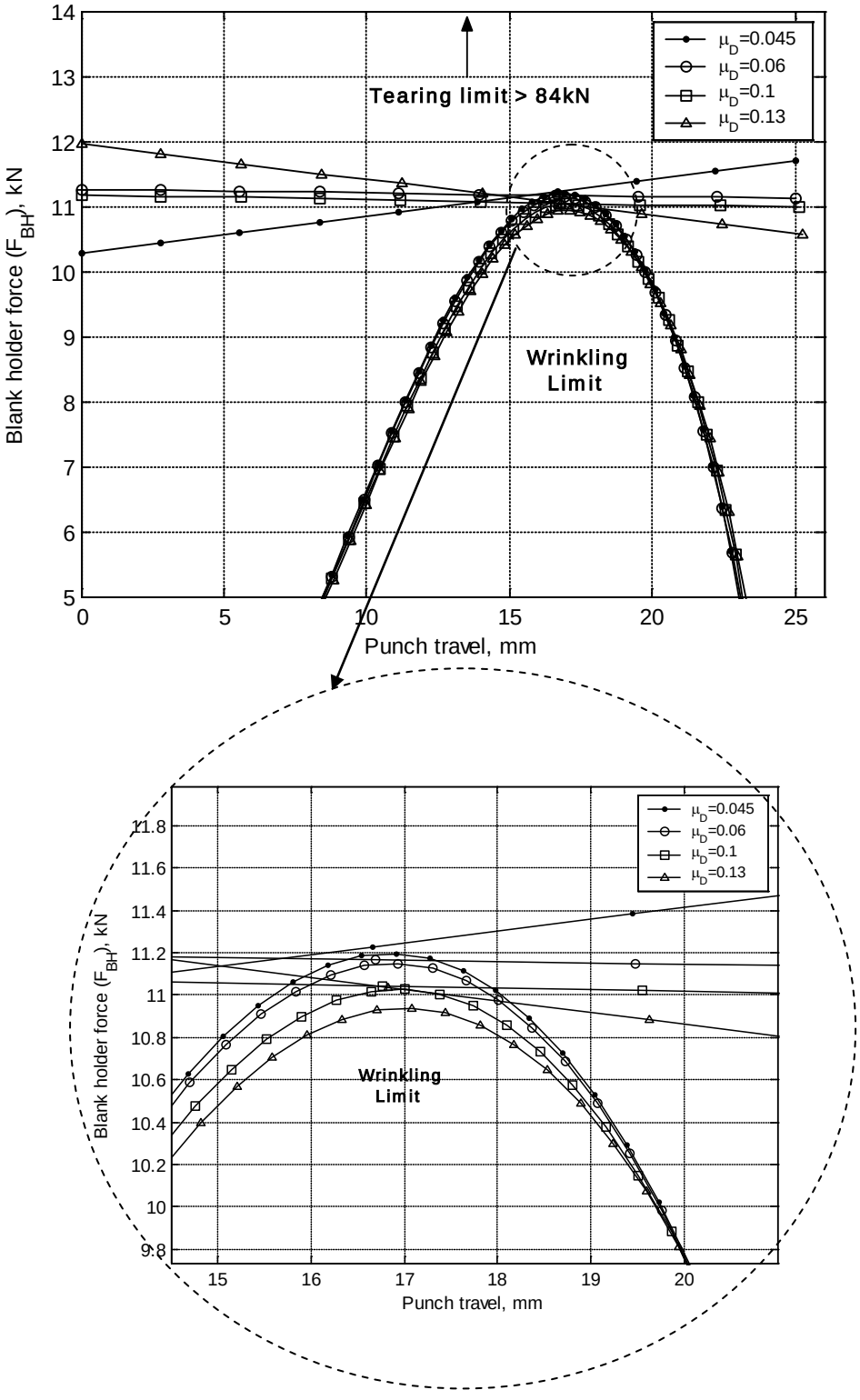

Fig. 5-47: BHF scheme for a drawing ratio of 1.95

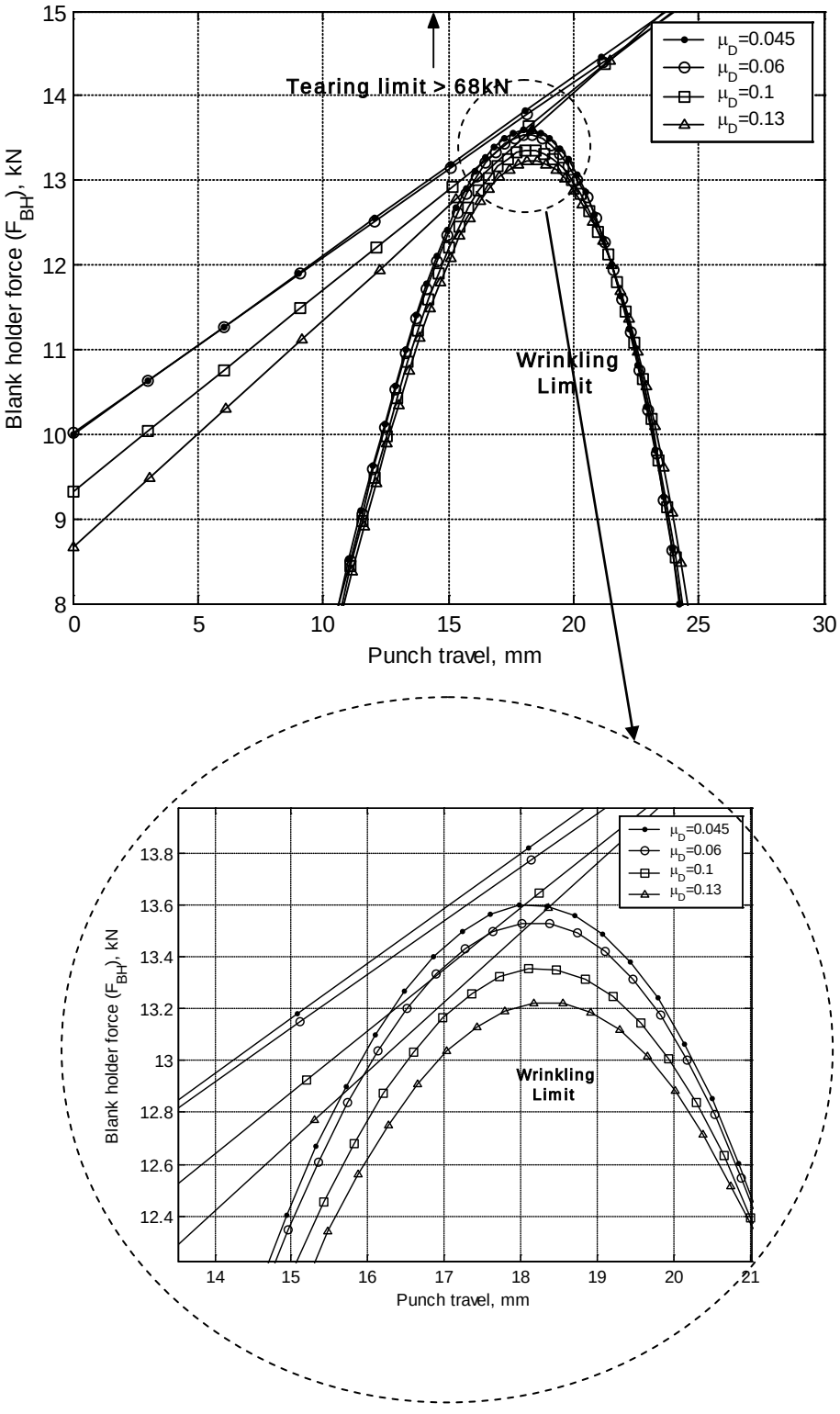

Fig. 5-48: BHF scheme for a drawing ratio of 2.0

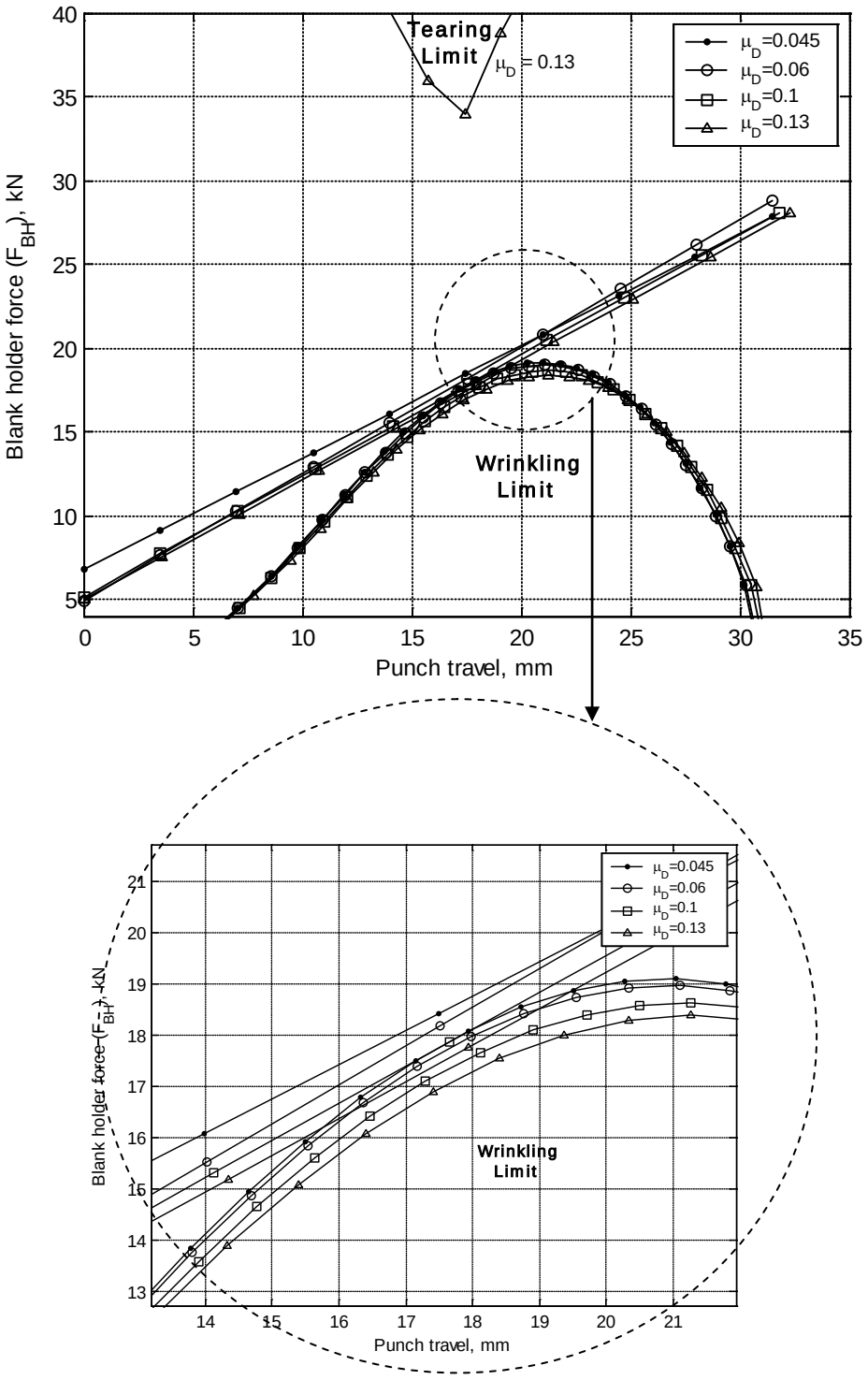

Fig. 5-49: BHF scheme for a drawing ratio of 2.1

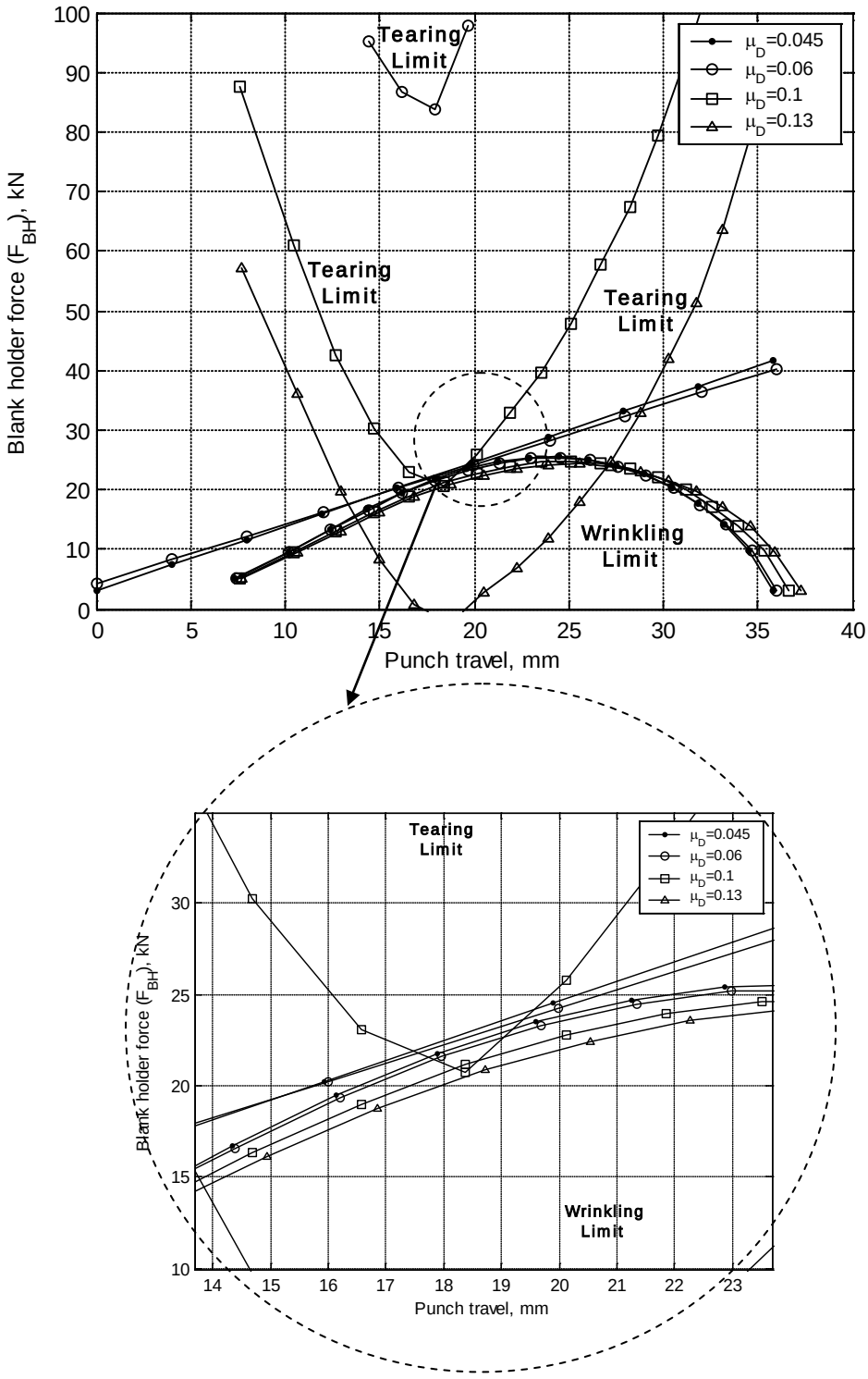

Fig. 5-50: BHF scheme for a drawing ratio of 2.2

The relation between the drawing ratio and the BHF function slope (v_1) is shown in Fig. 5-51. For all die coefficients of friction, there is a general trend for the slope to increase with increasing the drawing ratio in a linear manner. The difference in the slope of the four coefficients of friction at each drawing ratio is relatively small. Thus, it possible to deduce a general linear relation between the drawing ratio (B_0) and the BHF function slope (v_1) for all coefficients of friction. This can be achieved by fitting the data points in Fig. 5-51 to a linear function to give the following relation:

$$v_1 = -8.143 + 4.189\, B_0 \qquad (5.4)$$

The relation between the drawing ratio and the BHF function intercept (v_0) is nearly linear as shown in Fig. 5-52. There is a tendency for the intercept value to decrease with the increase in the drawing ratio. A similar general relation to that given in equation (5.4) can be reached for the relation between the drawing ratio and the BHF function intercept as follows.

$$v_0 = 68.544\text{-}29.660\, B_o \qquad (5.5)$$

By substituting equations (5.4) and (5.5) into equation (4.2), a general relation between the BHF and the drawing ratio and the punch travel can be concluded as follows.

$$F_{BH} = 68.544 – 29.660B_0 - 8.143L + 4.189B_0L \qquad (5.6)$$

This equation can be useful in industry if it is required to determine the optimum linear BHF scheme for any drawing ratio. It is worth noting that the relations in equations (5.4), (5.5), and (5.6) are only applicable to the cup under study. Further analysis will need to be carried out for other cups in order to determine if the BHF slope and intercept vary linearly with the drawing ratio for any cup.

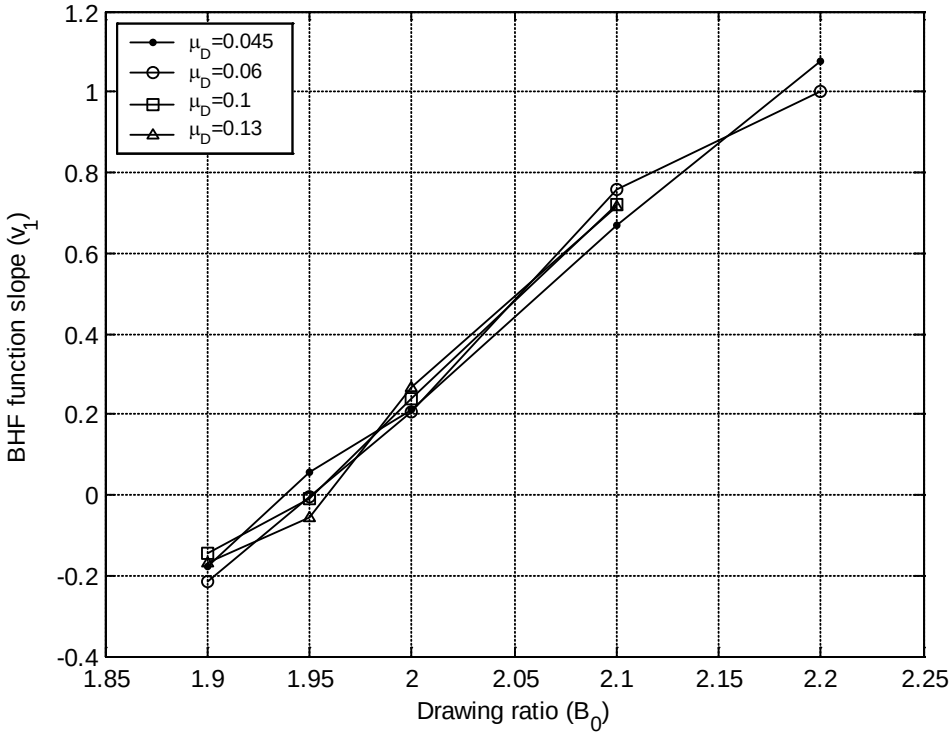

Fig. 5-51:Drawing ratio vs. BHF function slope

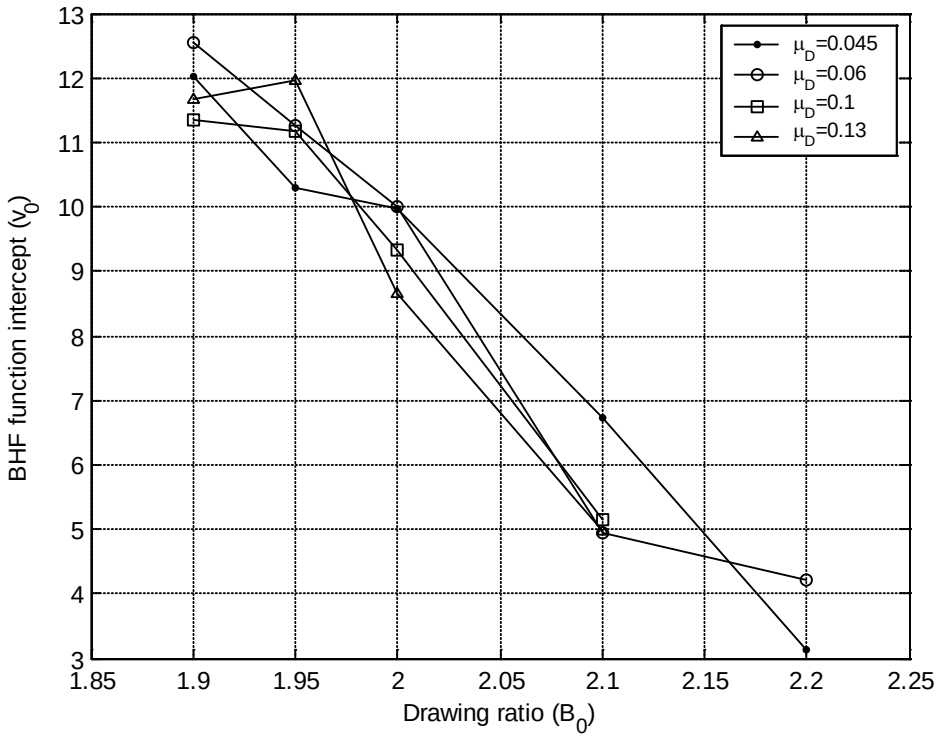

Fig. 5-52: Drawing ratio vs. BHF function intercept

CHAPTER 6

CONCLUSION AND RECOMMENDATIONS

The aim of the present study was to develop an optimization strategy that determines the optimum BHF scheme while minimizing punch force and avoiding process limits in the cup drawing process. The optimization process was applied to a developed analytical model that solves for the stresses and strains over the deforming sheet of the cup. The analytical model was verified with experimental results from the literature and compared with a developed finite element model. A parametric study was carried out using the analytical model to show the effect of some die, process, and material parameters on the process.

6.1 Conclusion

From the results of the present study, the following conclusions can be made:

1. The results for punch travel vs. flange radius reduction, punch travel vs. punch force, and strains distributions shows good correlation with the experimental results.
2. The comparison between the results of the analytical model and the finite element model shows good correlation. Both models have almost the same punch travel – punch force curve. Also, the punch travel vs. reduction in flange radius and circumferential strain show good agreement with the finite element model. However, the analytical model seems to under predict the strains and stresses at the punch profile region. The present study as well as other published work suggest that such analysis can be reliable up to the end of the cup wall. However, results at the punch profile and punch bottom are not accurate enough.
3. The parametric study conducted on the AL7075-T6 cup is found to be useful and some relations were concluded. The effect of the die profile radius is found to have a nearly linear relation with the maximum punch force as follows.

$$\left(F_p\right)_{\max} = 80.22 - 0.7\rho_d \quad \text{(kN)} \tag{5.2}$$

Also, a general approximate linear relation is deduced for the effect of the die coefficient of friction and drawing ratio on the maximum punch force, which is given as follows.

$$(F_p)_{\max} = -66.7 + 62.5\ B_0 + 115.6\ \mu_D \quad \text{(kN)} \tag{5.3}$$

4. Some relations are deduced from the optimization of the BHF scheme. The slope (v_1) of the optimum linear scheme has a negative value at low drawing ratios and shifts to positive values for higher drawing ratios. Also, it is found to have a nearly linear relation with the drawing ratio. Similarly, the BHF function intercept (v_0) shows a nearly linear relation with the drawing ratio. These findings helped in obtaining a general relation for the optimum BHF in terms of the drawing ratio and punch travel for the analyzed cup as follows:

$$F_{BH} = 68.5441 - 29.6604B_0 - 8.1433L + 4.1893B_0L \tag{5.6}$$

6.2 Recommendations

There are still some efforts that can be realized in this field, which include the following:

1. The analytical model requires more development to understand the behavior of the deforming sheet at the wall and punch profile regions. The effect of bending and unbending, shear stresses, and normal anisotropy should be investigated to determine how they contribute to the overall results.
2. Optimization of the BHF scheme needs to be carried out on other cup models in order to determine the validity of the linear relation between the BHF function slope and intercept with the drawing ratio.
3. Optimization can be carried out for other BHF functions to determine if there are other types of functions that can give better results than the linear function.

LIST OF REFERENCES

[1] Chung, S.Y. and Swift, H.W. (1951). Cup Drawing from a Flat Blank: Part 1: Experimental Investigation, Part 2: Analytical Investigation. *Proceedings of the Institution of Mechanical Engineering, 165*, 199-223.

[2] Woo, D.M. (1964). Analysis of the Cup-Drawing Process. *Journal of Mechanical Engineering Sciences, 6*, 116-131.

[3] Woo, D.M. (1968). On the Complete Solution of the Deep-Drawing Problem. *International Journal of Mechanical Sciences, 10*, 83-94.

[4] Woo, D. M. (1976, October). Analysis of Deep-Drawing over a Tractrix Die. *Journal of Engineering Materials and Technology, Transactions of the ASME, 98 Ser H* (4), 337-341.

[5] Al-Makky, M. M., and Woo, D. M. (1980). Deep-Drawing through Tractrix Type Dies. *International Journal of Mechanical Sciences, 22* (8), 467-480.

[6] Kaftanoğlu, B. and Alexander, J.M. (1970). On Quasistatic Axisymmetrical Stretch Forming. *International Journal of Mechanical Sciences, 12*, 1065-1084.

[7] Kaftanoğlu, B. and Tekkaya, A.E. (1981, Oct). Complete Numerical Solution of the Axisymmetrical Deep-Drawing Problem. *Journal of Engineering Materials and Technology, Transactions of the ASME. 103*, 326-332.

[8] Reissner, J. and Ehrismann, R. (1987). Computer-Aided Deep-Drawing of Two-Part Cans. *CIRP Annals, 36*, 199-202.

[9] Reissner, J. and Schmid, W. Tiefziehen, in: Lange, K. (ed.) (1990), *Umformtechnik Handbuch für Industrie und Wissenschaft*. Springer Verlag: Berlin (in German).

[10] Tatenami, T., Nakamura, Y., and Saito, K. (1982). An Analysis of Deep-drawing Process Combined with Bending. *Proceedings of the Numerical Methods for Industrial Forming Processes*, 687-696.

[11] Nakamura, Y, Tatenami, T, and Saito, K. (1982). Numerical Solution of Deep Drawing through Tractrix Die. *Proceedings of the Numerical Methods for Industrial Forming Processes*, 677-686.

[12] Mahdavian, S.M. and He, D. (1995 Apr). Product thickness analysis in pure cup-drawing. *Journal of Materials Processing Technology. 51,* 387-406.

[13] Chang, Der-Form and Wang, J. E. (1998, Aug.). Analysis of draw-redraw processes. *International Journal of Mechanical Sciences, 40*, 793-804.

[14] Noh, T.S. and Yang, D.Y. (1987). An Analysis of Hydroforming of Regular Polygonal Boxes. *International Journal of Mechanical Sciences, 29,* 139.

[15] Sowerby, R., Duncan, J. L., and Chu, E. (1986). The Modelling of Sheet Metal Stampings. *International Journal of Mechanical Sciences, 28*, 415.

[16] Gloeckl, H. and Lange, K. (1983). Computer-Aided Design of Blanks for Deep-Drawn Irregular Shaped Components. *Proceeding of the 11th North American Manufacturing Research Conference,* 243-251.

[17] Yoshida, K. and Miyauchi, K. (1977). Experimental Studies of Material Behavior as Related to Sheet Metal Forming. *Proceedings of Mechanics of Sheet Metal Forming Symposium, General Motors Research Labs, Warren, Michigan,* 19-52.

[18] Hansen, Bjarne G., Bay, Niels and Malberg, Michael P. (1995). A New Analysis and Verification Method of the Axisymmetrical Deep Drawing Process. *Proceedings of the Fifth International Conference on Numerical Methods in Industrial Forming Processes - Numiform 95, Balkema, Rotterdam,* 711-716.

[19] Wong, N.K., Arkun, B.H., Roberts, W.T. and Wilson, D.V. (1980, Mars). The Formability of Steel Sheets at Moderately Elevated Temepratures. *Less Memoires Scientifiques de la Revue de Metallurgie, 77e annee* (3), 413-422.

[20] Wifi, A.S. (1976). An Incremental Complete Solution of the Stretch Forming and Deep Drawing of a Circular Blank Using a Hemispherical Punch. *International Journal of Mechanical Sciences, 18* (23), 1976.

[21] Wang, N.M. and Budiansky, B. (1978). Analysis of Sheet Metal Stamping by a Finite-Element Method. *Journal of Applied Mechanics (Transactions of ASME, E), 45*, 73-82.

[22] Kobayashi, S. and Kim, J.H. (1977). Deformation Analysis of Axisymmetric Sheet Metal Forming Processes by the Rigid-Plastic Finite Element Method. *Proceedings of Mechanics of Sheet Metal Forming Symposium, General Motors Research Labs, Warren, Michigan,* 341-365.

[23] Yamada, Y., Wifi, A.S., and Hirakawa, T. (1978). Analysis of Large Deformation and Stress in Metal Forming Processes by the Finite Element Method.

Proceedings of IUTAM Symposium on Metal Forming Plasticity, Tutzing, F.R.G., 158-176.

[24] Saran, M.J., Schedin, E., Samuelsson, A., Melander, A. and Gustafsson, C. (1990). Numerical and Experimental Investigations of Deep Drawing of Metal Sheets. *Journal of Engineering for Industry, Transactions of the ASME, 112* (3) 272-277.

[25] Harpell, E., Lamontagne, C., and Worswick, M. J. (1996). Deep Drawing and Stretching of Al 5754 Sheet: LS-DYNA3d Simulation and Validation. *Proceedings of the 3rd International Conference, NUMISHEET '96, Numerical Simulation of 3-D Sheet Metal Forming Process, Dearborn, Michigan*, 386-393.

[26] Hayashida, Y., Maeda, Y., Matsui, K., Hashimoto, N., Hattori, S., Yangawa, M., Chung, K., Barlat, F., Brem, J.C., Lege, D.J., and Murtha, S.J. (1995). FEM analysis of Punch Stretching and Cup Drawing Tests for Aluminum Alloys using Planar Anisotropic Yield Function. *Proceedings of the Fifth International Conference on Numerical Methods in Industrial Forming Processes - Numiform 95, Balkema, Rotterdam,* 717-722.

[27] Moreira, L.P., Ferron, G., and Ferron, G. (2000, December) Experimental and numerical analysis of the cup drawing test for orthotropic metal sheets. *Journal of Materials Processing Technology, 108* (1), 78-86.

[28] Senior, B. W. (1981). Flange Wrinkling in Deep-Drawing Operations. *Journal of Mechanical Physical Solids, 4*, 235-246.

[29] Kawai, N. (1961). Critical Conditions of Wrinkling in Deep Drawing of Sheet Metals. *Bulletin of JSME, 4*, 169-192.

[30] Améziane-Hassani, H., and Neale, K.W. (1991). On the Analysis of Sheet Metal Wrinkling. *International Journal of Mechanical Sciences, 33* (1), 13-30.

[31] Kim, J.B., Yang, D.Y., Yoon, J.W., and Barlat, F. (1999). An Analysis of Wrinkling Initiation and Growth of Anisotropic Sheet in Deep Drawing Process With Controlled Blank Holding Force. *Numisheet '99, Besancon-France.* 335-340.

[32] Cao, J. and Wang, X. (1999). An Analytical Model for Plate Wrinkling Under Tri-Axial Loading and its Application. *International Journal of Mechanical Science, 42* (3), 617-633.

[33] De Magalhães Correia, J.P., Ferron, G. and Moreira, L.P. (2003). Analytical and numerical investigation of wrinkling for deep-drawn anisotropic metal sheets. *International Journal of Mechanical Sciences, 45*, 1167-1180.

[34] Deng, Z., Bleck, W., Lovell, M.R., and Papamantellos, K. (1999). A General approach for predicting the drawing fracture load and limit drawing ratio of an axisymmetric drawing process. *Metallurgical and Materials Transactions, Vol. 30A* (10), 2619-2627.

[35] Keeler S.P. and Backofen, W.A. (1963). Plastic Instability and Fracture in Sheets Stretched Over Rigid Punches, *Transactions of the ASM, 56*, 25-48.

[36] Lahoti, G. D., Nagpal, V., Altan, T. (1994). Prediction of Limit Strains in Biaxial Stretching of Sheets Using Marciniak's Approach. *Advanced Technology of Plasticity, 1*, 712-719.

[37] El-Sebaie, M.G. and Mellor, P.B. (1972). Plastic Instability Conditions in the Deep-Drawing of a Circular Blank of Sheet Metal. *International Journal of Mechanical Sciences, 14*, 535-556.

[38] Sonis, P, Reddy, N.V., and Lal, G.K. (2003). On Multistage Deep Drawing of Axisymmetric Components. *Journal of Manufacturing Science and Engineering, Transactions of the ASME, 125*, 352-362.

[39] Marciniak, Z, and Duncan, J.L. (1992). *Mechanics of Sheet Metal Forming.* Great Britain: Edward Arnold.

[40] Ahmetoglu, M.A., Coremans, A., Kinzel, G. L., and Altan, T. (1993). Improving Drawability by Using Variable Blank Holder Force and Pressure in Deep Drawing of Round and Non-Symmetric Parts. *SAE Special Publications, 944, Sheet Metal and Stamping Symposium*, pp. 113-120.

[41] Lei, Junxiang. (1998, September). Prediction and control of both wrinkle limit and fracture limit on cylindrical cup deep-drawing. *Journal of University of Science and Technology Beijing: Mineral Metallurgy Materials (Eng Ed), 5* (4), 237-240.

[42] Lei, Junxiang and Kang, Y. (1999, September). Prediction and control of both wrinkle limit and fracture limit on cylindrical cup deep-drawing (II). *Journal of University of Science and Technology Beijing: Mineral Metallurgy Materials (Eng Ed), 6* (3), 201-204.

[43] Thiruvarudchelvan, S. and Lewis, W. (1990). Deep drawing with Blank Holder Force Approximately Proportional to the Punch Force, *Transactions of the ASME, Journal of Engineering for Industry, 112* (3), 278-285.

[44] Thiruvarudchelvan, S. and Loh, N.H. (1994). Deep Drawing of Cylindrical Cups with Friction-actuated Blank Holding. *Journal of Materials Processing Technology, 40*, 343-358.

[45] Cao, J. and Boyce, M.C. (1995). Optimization of Sheet Metal Forming Processes by Instability Analysis and Control. *Proceedings of the Fifth International Conference on Numerical Methods in Industrial Forming Processes - Numiform 95, Balkema, Rotterdam*, 675-679.

[46] Sheng, Z.Q., Jirathearanat, S., and Altan, T. (2004, April). Adaptive FEM simulation for prediction of variable blank holder force in conical cup drawing. *International Journal of Machine Tools and Manufacture, 44* (5), 487-494.

[47] Lorenzo, R. Di, Fratini, L., and Micari, F. (1999), Optimal blankholder force path in sheet metal forming processes: an AI based design procedure, *Annals of CIRP, 48* (1), 231-234.

[48] Moshksar, M. M. and Zamanian, A. (1996). Optimization of the Tool Geometry in the Deep Drawing of Aluminum. *Journal of Materials Processing Technology, 72*, 363-370.

[49] Browne, M.T. and Hillery, M.T. (2001). Optimizing the Variables when Deep-Drawing C.R.1 Cups. *Journal of Materials Processing Technology, 136*, 64-71.

[50] Colgan, M., Monaghan, J. (2003). Deep drawing process: Analysis and experiment. *Journal of Materials Processing Technology, 132* (1-3), 35-41.

[51] Korhonen, A.S. (1982). Drawing Force in Deep Drawing of Cylindrical Cup with Flat-Nosed Punch. *Journal of Engineering for Industry, Transactions of the ASME, 104* (1), 29-37.

[52] El-Gizawy, A. S. and Younan, M.Y. (2004). *Modeling and Management of Process Induced Shape Distortion in Sheet Forming Processes*. Annual Progress Report. Unpublished Work. University of Missouri and the American University in Cairo.

[53] Hibbitt, Karlsson and Sorensen. *ABAQUS/Explicit User's Manual*

[54] Hibbitt, Karlsson and Sorensen. *Getting Started with ABAQUS/Explicit: Interactive Version*

[55] Chapra, Steven C. and Canale, Raymond P. (1998). *Numerical Methods for Engineers: With Programming and Software Applications.* McGraw-Hill, Inc.: New York, NY.

[56] Rao, Singiresu S. (1996). *Engineering Optimization*. John Wiley and Sons, Inc.: New York.

[57] Goldberg, David (1989). *Genetic Algorithms in Search, Optimization and Machine Learning*.

[58] Pearce, Roger (1991). *Sheet Metal Forming*. Adam Hilger: Bristol.

APPENDIX A

MATHEMATICAL DERIVATIONS

A1: Numerical Integration of the Force Equilibrium Equation in Region I

The force equilibrium equation in region I was given in chapter 3 as:

$$(\sigma_r)_{i,j} = (\sigma_r)_{i,j-1} + \int_{r_{i,j-1}}^{r_{i,j}} \left(\frac{\sigma_\theta - \sigma_r}{r}\right) dr + \frac{2\mu_{BH}}{t} \int_{r_{i,j-1}}^{r_{i,j}} \sigma_t dr$$

By using the trapezoidal rule for numerical integration [55]:

$$(\sigma_r)_{i,j} = (\sigma_r)_{i,j-1} + \frac{(r_{i,j} - r_{i,j-1})}{2}\left[\left\{\left(\frac{\sigma_\theta - \sigma_r}{r}\right)_{i,j} + \left(\frac{\sigma_\theta - \sigma_r}{r}\right)_{i,j-1}\right\} + \frac{2\mu_{BH}}{t}\left\{(\sigma_t)_{i,j} + (\sigma_t)_{i,j-1}\right\}\right]$$

$$(\sigma_r)_{i,j} = (\sigma_r)_{i,j-1} + (r_{i,j} - r_{i,j-1})\left[\frac{1}{2}\left\{\left(\frac{\sigma_\theta - \sigma_r}{r}\right)_{i,j} + \left(\frac{\sigma_\theta - \sigma_r}{r}\right)_{i,j-1}\right\} + \frac{\mu_{BH}}{t}\left[(\sigma_t - \sigma_r)_{i,j} + (\sigma_t - \sigma_r)_{i,j-1}\right]\right] + \frac{\mu_{BH}}{t}(\sigma_r)_{i,j}(r_{i,j} - r_{i,j-1}) + \frac{\mu_{BH}}{t}(\sigma_r)_{i,j-1}(r_{i,j} - r_{i,j-1})$$

$$= (\sigma_r)_{i,j-1} + (r_{i,j} - r_{i,j-1})\left[\frac{1}{2}\left\{\left(\frac{\sigma_\theta - \sigma_r}{r}\right)_{j} + \left(\frac{\sigma_\theta - \sigma_r}{r}\right)_{j-1}\right\} + \frac{\mu_{BH}}{t}\left[(\sigma_t - \sigma_r)_{i,j} + (\sigma_t - \sigma_r)_{i,j-1}\right]\right] + \frac{\mu_{BH}}{t}(\sigma_r)_{i,j}(r_{i,j} - r_{i,j-1}) + \frac{\mu_{BH}}{t}(\sigma_r)_{i,j-1}(r_{i,j} - r_{i,j-1})$$

This gives,

$$(\sigma_r)_{i,j}\left[1 - \frac{\mu_{BH}}{t}(r_{i,j} - r_{i,j-1})\right] = (\sigma_r)_{i,j-1}\left[1 + \frac{\mu_{BH}}{t}(r_{i,j} - r_{i,j-1})\right] + \left[\frac{1}{2}\left\{\left(\frac{\sigma_\theta - \sigma_r}{r}\right)_{i,j} + \left(\frac{\sigma_\theta - \sigma_r}{r}\right)_{i,j-1}\right\} + \frac{\mu_{BH}}{t}\left[(\sigma_t - \sigma_r)_{i,j} + (\sigma_t - \sigma_r)_{i,j-1}\right]\right](r_{i,j} - r_{i,j-1})$$

Thus, the final equation is

$$(\sigma_r)_{i,j} = \frac{1}{1-\frac{\mu_{BH}}{t_a}\left(r_{i,j}-r_{i,j-1}\right)}\left[(\sigma_r)_{i,j-1}\left(1+\frac{\mu_{BH}}{t_a}\left(r_{i,j}-r_{i,j-1}\right)\right)\right.$$
$$\left.+\left\{\frac{1}{2}\left(\left(\frac{\sigma_\theta-\sigma_r}{r}\right)_{i,j}+\left(\frac{\sigma_\theta-\sigma_r}{r}\right)_{i,j-1}\right)+\frac{\mu_{BH}}{t_a}\left((\sigma_t-\sigma_r)_{i,j}+(\sigma_t-\sigma_r)_{i,j-1}\right)\right\}\left(r_{i,j}-r_{i,j-1}\right)\right] \quad (3.31)$$

A2: Equations used in the determination of the contact angle θ

The following equations are based on the geometrical relations between the deforming sheet and the process tools shown in Fig. 3-15.

Equation 1

Assuming the deforming sheet is straight at the cup wall, the cross section areas of each region can be written as:

Region	Cross section area
I	$a_I = \pi\left(r_a^2 - r_b^2\right)$
II	$a_{II} = \pi\left(r_b^2 - r_c^2\right)$
III	$a_{III} = 2\pi\lambda_d \rho_d^{'}\theta$ Where, $\lambda_d = r_d + \rho_d - \rho_d^{'}\frac{(1-\cos\theta)}{\theta}$ = the centroid of the curved surface on the die profile
	$a_{IV} = 2\pi\lambda_W T$ Where, $\lambda_W = r_f + \left(\rho_p^{'}\tan\theta + \frac{1}{2}T\right)\cos\theta$ = the centroid of the wall
V	$a_V = 2\pi\lambda_p\rho_p^{'}\theta$ Where, $\lambda_p = r_f + \rho_p^{'}\frac{(1-\cos\theta)}{\theta}$ = the centroid of the curved surface on the punch profile
VI	$a_{VI} = \pi r_f^2$

The current total surface area of the sheet is: $a_I + a_{II} + a_{III} + a_{IV} + a_V + a_{VI}$

While, the initial total surface area of the sheet is: πR_a^2

Due to volume constancy of the sheet, the current volume equals the initial volume, thus:

$$\begin{aligned}\pi R_a^2 t_0 &= a_I t_a + a_{II} t_F + a_{III} t_D + a_{IV} t_W + a_V t_P + a_{VI} t_B \\ &= \pi\left(r_a^2 - r_b^2\right)t_a + \pi\left(r_b^2 - r_c^2\right)t_F + 2\pi\left(r_d + \rho_d - \rho_d^{'}\frac{(1-\cos\theta)}{\theta}\right)\rho_d^{'}\theta\, t_D \\ &\quad + 2\pi\left(r_f + \left(\rho_p^{'}\tan\theta + \frac{1}{2}T\right)\cos\theta\right)T\, t_W + 2\pi\left(r_f + \rho_p^{'}\frac{(1-\cos\theta)}{\theta}\right)\rho_p^{'}\theta\, t_P + \pi\, r_f^2 t_B\end{aligned}$$

By arranging terms, the final equation is:

$$\begin{aligned}&t_W\cos(\theta)T^2 + 2t_W[r_f + \rho_p^{'}\sin(\theta)]T + [2\rho_p^{'}t_P r_f + 2r_d\rho_d^{'}t_D + 2\rho_d\rho_d^{'}t_D]\theta \\ &-[2\rho_p^{'2}t_P - 2\rho_d^{'2}t_D]\cos(\theta) - R_a^2 t_o + r_f^2 t_B + 2\rho_p^{'2}t_P - 2\rho_d^{'2}t_D + [r_b^2 - r_c^2]t_F \\ &+[r_a^2 - r_b^2]t_a = 0\end{aligned} \tag{3.34}$$

Equation 2

From the geometry of the deforming sheet, which is shown in Fig. 3-15, the tangent line between the die and punch profiles is written as:

$$\begin{aligned}T^2 &= \left[\left(\rho_d^{'} + \rho_p^{'}\right)\cos\theta - H\right]^2 + \left[K - \left(\rho_d^{'} + \rho_p^{'}\right)\sin\theta\right]^2 \\ &= \left(N\cos\theta - H\right)^2 + \left(K - N\sin\theta\right)^2 \\ &= H^2 + K^2 + N^2 + 2N\left(-H\cos\theta - K\sin\theta\right)\end{aligned}$$

This gives:

$$H^2 - [2N\cos(\theta)]H + [K^2 + N^2 - 2NK\sin(\theta) - T^2] = 0 \tag{3.55}$$

Equation 3

From the angles between the sheet and the punch profile shown in Fig. 3-15,

$$\theta = \frac{1}{2}\pi - \left(\beta + \gamma\right)$$

Where, $\beta = \tan^{-1}\left(\frac{H}{K}\right)$ and $\gamma = \tan^{-1}\left(\frac{T}{N}\right)$

Therefore,

$$\theta = \frac{1}{2}\pi - \left[\tan^{-1}\left(\frac{H}{K}\right) + \tan^{-1}\left(\frac{T}{N}\right)\right] \tag{3.56}$$

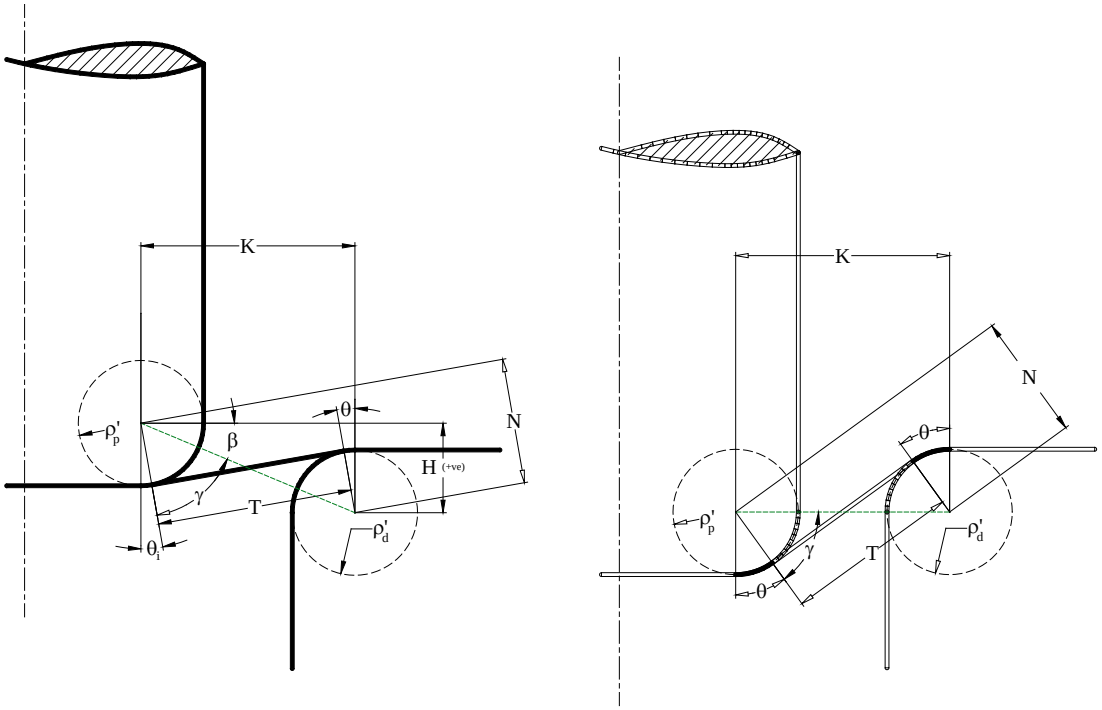

(a) H = +ve (b) H = 0

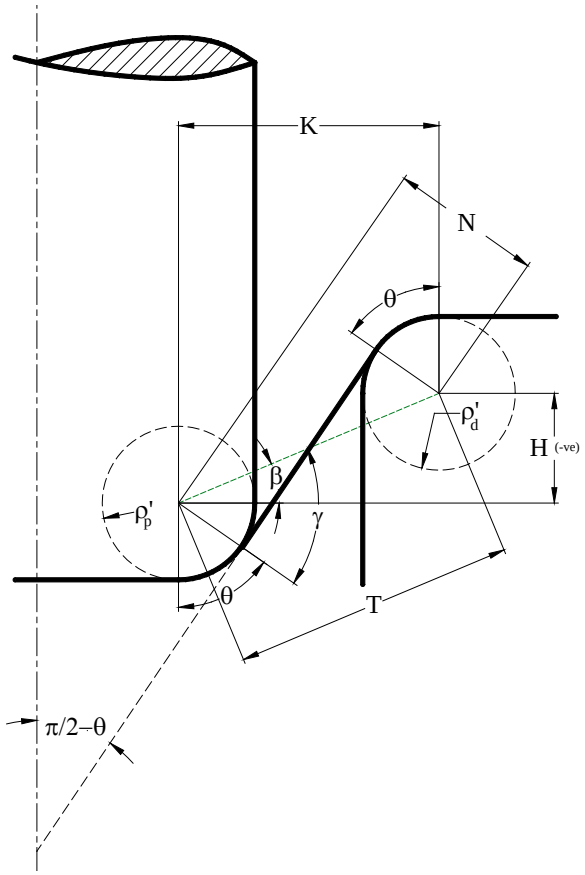

(c) H = -ve

Fig. 3-15: Geometrical relations in deep drawing at various stages of deformation

APPENDIX B

PSEUDO CODE OF THE ANALYTICAL MODEL

Cup

procedure *Cup*
begin
  get Input Data
  loop stage i
    call region I (rim)
    call region II (flange)
    call Theta guess
    call Boundary Search to minimize $\Delta\varepsilon_f = (\varepsilon_\theta - \varepsilon_r)$ at r_f
    evaluate regions III to VI with θ that gives minimum $\Delta\varepsilon_f$
    call *wrinkling*
    if $F_B < (F_B)_{cr}$
      then end of cup
      else continue
    call *fracture*
    if $(F_p) > (F_p)_{cr}$
      then end of cup
      else continue
    if $r_a < r_c$
      then end of cup
      else i = i + 1
  until end of cup
end

The program starts with calling a function called *Input data* that includes the input data for the cup solution. These data include:

- Cup geometry
- Sheet metal blank material properties
- Loading conditions
- Finite difference grid

Stress Strain

procedure *Stress-Strain*
begin
evaluate strains from equations (3.11) and (3.12)
evaluate incremental strains from equations (3.13), (3.14), and (3.15)
evaluate effective incremental strain and total effective strain from equations (3.16) and (3.17) respectively
evaluate effective stress from equation (3.18)
end

Rim

procedure *Rim*
begin
$t_a = t_a$ of previous stage
call *Rim-ta* to search for minimum F_{error} from equation (3.33)
call *Rim-rb* to search for r_b that gives $(\sigma_t)_b = 0$
end

Rim ta

procedure *Rim-ta*
begin
search for minimum F_{error} from equation (3.33)
loop j = 1 → Rend [*Rim (region I) end*]
evaluate radial position $r_{i,j}$ from equation (3.22)
call Stress-Strain to evaluate strains, and effective strain and stress from sub-function
evaluate stress difference $[(\sigma_\theta)_{i,j} - (\sigma_r)_{i,j}]$ from equation (3.19) and $[(\sigma_t)_{i,j} - (\sigma_r)_{i,j}]$ from equation (3.20)
evaluate radial stress $(\sigma_r)_{i,j}$ from equilibrium equation (3.31)
if $(\sigma_t)_{i,j} > 0$ or $r_{i,j} < r_c$
then end loop
end
until tolerance of $F_{error} < 1x10^{-6}$
end

Rim rb

procedure *Rim-rb*

begin

search for r_b that gives $(\sigma_t)_b = 0$

evaluate radial position $r_{i,b}$ from equation (3.22)

call Stress-Strain to evaluate strains, and effective strain and stress from sub-function

evaluate stress difference $[(\sigma_\theta)_{i,b} - (\sigma_r)_{i,b}]$ from equation (3.19) and $[(\sigma_t)_{i,b} - (\sigma_r)_{i,b}]$ from equation (3.20)

evaluate radial stress $(\sigma_r)_{i,b}$ from equilibrium equation (3.31)

until tolerance of (σ_t) at $r_b < 1x10^{-6}$

end

Flange

procedure *Flange*

begin

loop j = Rend →Fend [*Flange (region II) end*]

repeat

$t_{i,j} = t_{i,j-1}$

evaluate radial position $r_{i,j}$ from equation (3.24)

call Stress-Strain to evaluate strains, and effective strain and stress from sub-function

evaluate stress difference $[(\sigma_\theta)_{i,j} - (\sigma_r)_{i,j}]$ from equation (3.19) and $(\sigma_r)_{i,j}$ from equation (3.20)

evaluate radial stress $(\sigma_r)'_{i,j}$ from equilibrium equation (3.33)

until t_{error} from equation (3.44) is less than 0.01%

if $r_{i,j} < r_c$

then end loop

else continue loop

end

$t_{i,c} = t_{i,Fend}$

repeat for boundary point 3 at radius r_c

evaluate radial position $r_{i,c}$ from equation (3.24)

call Stress-Strain to evaluate strains, and effective strain and stress from sub-function

evaluate stress difference $[(\sigma_\theta)_{i,c} - (\sigma_r)_{i,c}]$ from equation (3.19) and $(\sigma_r)_{i,c}$ from equation (3.20)

evaluate radial stress $(\sigma_r)'_{i,c}$ from equilibrium equation (3.33)

until t_{error} from equation (3.44) is less than 0.01%

end

Theta Guess

procedure *Theta Guess*
begin
  assume a mean thickness of each region equals to those of previous stage
  assume a value of theta equals that of previous stage
  repeat
    evaluate T from equation (3.52)
    evaluate H from equation (3.55)
    evaluate θ_{new} from equation (3.56)
    $\theta_{error} = (\theta - \theta_{new})$x100/ θ_{new} (equation (3.57))
    $\theta = \theta_{new}$
  until $\theta_{error} < 0.01$
end

Boundary Search

procedure *Boundary Search*
begin
  initial search point $\theta = \theta_{guess}$
  search for minimum of equation (3.58)
    call Die Profile
    call Cup Wall
    call Punch Profile
  until tolerance of $\Delta\varepsilon_f < 1\text{x}10^{-6}$
end

Pseudo code for Die Profile, Cup Wall, and Punch Profile sub-functions which correspond to regions III, IV, and V respectively are the same as the Flange sub-function for region II. This is because the calculations for regions III, IV, and V are the same as region II except for the equilibrium equations, continuity equations and calculations termination. The differences were discussed earlier in the Numerical Solution section 3.5.2.

Wrinkling

procedure *wrinkling*
begin
evaluate p_{cr} from equation (4.3)
evaluate $(F_B)_{cr}$ from equation (4.4)
end

Fracture

Procedure *fracture*
begin
evaluate $(F_p)_{cr}$ from equation **(4.5**)
end

APPENDIX C

REAL CODED GENETIC ALGORITHMS

Genetic Algorithms (GAs) is among the most famous global search techniques. A detailed description of the approach is found in Goldberg [57]. GAs use three concepts that are deduced from natural evolution: selection, reproduction and mutation. The GAs used in the present study is a special type known as real-coded genetic algorithms, which is suitable to continuous function problems. The main steps involved in solving a problem using real-coded GAs are the following:

1. Initialize an initial population of solutions

The first step in the search is to generate initial search points. Each search point is called a chromosome which is made up of a number of variables values called genes and the number of points in the search space is called the population. The initial population of solutions is normally a randomly generated number of possible solutions to the problem the GA is expected to solve. It does not matter how good those solutions are, they are just a starting point for the GA to perform the search.

2. Evaluate the fitness of individuals in the population

A chromosome is evaluated by a fitness function to determine the quality of the solution. The fitness of each chromosome is a measure of its importance relative to the objective function. This fitness function is problem-specific and defines the genetic algorithm's objective for the current problem. For example, for a minimization problem with an objective function F(X),

Given a chromosome X_k , $k \in \{1,\ldots.., N\}$ and N = population size

Then, the fitness function is: $f_k(X_k) = \max F(X) - F(X_k)$

3. Select chromosomes with the highest fitness value

In each generation the chromosomes with the highest fitness values are selected to be passed on to the next generation. The number of selected high

fitness chromosomes is a proportion Q of the population N. The other M (N-Q) chromosomes in the N population are altered by using mutation and cross-over operations. These operations change the remaining M chromosomes in order to search for other possible function values with high fitness.

4. Mutate the genes of the offspring chromosomes

This mutation occurs according to some user-defined probability and serves to introduce some variability into the genes. Without mutation, offspring chromosomes would be limited to only the genes available within the initial population. The following mutations were used in the present study:

a. Uniform Mutation: For a given chromosome $X=\{x_1, x_2,\ldots,x_k, \ldots,x_n\}$, x_k is replaced by a random number between $[left_k, right_k]$, where left and right are the bounds on the variable x_k. It is to be noted that k is selected randomly between 1 and n. The effect of uniform mutation is the application of random search along one of the variables while keeping the others constant.

b. Whole Uniform Mutation: For a given chromosome $X=\{x_1, x_2,\ldots,x_n\}$, uniform mutation is applied on all variables. This operator is useful in the early stages of search in order to search over a larger space.

c. Boundary Mutation: For a given chromosome $X=\{x_1, x_2,\ldots,x_k, \ldots,x_n\}$ and randomly chosen $k \in \{1,\ldots,n\}$, x_k is replace with either $left_k$ or $right_k$, which are chosen at random. This operator is useful as a search element for the optima when they lie close to the boundary.

d. Non-Uniform Mutation: For a given chromosome $X=\{x_1, x_2,\ldots,x_k, \ldots,x_n\}$and for a random $k\in\{1,\ldots,n\}$, x_k is replace with $x_k^{'}$, where $x_k^{'}$ is randomly selected from either of the following two equations:

(1) $x_k^{'} = x_k + \Delta(t , right_k - x_k)$

(2) $x_k^{'} = x_k - \Delta(t , x_k - right_k)$

Where, $\Delta(t, y) = y \cdot r\left(1 - \frac{t}{T}\right)^6$

t = the number of the current generation

T = maximum number of generations

r = random value between [0,1]

The effect of such operator is the change in the variables value towards one of its boundaries.

5. Crossover the selected chromosomes to produce new offspring chromosomes

This crossover occurs according to some user-defined probability and results in new chromosomes having characteristics taken from both of the parent chromosomes. The crossovers used in the present study are:

a. Arithmetical Crossover: This operator has some kind of an averaging effect. For two chromosomes,

$X_1=\{x_{11}, x_{21},x_{31}, \ldots,x_{n1}\}$

$X_1=\{x_{12}, x_{22}, x_{k2}, \ldots,x_{n2}\}$

A random number α is generated between [0,1], then replace X_1 and X_2 with Y_1 and Y_2 as follows:

$Y_1 = \alpha X_1 + (1-\alpha)X_2$
$Y_2 = (1-\alpha) + \alpha X_2$

b. Simple Crossover: The effect of such operator is the search on the partial dimensions of each chromosome. For given chromosomes,

$X_1=\{x_{11}, x_{21},x_{31}, \ldots,x_{k1,}\ldots,x_{n1}\}$

$X_2=\{x_{12}, x_{22}, x_{k2}, \ldots,x_{k2,}\ldots,x_{n2}\}$

A random location k is selected and X_1 and X_2 are replaced with Y_1 and Y_2, where

$Y_1 = \{x_{11}, x_{21},x_{31}, \ldots,(x_{k1})_{1,} ,(x_{k+1})_2\ldots,x_{n1}\}$

$Y_2 = \{x_{12}, x_{22},x_{32}, \ldots,(x_{k1})_{2,} ,(x_{k+1})_1\ldots,x_{n2}\}$

c. Heuristic Crossover: For chromosomes X_1 and X_2 where, $f(X_2) > f(X_1)$, X_3 is generated along the higher fitness where,

$X_3 = r (X_2 – X_1) + X_2$, where r = random number between [0,1]

If X_3 exceeds the boundaries for the variables, then its value is repaired such that it stops at the boundary of the exceeded variable.

6. Evaluate each of the chromosomes in the new population

Once mutations and crossovers are applied to the M chromosomes, a new generation is started and same steps from 3 to 5 are repeated.

After the evolution of the initial population through many generations, the chromosomes (or solutions) within the final population will generally be much better as a whole than the chromosomes within the initial population. Also, the best chromosome in the final population will generally be near optimal if the genetic algorithm was run for enough generations. Search is terminated when the total number of specified generations is satisfied.

General Pseudocode of the Real-Coded GA

procedure Real-Coded GA Algorithm
begin

let $F(x_1,\ldots,x_n)$ be an objective function to be optimized, where $(x_1,\ldots,x_n)$ are the independent variables, where each variable x_i ranges between a lower and an upper limit [L, U].

convert the function F from a minimization to a maximization problem, where a new function $f(F)$ is to be maximized. The new function is known as the fitness function.

generate a random population P of N chromosomes

for a pre-specified number of generations (iterations)

use the *selection* operator to fill a new population with N-M high fitness chromosomes, where M is the total number of offspring chromosomes due to the application of the mutation and cross-over operators

use the *selection* operator along with the *mutation* and *cross-over* operators to fill the remaining M locations in the population.

evaluate the objective function (and fitness) value for the new population for the chromosomes that where changed by cross-over and mutation, and retain the fitness values of the unchanged chromosomes.

end

end

APPENDIX D

FINITE ELEMENT MODEL AND ABAQUS INPUT FILES

D1: Finite Element Model

Meshing

The problem was solved using axisymmetric model. The deep-drawing process has 4 parts, namely sheet, die, punch and blank holder. The die, punch, and blank holder were modeled as analytical rigid surfaces. An analytical rigid surface is a geometric surface with profiles that can be expressed with straight and curved line segments. It is associated with a rigid body reference node, which governs the motion of the surface. It is useful to use analytical rigid surfaces instead of element-based rigid surfaces due to two main reasons. First, modeling a body using analytical surfaces gives smooth curves. Thus, it reduces contact noise and provides a between approximation to the physical contact constraint. Also, computation time cost is reduced when using analytical rigid surfaces compared to element-based rigid surfaces. Parts of the deep drawing process are shown in Fig. D-1. Solid axisymmetric elements (CAX4R) were used in the meshing of the sheet, which is a 4-noded reduced integration element.

For the two models considered in this study, the sheet was meshed with 4 elements across the thickness to better show the variation of stresses and strains. The meshed blank is shown in Fig. D-2.

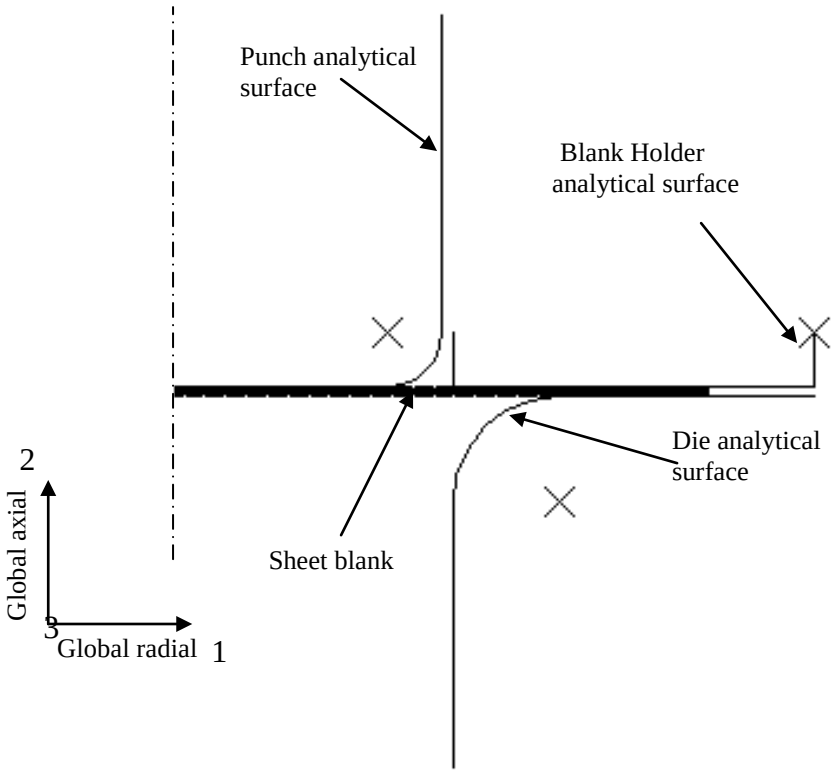

Fig. D-1: Deep-drawing parts showing die, punch, and blank holder as rigid analytical surfaces with reference nodes (marked as X)

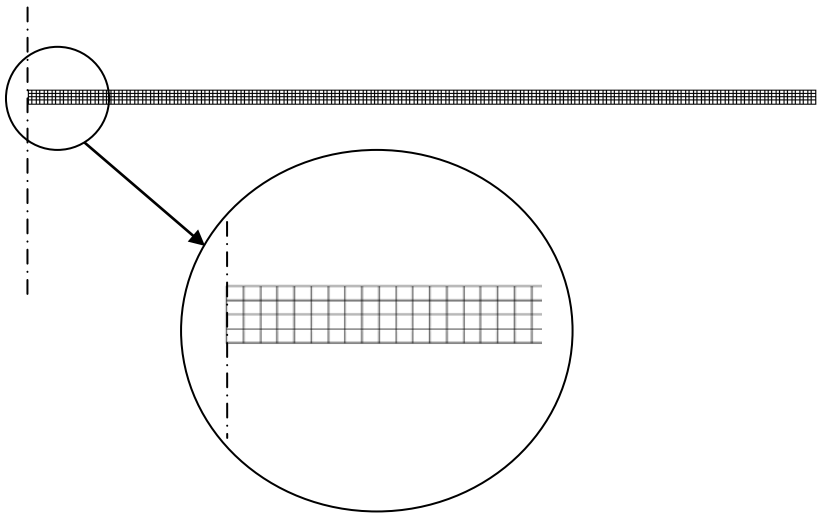

Fig. D-2: Meshed blank

Modeling of contact

Friction

The finite element model contains three surface contact pairs; sheet-blank holder, sheet-die, and sheet-punch. By default, ABAQUS assumes that contact is frictionless. So, the coefficient of friction has to be defined to describe the surface interaction between each two bodies. Friction is assumed constant coulomb friction.

Contact Formulation

For surface-to-surface contact modeling in ABAQUS/Explicit, kinematic contact formulation is the most suitable, where it was used for the three contact pairs. It achieves accurate fulfillment of the contact conditions using a predictor/corrector method. At first, the increment proceeds under the assumption that contact does not occur. If at the end of the increment there is an overclosure, the acceleration is modified to obtain a corrected configuration in which the contact constraints are imposed. Also, this type of contact algorithm gives a plastic impact and energy dissipation upon impact. For a fine mesh, like the case at hand, this loss in energy is insignificant. Kinematic contact is useful since it avoids sheet from bouncing upon punch impact.

Material Properties

The material flow curve is given as tabulated values for stresses and strains from zero strain up to a strain value of one.

Boundary Conditions and Loading

The problem under consideration is modeled as an axisymmetric problem. So, the sheet is fixed in the global radial direction at the nodes lying on the axis of symmetry (see Fig. D-1 for directions). Analytical rigid surfaces were constrained from their reference points by allowing them to move in the following manner:

- Blank holder is allowed to move in the global axial direction
- Die fixed in all directions
- Punch is allowed to move in the global axial direction

A concentrated load was applied at the blank holder reference node in the negative global axial direction with a value equal to the actual applied blank holder force. In case of a varying blank holder force, the load is applied in a varying scheme with the process time.

The dynamic solution using ABAQUS/Explicit solves for the dynamic equilibrium of the model. So, the velocity of the punch should be determined to analyze the problem. It is required to solve the problem in a quasi-static condition. Since a static solution is defined as a long-time solution, it is computationally impractical to solve the problem in its large natural time scale because it would require a large number of small time increments. A large velocity, which means smaller process time, is required to have an economical solution. However, as velocity increases, the state of static equilibrium converts into a state of dynamic equilibrium in which inertia forces become apparent. It is required to model the process in the shortest time period in which inertial forces remain insignificant.

In a static analysis the lowest frequency mode of the sheet usually dominates the response of deformation. In other words, the first mode shape of the blank is considered the limit of having a near static process. Thus, the time period of the lowest frequency mode of the sheet metal blank is taken as the step time of the process. This requires performing a frequency analysis for the blank to determine the first mode shape frequency. Then the process time required to complete the punch stroke is the reciprocal of the frequency. To determine the velocity of the punch, the required punch stroke is divided by the process time. The process loading was modeled in one step, which is the motion of the punch to give the total stroke with the calculated velocity.

D2: ABAQUS Input Files

Model 1 (shown in Fig. 3-21)

Note: only sample nodes and elements representing boundaries of the sheet are provided in the following input file. The total number of nodes is 1005 nodes and the total number of elements is 800 elements.

1. Frequency Analysis Input File

```
*Heading
 MODEL 1 - FREQUENCY ANALYSIS
**
**
*Node,NSET=ALLNODES
      1,          0.,          0.
    201,         50.,          0.
    202,          0.,       0.2225
    402,         50.,       0.2225
    403,          0.,        0.445
    603,         50.,        0.445
    604,          0.,       0.667
    804,         50.,       0.6675
    805,          0.,        0.89
   1005,         50.,        0.89
*Element,type=CAX4R,ELSET=SHEET
  1,    1,    2,  203,  202
200,  200,  201,  402,  401
201,  202,  203,  404,  403
400,  401,  402,  603,  602
401,  403,  404,  605,  604
600,  602,  603,  804,  803
601,  604,  605,  806,  805
800,  803,  804, 1005, 1004
**
**
*Orientation,name=SHEETGLOB
 1,0,0,0,1,0
 1,0
**
**
*Solid Section,elset=SHEET,orientation=SHEETGLOB,material=AL7075-T6
**
**
** NODE AND ELEMENT SETS
** ######################
*Nset,nset=SheetSYMM,generate
 1,805,201
*Elset,elset=SheetSYMM,generate
 1,601,200
*Nset,nset=SheetEND,generate
 201,1005,201
*Elset,elset=SheetEND,generate
 200,800,200
**
**
** SHEET SURFACES
** ###############
*Elset,elset=SHEET_TOP,generate
 601,800,1
*Surface,type=ELEMENT,name=SHEET_TOP
 SHEET_TOP,S3
*Elset,elset=SHEET_BOT,generate
 1,200,1
*Surface,type=ELEMENT,name=SHEET_BOT
 SHEET_BOT,S1
**
** MATERIALS
** #########
*Material,name=AL7075-T6
*Density
 2.796e-09,
*Elastic
 65000., 0.33
*Plastic
520.000,0.00
557.195,0.02
588.230,0.04
607.180,0.06
620.995,0.08
631.926,0.10
641.000,0.12
648.774,0.14
```

```
655.584,0.16
661.651,0.18
667.124,0.20
672.115,0.22
676.704,0.24
680.953,0.26
684.911,0.28
688.616,0.30
692.100,0.32
695.389,0.34
698.504,0.36
701.464,0.38
704.283,0.40
706.976,0.42
709.552,0.44
712.023,0.46
714.397,0.48
716.681,0.50
718.882,0.52
721.007,0.54
723.061,0.56
725.047,0.58
726.972,0.60
728.839,0.62
730.650,0.64
732.411,0.66
734.122,0.68
735.789,0.70
737.411,0.72
738.993,0.74
740.536,0.76
742.041,0.78
743.512,0.80
744.949,0.82
746.354,0.84
747.729,0.86
749.074,0.88
750.392,0.90
751.683,0.92
752.948,0.94
754.189,0.96
755.406,0.98
756.600,1.00
**
**
** BOUNDARY CONDITIONS
** ####################
*Boundary
 SheetSYMM,XSYMM
 SheetEND,2
**
** Frequency analysis(the first 10 mode shapes)
**
*STEP
*FREQUENCY
 10,
*END STEP
```

2. Analysis Input File

```
*Heading
 MODEL 1
**
**
*Node,NSET=ALLNODES
      1,          0.,          0.
    201,          50.,           0.
    202,           0.,       0.2225
    402,          50.,       0.2225
    403,           0.,       0.445
    603,          50.,        0.445
```

```
   604,          0.,       0.667
   804,         50.,       0.6675
   805,          0.,        0.89
  1005,         50.,        0.89
*Element,type=CAX4R,ELSET=SHEET
  1,    1,    2,  203,  202
200,  200,  201,  402,  401
201,  202,  203,  404,  403
400,  401,  402,  603,  602
401,  403,  404,  605,  604
600,  602,  603,  804,  80
601,  604,  605,  806,  805
800,  803,  804, 1005, 1004
**
**
*Orientation,name=SHEETGLOB
 1,0,0,0,1,0
 1,0
**
**
*Solid Section,elset=SHEET,orientation=SHEETGLOB,material=AL7075-T6
**
**
** DIE DEFINITION
** #############
*Node
 5000,36.068,-10,0
*Nset,nset=DIEREFP
 5000
*Surface,type=SEGMENTS,name=DIE_SURFACE
 START,26.068,-35
 LINE,26.068,-10
 CIRCL,36.068,0,36.068,-10
 LINE,60,0
*Rigid Body,ref node=DIEREFP,analytical surface=DIE_SURFACE
**
**
** PUNCH DEFINITION
** ###############
*Node
 6000,20,5.89,0
*Nset,nset=PUNCHREFP
 6000
*Surface,type=SEGMENTS,name=PUNCH_SURFACE
 START,25,35.89
 LINE,25,5.89
 CIRCL,20,0.89,20,5.89
 LINE,0,0.89
*Rigid Body,ref node=PUNCHREFP,analytical surface=PUNCH_SURFACE
**
**
** BLANKHOLDER INSTANCE
** ####################
*Node
 7000,60,5.89,0
*Nset,nset=BHREFP
 7000
*Element,type=MASS,elset=EMASS
 10000,7000
*Mass,elset=EMASS
 0.01,
*Surface,type=SEGMENTS,name=BHOLDER_SURFACE
 START,60,5.89
 LINE,60,0.9
 CIRCL,59.99,0.89,59.99,0.9
 LINE,26.058,0.89
 CIRCL,26.068,0.9,26.078,0.9
 LINE,26.068,5.89
*Rigid Body,ref node=BHREFP,analytical surface=BHOLDER_SURFACE
**
**
** NODE AND ELEMENT SETS
** ####################
*Nset,nset=SheetSYMM,generate
 1,805,201
```

```
*Elset,elset=SheetSYMM,generate
 1,601,200
*Nset,nset=SheetEND,generate
 201,1005,201
*Elset,elset=SheetEND,generate
 200,800,200
**
**
** SHEET SURFACES
** ###############
*Elset,elset=SHEET_TOP,generate
 601,800,1
*Surface,type=ELEMENT,name=SHEET_TOP
 SHEET_TOP,S3
*Elset,elset=SHEET_BOT,generate
 1,200,1
*Surface,type=ELEMENT,name=SHEET_BOT
 SHEET_BOT,S1
**
**
** MATERIALS
** #########
*Material,name=AL7075-T6
*Density
 2.796e-09,
*Elastic
 65000., 0.33
*Plastic
520.000,0.00
557.195,0.02
588.230,0.04
607.180,0.06
620.995,0.08
631.926,0.10
641.000,0.12
648.774,0.14
655.584,0.16
661.651,0.18
667.124,0.20
672.115,0.22
676.704,0.24
680.953,0.26
684.911,0.28
688.616,0.30
692.100,0.32
695.389,0.34
698.504,0.36
701.464,0.38
704.283,0.40
706.976,0.42
709.552,0.44
712.023,0.46
714.397,0.48
716.681,0.50
718.882,0.52
721.007,0.54
723.061,0.56
725.047,0.58
726.972,0.60
728.839,0.62
730.650,0.64
732.411,0.66
734.122,0.68
735.789,0.70
737.411,0.72
738.993,0.74
740.536,0.76
742.041,0.78
743.512,0.80
744.949,0.82
746.354,0.84
747.729,0.86
749.074,0.88
750.392,0.90
751.683,0.92
```

```
752.948,0.94
754.189,0.96
755.406,0.98
756.600,1.00
**
** BOUNDARY CONDITIONS
** ####################
*Boundary
 BHREFP,1,1
 BHREFP,6,6
 DIEREFP,1,1
 DIEREFP,2,2
 DIEREFP,6,6
 PUNCHREFP,1,1
 PUNCHREFP,6,6
 SheetSYMM,XSYMM
**
** STEP: MOVE_PUNCH
** #################
*Step,NLGEOM=YES
 Move Punch by a prescribed distance
*Dynamic,Explicit
 ,0.002483
*Boundary,type=VELOCITY
 PUNCHREFP,2,2,-12082
**
** LOADS
**
** Name: BHOLDER_LOAD   Type: Constant
*Cload
 BHREFP,2,-17000
**
**
** INTERACTIONS
** ************
** Interaction: BHOLDER-SHEET_CONTACT
**
*Surface Interaction,name=BHOLDER_FRICTION
*Friction
 0.13,
*Contact Pair,interaction=BHOLDER_FRICTION,CPSET=BHSHE
 SHEET_TOP,BHOLDER_SURFACE
**
**
** Interaction: DIE-SHEET_CONTACT
**
*Surface Interaction,name=DIE_FRICTION
*Friction
 0.13,
*Contact Pair,interaction=DIE_FRICTION
 SHEET_BOT,DIE_SURFACE
**
**
** Interaction: PUNCH-SHEET_CONTACT
**
*Surface Interaction,name=PUNCH_FRICTION
*Friction
 0.13,
*Contact Pair, interaction=PUNCH_FRICTION,CPSET=PUNSHE
 SHEET_TOP,PUNCH_SURFACE
**
**
** OUTPUT REQUESTS
** ################
**  Requesting output variables for postprocessing (OUTPUT and HISTORY FIELDS)
**
**
** FIELD OUTPUT: F-Output-1
** ************************
*Output,field
*Element Output,elset=SHEET,VARIABLE=PRESELECT
*Node Output,nset=allnodes,VARIABLE=PRESELECT
*Node Output,nset=DIEREFP,VARIABLE=PRESELECT
*Node Output,nset=PUNCHREFP,VARIABLE=PRESELECT
*Node Output,nset=BHREFP,VARIABLE=PRESELECT
```

```
**
**
** HISTORY OUTPUT: SheetEnd_History
** ********************************
*Output, history
*Node Output, nset=SheetEND
 U1
*Node Output, nset=SheetSYMM
 U2
*CONTACT OUTPUT,CPSET=BHSHE,VARIABLE=PRESELECT
 CFN
 CFT
*CONTACT OUTPUT,CPSET=PUNSHE,VARIABLE=PRESELECT
 CFN
 CFT
*End Step
```

Model 2 (shown in Fig. 3-20)

Note: only sample nodes and elements representing boundaries of the sheet are provided in the following input file. The total number of nodes is 1505 nodes and the total number of elements is 1200 elements.

1. Frequency Analysis Input File

```
*Heading
 MODEL 2 - FREQUENCY ANALYSIS
**
*Node,NSET=ALLNODES
      1,          0.,          0.
    301,        100.,          0.
    302,          0.,       0.175
    602,        100.,       0.175
    603,          0.,        0.35
    903,        100.,        0.35
    904,          0.,       0.525
   1204,        100.,       0.525
   1205,          0.,         0.7
   1505,        100.,         0.7
*Element,type=CAX4R,ELSET=SHEET
   1,    1,    2,  303,  302
 300,  300,  301,  602,  601
 301,  302,  303,  604,  603
 600,  601,  602,  903,  902
 601,  603,  604,  905,  904
 900,  902,  903, 1204, 1203
 901,  904,  905, 1206, 1205
1200, 1203, 1204, 1505, 1504
**
**
*Orientation,name=SHEETGLOB
 1,0,0,0,1,0
 1,0
**
*Solid Section,elset=SHEET,orientation=SHEETGLOB,material=BRASS70-30
**
**
** NODE AND ELEMENT SETS
** ######################
*Nset,nset=SheetSYMM,generate
 1,1205,301
*Elset,elset=SheetSYMM,generate
 1,901,300
*Nset,nset=SheetEND,generate
 301,1505,301
```

```
*Elset,elset=SheetEND,generate
 300,1200,300
**
**
** SHEET SURFACES
** ###############
*Elset,elset=SHEET_TOP,generate
 901,1200,1
*Surface,type=ELEMENT,name=SHEET_TOP
 SHEET_TOP,S3
*Elset,elset=SHEET_BOT,generate
 1,301,1
*Surface,type=ELEMENT,name=SHEET_BOT
 SHEET_BOT,S1
**
** MATERIALS
** #########
*Material,name=BRASS70-30
*Density
 8.470e-09,
*Elastic
 110000., 0.34
*Plastic
65.80,0.00
173.08,0.02
231.57,0.04
274.57,0.06
309.83,0.08
340.27,0.10
367.35,0.12
391.92,0.14
414.53,0.16
435.55,0.18
455.26,0.20
473.85,0.22
491.49,0.24
508.29,0.26
524.36,0.28
539.78,0.30
554.61,0.32
568.91,0.34
582.73,0.36
596.12,0.38
609.10,0.40
621.71,0.42
633.98,0.44
645.92,0.46
657.57,0.48
668.95,0.50
680.06,0.52
690.92,0.54
701.56,0.56
711.97,0.58
722.18,0.60
732.20,0.62
742.03,0.64
751.68,0.66
761.16,0.68
770.49,0.70
779.66,0.72
788.68,0.74
797.56,0.76
806.31,0.78
814.93,0.80
823.43,0.82
831.80,0.84
840.06,0.86
848.21,0.88
856.26,0.90
864.20,0.92
872.04,0.94
879.79,0.96
887.44,0.98
895.00,1.00
**
```

```
**
** BOUNDARY CONDITIONS
** ####################
*Boundary
 SheetSYMM,XSYMM
 SheetEND,2
**
** Frequency analysis(the first 10 mode shapes)
**
*STEP
*FREQUENCY
 10,
*END STEP
```

2. Constant BHF Analysis Input File

```
*Heading
 ANALYSIS CUP
**
**
*Node,NSET=ALLNODES
      1,          0.,          0.
    301,         100.,          0.
    302,          0.,        0.175
    602,         100.,        0.175
    603,          0.,         0.35
    903,         100.,         0.35
    904,          0.,        0.525
   1204,         100.,        0.525
   1205,          0.,          0.7
   1505,         100.,          0.7
*Element,type=CAX4R,ELSET=SHEET
   1,    1,    2,  303,  302
 300,  300,  301,  602,  601
 301,  302,  303,  604,  603
 600,  601,  602,  903,  902
 601,  603,  604,  905,  904
 900,  902,  903, 1204, 1203
 901,  904,  905, 1206, 1205
1200, 1203, 1204, 1505, 1504
**
**
*Orientation,name=SHEETGLOB
 1,0,0,0,1,0
 1,0
**
**
*Solid Section,elset=SHEET,orientation=SHEETGLOB,material=BRASS70-30
**
**
** DIE DEFINITION
** #############
*Node
 5000,56.25,-5,0
*Nset,nset=DIEREFP
 5000
*Surface,type=SEGMENTS,name=DIE_SURFACE
 START,51.25,-80
 LINE,51.25,-5
 CIRCL,56.25,0,56.25,-5
 LINE,110,0
*Rigid Body,ref node=DIEREFP,analytical surface=DIE_SURFACE
**
**
** PUNCH DEFINITION
** ###############
*Node
 6000,37,13.7,0
*Nset,nset=PUNCHREFP
 6000
*Surface,type=SEGMENTS,name=PUNCH_SURFACE
```

```
 START,50,80.7
 LINE,50,13.7
 CIRCL,37,0.7,37,13.7
 LINE,0,0.7
*Rigid Body,ref node=PUNCHREFP,analytical surface=PUNCH_SURFACE
**
**
** BLANKHOLDER INSTANCE
** ####################
*Node
 7000,110,5.7,0
*Nset,nset=BHREFP
 7000
*Element,type=MASS,elset=EMASS
 10000,7000
*Mass,elset=EMASS
 0.01,
*Surface,type=SEGMENTS,name=BHOLDER_SURFACE
 START,110,5.7
 LINE,110,0.71
 CIRCL,109.99,0.7,109.99,0.71
 LINE,51.26,0.7
 CIRCL,51.25,0.71,51.26,0.71
 LINE,51.25,5.7
*Rigid Body,ref node=BHREFP,analytical surface=BHOLDER_SURFACE
**
**
** NODE AND ELEMENT SETS
** ######################
*Nset,nset=SheetSYMM,generate
 1,1205,301
*Elset,elset=SheetSYMM,generate
 1,901,300
*Nset,nset=SheetEND,generate
 301,1505,301
*Elset,elset=SheetEND,generate
 300,1200,300
**
**
** SHEET SURFACES
** ###############
*Elset,elset=SHEET_TOP,generate
 901,1200,1
*Surface,type=ELEMENT,name=SHEET_TOP
 SHEET_TOP,S3
*Elset,elset=SHEET_BOT,generate
 1,300,1
*Surface,type=ELEMENT,name=SHEET_BOT
 SHEET_BOT,S1
**
**
** MATERIALS
** #########
*Material,name=BRASS70-30
*Density
 8.470e-09,
*Elastic
 110000., 0.34
*Plastic
65.80,0.00
173.08,0.02
231.57,0.04
274.57,0.06
309.83,0.08
340.27,0.10
367.35,0.12
391.92,0.14
414.53,0.16
435.55,0.18
455.26,0.20
473.85,0.22
491.49,0.24
508.29,0.26
524.36,0.28
539.78,0.30
```

```
554.61,0.32
568.91,0.34
582.73,0.36
596.12,0.38
609.10,0.40
621.71,0.42
633.98,0.44
645.92,0.46
657.57,0.48
668.95,0.50
680.06,0.52
690.92,0.54
701.56,0.56
711.97,0.58
722.18,0.60
732.20,0.62
742.03,0.64
751.68,0.66
761.16,0.68
770.49,0.70
779.66,0.72
788.68,0.74
797.56,0.76
806.31,0.78
814.93,0.80
823.43,0.82
831.80,0.84
840.06,0.86
848.21,0.88
856.26,0.90
864.20,0.92
872.04,0.94
879.79,0.96
887.44,0.98
895.00,1.00
**
**
** BOUNDARY CONDITIONS
** ####################
*Boundary
 BHREFP,1,1
 BHREFP,6,6
 DIEREFP,1,1
 DIEREFP,2,2
 DIEREFP,6,6
 PUNCHREFP,1,1
 PUNCHREFP,6,6
 SheetSYMM,XSYMM
**
**
** STEP: MOVE_PUNCH
** #################
*Step,NLGEOM=YES
 Move Punch by a prescribed distance
*Dynamic,Explicit
 ,0.01722
*Boundary,type=VELOCITY
 PUNCHREFP,2,2,-4644.56
**
** LOADS
**
** Name: BHOLDER_LOAD   Type: COnstant
*Cload
 BHREFP,2,-100000
**
**
** INTERACTIONS
** ************
** Interaction: BHOLDER-SHEET_CONTACT
**
*Surface Interaction,name=BHOLDER_FRICTION
*Friction
 0.06,
*Contact Pair,interaction=BHOLDER_FRICTION,CPSET=BHSHE
 SHEET_TOP,BHOLDER_SURFACE
```

```
**
**
** Interaction: DIE-SHEET_CONTACT
**
*Surface Interaction,name=DIE_FRICTION
*Friction
 0.06,
*Contact Pair,interaction=DIE_FRICTION
 SHEET_BOT,DIE_SURFACE
**
**
** Interaction: PUNCH-SHEET_CONTACT
**
*Surface Interaction,name=PUNCH_FRICTION
*Friction
 0.06,
*Contact Pair, interaction=PUNCH_FRICTION,CPSET=PUNSHE
 SHEET_TOP,PUNCH_SURFACE
**
**
** OUTPUT REQUESTS
** ################
**  Requesting output variables for postprocessing (OUTPUT and HISTORY FIELDS)
**
**
** FIELD OUTPUT: F-Output-1
** ************************
*Output,field
*Element Output,elset=SHEET,VARIABLE=PRESELECT
*Node Output,nset=allnodes,VARIABLE=PRESELECT
*Node Output,nset=DIEREFP,VARIABLE=PRESELECT
*Node Output,nset=PUNCHREFP,VARIABLE=PRESELECT
*Node Output,nset=BHREFP,VARIABLE=PRESELECT
**
**
** HISTORY OUTPUT: SheetEnd_History
** ********************************
*Output, history
*Node Output, nset=SheetEND
 U1
*Node Output, nset=SheetSYMM
 U2
*CONTACT OUTPUT,CPSET=BHSHE,VARIABLE=PRESELECT
 CFN
 CFT
*CONTACT OUTPUT,CPSET=PUNSHE,VARIABLE=PRESELECT
 CFN
 CFT
*End Step
```

3. Linear BHF Analysis Input File

The input file for the linear BHF is the same as the one for the constant BHF except at the LOADS definition, where it is replaced with the following:

```
** LOADS
**
** Name: BHOLDER_LOAD   Type: Linearly varying force
*Amplitude,Definition=Tabular,Name=BHF
 0,4638.9,0.01722,92174.9
*Cload,Amplitude=BHF
 BHREFP,2,-1
```